

A Hybrid Approach to Neutron Transport with Thermal-hydraulic Feedback for Reactor Transient Analysis

Présentée le 18 mars 2021

Faculté des sciences de base
Laboratoire de physique des réacteurs et de comportement des systèmes
Programme doctoral en énergie

pour l'obtention du grade de Docteur ès Sciences

par

Alexander AURES

Acceptée sur proposition du jury

Prof. K. A. J. Mulleners, présidente du jury
Prof. A. Pautz, Dr W. Zwermann, directeurs de thèse
Dr S. Kliem, rapporteur
Prof. N. Garcia-Herranz, rapporteuse
Prof. H.-M. Prasser, rapporteur

To Felix

Acknowledgements

First and foremost, I would like to express my sincere gratitude to my thesis director Prof. Andreas Pautz for giving me the opportunity to perform a doctoral research in this field, and for all the valuable suggestions during my work.

Special thanks belongs to my advisor and thesis co-director Dr. Winfried Zwermann (Gesellschaft für Anlagen- und Reaktorsicherheit (GRS) gGmbH). His continuous support, guidance, and the valuable discussions on reactor physics and uncertainty and sensitivity analysis were essential for the success of my thesis.

I would like to acknowledge the members of my thesis committee, Prof. Nuria García-Herranz, Dr. Sören Kliem, and Prof. Horst-Michael Prasser. Their time devoted to evaluating my thesis and their valuable comments are highly appreciated.

I want to thank my colleagues at GRS for their support and for providing a great work environment. Special thanks goes to Dr. Kiril Velkov and to Dr. Robert Kilger for providing support throughout my thesis. My sincere appreciation goes to Dr. Friederike Bostelmann for all the discussions, the benefit from her expertise, and for her friendship. I would like to thank Dr. Matías Zilly for showing me how to use KMACS, Dr. Matthias Küntzel for showing me how to hack KMACS and for patiently answering all my programming-related questions. I have greatly benefited from discussions with Dr. Nadine Berner about statistics related to uncertainty analysis. Special thanks goes to Dr. Vera Koppers, Daniel von der Cron, Philipp Schöffel, Dr. Fabian Weyermann, and Josef Scheuer for their help regarding the application of ATHLET. For nodal diffusion calculations and group constants generation, the discussions with Dr. Yann Périn and Jérémy Bousquet were very helpful.

Special thanks goes to Dr. Yurii Bilodid (Helmholtz-Zentrum Dresden-Rossendorf) for help with questions about DYN3D, and Dr. Petra Malá (Paul Scherrer Institute) and Dr. Mathieu Hursin (École polytechnique fédérale de Lausanne) for their support and interest in my work.

Finally, I would like to thank my wife Kerstin for her support and great patience throughout the time I spent working on my thesis.

München, November 28, 2020

A. A.

Abstract

Understanding the time-dependent behaviour of a nuclear reactor following an intended or unintended change of the reactor conditions is of crucial importance to the safe operation of nuclear reactors. Safety evaluations of nuclear reactors involve the analysis of normal and abnormal reactor operation states with adequate and validated simulation tools.

There is a growing interest in supplementing the results of best-estimate reactor calculations with uncertainties. A major source of uncertainty in reactor calculations is the nuclear data. The propagation of uncertainties allows to study their impact on response values of reactor calculations and to establish safety margins in nuclear reactor safety evaluations.

For the simulation of reactor transients, the two-step approach consisting of the generation of group constants in infinite lattice geometry and the full-core calculation using a neutron-kinetic/thermal-hydraulic code system has been state-of-the-art. Nowadays, Monte Carlo codes allow for the determination of group constants based on a three-dimensional full-core model. Thus, effects from neighbouring fuel assemblies can be considered.

In this thesis, the applicability of the neutron-kinetic code DYN3D coupled with the thermal-hydraulic system code ATHLET for the simulation of transients in small reactor cores was assessed. Experimental reactivity accident tests carried out at the SPERT III research reactor were simulated. Appropriate group constants were generated with the Monte Carlo code Serpent. The overall good agreement between the calculated and the experimental results prove the applicability of the applied codes for the analysis of such reactor transients.

Nuclear data uncertainties were propagated through the simulations of two control rod withdrawal transients in a mini-core model of a pressurised water reactor. The random sampling-based method XSUSA in combination with the SCALE code package was used to determine varied two-group constants. Based on these two-group constants, 1,000 DYN3D-ATHLET calculations were performed and statistically analysed to obtain uncertainty information for the reactor power and the reactivity. Since the assumption of normality could not be maintained for the reactor power, distribution-

Abstract

free Wilks tolerance limits were applied. By sensitivity analyses, the number of delayed neutrons per fission of U-235 and the scattering cross sections of U-238 were identified as the major contributors to the reactor power uncertainty.

For a potential improvement of transient simulations, an approach was developed that was comprised of the determination of group constants using a Serpent full-core model at selected times during a transient simulation and the updating of the original infinite lattice group constants with these full-core group constants. Various challenges and possible solutions were identified. The applicability of the group constants obtained by a full-core model was assessed by their application in full-core diffusion calculations.

Keywords: SPERT III, transient analysis, uncertainty analysis, sensitivity analysis, Wilks tolerance limit, Serpent, DYN3D, ATHLET, XSUSA

Zusammenfassung

Für den sicheren Betrieb von Kernreaktoren ist das Verständnis des zeitabhängigen Verhaltens eines Kernreaktors nach einer beabsichtigten oder unbeabsichtigten Änderung des Reaktorzustands von entscheidender Bedeutung. Sicherheitsbewertungen von Kernreaktoren umfassen die Analyse normaler und anormaler Reaktorbetriebszustände mittels geeigneter und validierter Simulationswerkzeuge.

Es besteht ein wachsendes Interesse daran, die Ergebnisse realistischer Reaktorberechnungen mit Unsicherheiten zu ergänzen. Eine der wesentlichsten Ursachen für Unsicherheiten in Reaktorberechnungen bilden die nuklearen Daten. Die Berücksichtigung von Unsicherheiten ermöglicht es, deren Auswirkungen auf die Ergebnisse von Reaktorberechnungen zu untersuchen und Sicherheitsmargen in Sicherheitsbewertungen von Kernreaktoren festzulegen.

Für die Simulation von Reaktortransienten ist der zweistufige Ansatz Stand der Technik, bestehend aus der Erzeugung von Gruppenkonstanten in unendlicher Gittergeometrie und der Ganzkernberechnung unter Verwendung eines neutronenkinetischen/thermohydraulischen Codesystems. Heutzutage ermöglichen Monte-Carlo-Codes die Ermittlung von Gruppenkonstanten basierend auf einem dreidimensionalen Ganzkernmodell. Dadurch können Effekte von benachbarten Brennelementen berücksichtigt werden.

In dieser Arbeit wurde die Eignung des neutronenkinetischen Codes DYN3D gekoppelt mit dem thermohydraulischen Systemcode ATHLET für die Simulation von Transienten in kleinen Reaktorkernen untersucht. Es wurden experimentelle Reaktivitätsstörfallversuche simuliert, die am Forschungsreaktor SPERT III durchgeführt wurden. Entsprechende Gruppenkonstanten wurden mit dem Monte-Carlo-Code Serpent generiert. Die insgesamt gute Übereinstimmung zwischen den berechneten und experimentellen Ergebnissen belegt die Eignung der verwendeten Codes für die Analyse solcher Reaktortransienten.

Unsicherheiten nuklearer Daten wurden in Simulationen zweier Steuerstabverfahrentransienten in einem Minikernmodell eines Druckwasserreaktors berücksichtigt. Das Stichprobenverfahren mittels XSUSA in Kombination mit dem SCALE Programmpaket wurde angewendet, um variierte Zwei-Gruppenkonstanten zu ermitteln. Basie-

Zusammenfassung

rend auf den variierten Zwei-Gruppenkonstanten, wurden 1.000 DYN3D-ATHLET Simulationen durchgeführt und statistisch analysiert, um die Unsicherheiten der Reaktorleistung und der Reaktivität zu ermitteln. Da die Annahme der Normalität für die Reaktorleistung nicht aufrechterhalten werden konnte, wurden verteilungsfreie Wilks-Toleranzlimits angewendet. Durch Sensitivitätsanalysen wurden die Streuquerschnitte von U-238 und die Anzahl verzögerter Neutronen bei Spaltung von U-235 als die Hauptbeiträge zur Unsicherheit der Reaktorleistung ermittelt.

Für eine mögliche Verbesserung der Simulation von Transienten wurde ein Ansatz entwickelt, der aus der Ermittlung von Gruppenkonstanten mittels eines Serpent Ganzkernmodells an ausgewählten Zeitpunkten während der Simulation einer Transiente und aus der Aktualisierung der ursprünglichen Gruppenkonstanten aus der unendlichen Gittergeometrie mit den Gruppenkonstanten aus der Ganzkernrechnung bestand. Verschiedene Herausforderungen und mögliche Lösungswege wurden identifiziert. Die Eignung von Gruppenkonstanten, die mit einem Ganzkernmodell ermittelt wurden, wurde durch deren Anwendung in Ganzkerndiffusionsrechnungen untersucht.

Stichwörter: SPERT III, Transientenanalysen, Unsicherheitsanalysen, Sensitivitätsanalysen, Wilks Toleranzlimit, Serpent, DYN3D, ATHLET, XSUSA

Contents

Acknowledgements	i
Abstracts	iii
List of Figures	xi
List of Tables	xv
1 Introduction	1
1.1 Computational analysis of reactor transients	4
1.2 Nuclear data and their uncertainty	7
1.3 Objectives of this thesis	11
1.4 Thesis outline	12
2 Nuclear data, methods, and computational tools	15
2.1 Nuclear data in neutron transport	15
2.1.1 Evaluated nuclear data libraries	15
2.1.2 Continuous-energy cross section data	18
2.1.3 Groupwise cross section data and spatial homogenisation	19
2.2 Monte Carlo reactor physics code Serpent	21
2.3 TRITON-NEWT of the SCALE code package	24
2.4 Reactor dynamics code DYN3D	25
2.5 Thermal-hydraulic system code ATHLET	26
2.5.1 Coupling of the neutron-kinetic code DYN3D with the thermal-hydraulic system code ATHLET	28
2.6 Core simulator KMACS	31
2.7 Random sampling-based method XSUSA	32
3 Applicability of Serpent/DYN3D-ATHLET for the analysis of SPERT III experiments	35
3.1 SPERT III experiments	36
3.2 Models for steady-state and transient analysis	39

Contents

3.2.1	Serpent full-core models	40
3.2.2	Serpent infinite-lattice models and reflector models for the generation of group constant libraries	44
3.2.3	DYN3D steady-state models and DYN3D-ATHLET models	47
3.3	Results	50
3.3.1	Static nuclear core characteristics under cold-startup conditions	50
3.3.2	Reactivity accident tests	57
3.4	Summary and discussion	67
4	Impact of nuclear data uncertainties in transient analysis	71
4.1	TMI-1 mini-core model and reactor transients	73
4.1.1	TMI-1 mini-core model	73
4.1.2	Reactor transients	73
4.2	Methods and tools	75
4.2.1	Generation of randomly sampled two-group constants with XSUSA and SCALE	76
4.2.2	Transient analyses with DYN3D-ATHLET	78
4.3	Uncertainty analysis	79
4.3.1	Normally distributed data	80
4.3.2	Non-parametric tolerance limits	81
4.4	Sensitivity analysis	84
4.5	Uncertainty and sensitivity analysis results	85
4.5.1	Uncertainty analysis of the critical boron concentration	86
4.5.2	Uncertainty analysis of Transient 1	86
4.5.3	Uncertainty analysis of Transient 2	89
4.5.4	Sensitivity analyses of Transient 1 and Transient 2	91
4.6	Summary and discussion	95
5	Hybrid neutron transport approach for reactor transient analysis	97
5.1	Method description	98
5.2	Technical implementation	103
5.3	TMI-1 mini-core models for steady-state and transient analysis	105
5.3.1	Generation of group constants with Serpent models	105
5.3.2	DYN3D steady-state model and DYN3D-ATHLET model	108
5.4	Results	108
5.4.1	Comparison between full-core group constants and infinite-lattice group constants	109
5.4.2	Performance assessment of group constants from the full-core model and the infinite-lattice models	112

5.4.3	Modelling of partially controlled nodes in the nodal diffusion model with group constants from Serpent full-core calculations	116
5.4.4	Linear Extrapolaton of full-core group constants	117
5.5	Summary and discussion	119
6	Summary and recommendations for future research	121
6.1	Thesis summary	121
6.2	Recommendations for future research	125
A	Behaviour of Wilks Tolerance Limits in dependence on the sample size	129
	Bibliography	133
	Thesis-related publications	143
	Curriculum Vitae	145

List of Figures

1.1	Conventional two-step approach for full-core reactor calculations. . .	6
1.2	Microscopic fission cross section of ^{235}U ; data based on the ENDF/B-VII.1 nuclear data library at 293 K.	8
1.3	Total neutron multiplicity of both ^{233}U and ^{235}U as a function of the neutron energy; data based on the ENDF/B-VII.1 nuclear data library. .	9
1.4	Covariance matrix of the ^{235}U fission cross section in a 44-group structure.	10
1.5	Standard deviations for the ^{235}U total neutron multiplicity (nubar), the ^{235}U fission cross section, and the ^{238}U capture cross section in a 44-group structure.	11
2.1	^{241}Am (n, γ) cross section from ENDF/B-VIII.0 and various experimental data sets from the EXFOR library.	16
2.2	Pointwise ^{238}U (n, γ) cross section, reconstructed and Doppler broadened (300 K, 1200 K) with NJOY from the corresponding ENDF file of the JEFF-3.2 NDL.	18
2.3	^{238}U (n, γ) cross section based on ENDF/B-VII.1 in CE representation and 252-group representation for a temperature of 293 K.	20
2.4	Scheme for coupled time-dependent neutron-kinetic and thermal-hydraulic calculations for the analysis of reactor transients.	30
3.1	Drawing of the SPERT III reactor vessel.	37
3.2	Cutaway views of a control rod group and of the flux suppressors. . . .	39
3.3	Vertical view of the Serpent reference model of the SPERT III E-core. . .	40
3.4	Horizontal view of the Serpent reference model of the SPERT III E-core.	41
3.5	Infinite-lattice models used for the generation of two-group constants libraries with Serpent.	45
3.6	Reflector models used for the generation of two-group constants libraries with Serpent.	46
3.7	Relative differences of assembly powers between DYN3D - Serpent reference model, DYN3D - Serpent simplified model, of SPERT III E-core under cold-startup conditions and all rods out state.	53

List of Figures

3.8	Normalised axial power distribution of SPERT III E-core under cold-startup conditions and all rods out state.	54
3.9	Calculated integral reactivity worth of the control rod bank.	56
3.10	Calculated absolute integral reactivity worth of the transient rod. . . .	57
3.11	DYN3D-ATHLET results of <i>Test 43</i> under cold-startup conditions. . . .	59
3.12	Reactor period calculated from reactor power and determination of the stable reactor period of <i>Test 43</i>	60
3.13	DYN3D-ATHLET results of <i>Test 18</i> under cold-startup conditions. . . .	61
3.14	Determination of the stable reactor period of <i>Test 18</i>	61
3.15	DYN3D-ATHLET results of <i>Test 48</i> under cold-startup conditions. . . .	62
3.16	Determination of the stable reactor period of <i>Test 48</i>	62
3.17	DYN3D-ATHLET results of <i>Test 49</i> under cold-startup conditions. . . .	63
3.18	Determination of the stable reactor period of <i>Test 49</i>	64
3.19	DYN3D-ATHLET results of <i>Test 81</i> under hot-standby conditions. . . .	65
3.20	DYN3D-ATHLET results of <i>Test 79</i> under hot-standby conditions. . . .	65
3.21	DYN3D-ATHLET results of <i>Test 82</i> under hot-standby conditions. . . .	66
3.22	Reactor period calculated from reactor power over time of <i>Test 82</i>	67
4.1	Layout of the TMI-1 mini-core model.	74
4.2	Control rod position as a function of time for the studied transients. . .	75
4.3	Generation of varied two-group constants sets using XSUSA and TRITON/NEWT.	77
4.4	Performance of N NK/TH calculations with varied two-group constants libraries, followed by UQ/SA analysis of N resulting data sets.	79
4.5	Conservativity profiles of the one-sided, upper Wilks Tolerance Limit of coverage probability $\beta = 0.95$ and statistical confidence level $\gamma = 0.95$ for varying sample sizes N	83
4.6	Distribution of the critical boron concentration at the initial state of <i>Transient 1</i> and the estimated normal distribution.	86
4.7	Nominal reactivity and sample mean reactivity with 2σ -confidence interval for <i>Transient 1</i>	87
4.8	Nominal power, and mean, median, 2σ -confidence interval and the one-sided (95%,95%) WTL and the two-sided (95%,95%) WTL of the power output sample for <i>Transient 1</i>	87
4.9	Distributions of the power output sample of <i>Transient 1</i> at $t_1 = 12.005$ s and $t_2 = 20.005$ s.	88
4.10	Development of the control rod position and the Anderson-Darling test statistics of both the power output sample and the reactivity output sample, all of <i>Transient 1</i>	89

4.11	Nominal reactivity and sample mean reactivity with 2σ -uncertainty interval for <i>Transient 2</i>	90
4.12	Nominal power, and mean, median and one-sided, upper (95 %,95 %) WTL of the power output sample for <i>Transient 2</i>	91
4.13	<i>Transient 2</i> : Power curves of the entire sample; mean, median and one-sided, upper (95 %,95 %) WTL of the power output sample.	92
4.14	R^2 coefficients with confidence intervals and significance bounds of the major contributors to the power uncertainty for <i>Transient 1</i>	92
4.15	R^2 coefficients with confidence intervals and significance bounds of the major contributors to the power uncertainty for <i>Transient 2</i>	93
4.16	Estimated total R^2 coefficients for the power uncertainty of both <i>Transient 1</i> and <i>Transient 2</i> if ^{235}U and ^{238}U are considered.	94
5.1	Scheme for the hybrid approach with coupled time-dependent neutron-kinetic and thermal-hydraulic calculations in combination with Monte Carlo full-core calculations.	99
5.2	Linear extrapolation scheme to parameterise group constants from the Serpent full-core calculation with respect to thermal-hydraulic parameters.	100
5.3	Scheme for the assignment of uncontrolled and controlled group constants obtained by an original Monte Carlo full-core calculation and an additional Monte Carlo full-core calculation to model partially controlled nodes in the neutron-kinetic model.	102
5.4	Radial view of the Serpent full-core model of the TMI-1 mini-core. . . .	106
5.5	Layout of the UO_2 fuel assembly, left: uncontrolled, right: controlled. .	107
5.6	Radial reflector model.	108
5.7	Regions in the Serpent full-core model for which group constants are compared with those obtained by infinite-lattice models.	109
5.8	Relative difference between full-core group constants and infinite-lattice group constants of UO_2 nodes as generated with Serpent.	110
5.9	Relative difference between full-core group constants and infinite-lattice group constants of reflector nodes as generated with Serpent.	111
5.10	Relative difference of the radial core power distribution between DYN3D with infinite-lattice group constants, ADFs, and diffusion coefficient from TRC method, and Serpent reference calculation.	114
5.11	Relative difference of the radial core power distribution between DYN3D with full-core group constants, ADFs, and diffusion coefficient from TRC method, and Serpent reference calculation.	115
5.12	Calculated multiplication factor as a function of control rod insertion. .	117
5.13	Reactor power over time.	118

List of Figures

5.14	Linearly extrapolated fission and absorption cross sections based on Serpent full-core calculations, and fission and absorption cross sections obtained by infinite-lattice calculations.	119
A.1	One-sided, upper (95 %,95 %) WTLs for samples with a sample size of 59 and for a sample with a sample size of 1,000.	130
A.2	One-sided, upper (95 %,95 %) WTLs for samples with a sample size of 200 and for a sample with a sample size of 1,000.	130
A.3	One-sided, upper (95 %,95 %) WTLs for samples with a sample size of 500 and for a sample with a sample size of 1,000.	131

List of Tables

1.1	Delayed neutron parameters given in the six time-group representation for ^{233}U and ^{235}U for thermal neutron-induced fission.	10
3.1	Initial reactor conditions under which reactivity accident tests were performed.	38
3.2	Standard deviations of the reactivity accident test results at different system temperatures and initial power levels.	39
3.3	Selected dimensions used in the Serpent full-core models as well as in the Serpent infinite-lattice and reflector models.	43
3.4	Thermal-hydraulic parameter ranges of the two-group constants libraries for the cold-startup tests and the hot-standby tests.	46
3.5	Calculated initial positions of both the control rod bank and the transient rod for the simulations of the reactivity accident tests with DYN3D-ATHLET.	50
3.6	Critical position of the control rod bank.	51
3.7	Effective point kinetic parameters.	51
3.8	Serpent results of the effective delayed neutron fractions β_i , decay constants λ_i , and lifetimes τ_i , in the six-time group representation at cold-startup conditions.	52
3.9	Calculated and measured absolute excess reactivity and transient rod worth under cold-startup conditions.	55
3.10	Calculated and measured reactivity accident test results for cold-startup and hot-standby conditions.	69
4.1	Thermal-hydraulic parameters used for the parameterisation of the group constants.	78
5.1	DYN3D calculations with infinite-lattice group constants or full-core group constants compared to the Serpent reference result.	113

1 Introduction

Nuclear power plants are usually operated in steady state since they serve as base load units. However, revision and refueling procedures require shutdown and restart. Moreover, due to an increasing proportion of renewable energy sources with their fluctuating availability, the operational mode of nuclear power plants has moved towards load following operation. To set a nuclear power plant into full-load, no-load or partial-load operation, the control rod positions and possibly also the boron concentration are changed to add either positive or negative reactivity to the reactor core. In this way, the neutron population is adjusted eventually leading to the desired thermal power of the reactor core.

The understanding of the reactor dynamic behaviour following an intended or unintended change of the reactor conditions is of crucial importance to safe reactor operation. Therefore, safety evaluations of nuclear power plants comprise the analyses of normal and abnormal reactor operation states. Various accident scenarios need to be considered. Among the most relevant accident scenarios are, for example, loss of coolant accidents due to a rupture of a primary coolant pipe, loss of flow accidents due to a failure of one or more main cooling pumps, and reactivity initiated accidents (RIA). Typical RIA events are the unintended withdrawal or ejection of one or more control rods, boron dilution transients, and cool-down transients for reactor cores with a strongly negative moderator temperature coefficient.

Several neutrons are emitted in a nuclear fission reaction. While most of these neutrons appear promptly, that is within 10^{-14} s, a fraction of less than 1% of these neutrons is emitted upon the decay of radioactive fission products with a delay of a few seconds (Duderstadt and Hamilton, 1976). In a nuclear reactor with a thermal neutron spectrum, the neutrons undergo a series of scattering reactions and then some of

them are absorbed in radiative capture reactions, some of them leak out from the reactor, and some of them cause further fission reactions. A sustained fission chain reaction is achieved when, on average, one neutron survives and causes another fission reaction. This reactor state is referred to as critical. The critical state is not reached by the prompt neutrons alone and relies on the small fraction of the delayed neutrons. Since the emission time of the delayed neutrons is in the range of a few seconds, control measures can be applied to adjust the neutron population in the reactor core. However, the prompt neutron level reacts rapidly to a change of the reactor conditions. If in an accident scenario the reactor becomes supercritical on the prompt neutrons alone due to a change of the reactor conditions, a runaway increase of the neutron population and thus the fission power can only be prevented by intrinsic negative feedback effects (Stacey, 2007). In a light water reactor (LWR), the negative reactivity feedback results mainly from the Doppler broadening of the capture cross section resonances due to a fuel temperature increase and from a decrease of the moderator density leading to a reduction of the neutron moderation. However, in case the reactor has a high boron concentration, the reduction of the moderator density may cause a net positive reactivity insertion.

Due to the strong interaction between the neutron physics and the thermal-hydraulics, it is necessary to simulate both in coupled multi-physics simulations to accurately predict the behaviour of the reactor core or even the whole plant in normal and abnormal operation states. For the last decades, such multi-physics simulations were performed with a neutron-kinetic code that solves the neutron diffusion equation in a few-group energy representation on a coarse spatial mesh. The thermal-hydraulics was calculated with a thermal-hydraulic system code or a simplified thermal-hydraulic model implemented in the neutron-kinetic code. Despite these approximations, this conventional method yields results that are in good agreement with measured data, such as the core power distribution and the critical boron concentration. It became a well-established method in design and safety calculations of nuclear reactors. The nodal diffusion method, however, relies on energy-collapsed and spatially-homogenised cross sections that need to be generated with a lattice physics code.

Meanwhile, simulation codes based on high-fidelity methods have been developed and applied to full-core problems. Deterministic neutron transport codes simulate the neutron transport with a high resolution in terms of energy and space but still rely on multigroup (MG) cross section data and on approximations in the geometry modelling. However, stochastic neutron transport codes based on the Monte Carlo method use highly resolved cross section data in the continuous-energy (CE) representation and they can use models of arbitrarily complex geometry. Moreover, the Monte Carlo neutron transport code Serpent (Leppänen et al., 2015) provides the functionality

to generate group constants for the application in neutron diffusion codes. Group constants can be determined for a single fuel assembly model with reflective boundary conditions (infinite lattice) or for a region in a larger model where the actual three-dimensional neutron flux distribution is taken into account, i.e. the effect of the neighbouring assemblies and the neutron leakage is considered. The calculation of the full-core model with Serpent with the same nuclear data serves then as a reference, and the result can be compared to the nodal diffusion result.

In recent years, Monte Carlo codes became even capable of simulating time-dependent neutron transport including delayed neutron emission (Leppänen, 2013; Sjenitzer, 2013). Thermal-hydraulic calculations are performed on a fuel pin level or even computational fluid dynamic (CFD) calculations are carried out. However, the application of such high-fidelity methods for solving both the neutron-kinetics and the thermal-hydraulics often requires extensive computational resources and is therefore mostly limited to selected research projects that have access to such resources.

There has been a growing interest in supplementing the results of best-estimate reactor calculations, i.e. reactor calculations yielding the most realistic result, with uncertainties to enhance the meaningfulness of these results. The international benchmark activity *Benchmarks for Uncertainty Analysis in Modelling (UAM) for the Design, Operation and Safety Analysis of LWRs (LWR-UAM)* (Ivanov et al., 2016) launched by the Nuclear Energy Agency (NEA) of the Organisation for Economic Co-operation and Development (OECD) in the year 2005 promoted the development and application of uncertainty and sensitivity analysis methods for the individual steps of a typical LWR calculation sequence, starting with pin-cell calculations and ending with time-dependent coupled multi-physics calculations. The nuclear data were thereby identified as one major source of input uncertainty. While the impact of the nuclear data uncertainties on the output quantities of static pin-cell, fuel assembly, and steady-state reactor core calculations has been widely studied so far, there is only a limited experience with uncertainty and sensitivity analyses of reactor transient simulations.

In this thesis, RIA tests performed at the SPERT III E-core research reactor (Heffner and Wilson, 1961) are analysed to demonstrate the applicability of the conventional two-step approach—group constant generation and coupled neutron-kinetic/thermal-hydraulic (NK/TH) calculation using a nodal diffusion code and a thermal-hydraulic system code—for reactor transients in small reactor cores. Afterwards, the impact of nuclear data uncertainties on the outcome of coupled NK/TH simulations of two control rod withdrawal transients in a pressurised water reactor (PWR) mini-core is studied. Finally, the approach of generating group constants with a three-dimensional

Monte Carlo full-core model and their subsequent application in a nodal diffusion model is studied. In contrast to infinite-lattice group constants, the group constants from a full-core model are spatially homogenised and energy collapsed with the actual neutron flux distribution that incorporates the surrounding assemblies and the neutron leakage. In a next step, group constants are generated with a Monte Carlo full-core model at selected times during a reactor transient simulation performed with a NK/TH code system. An approach is explored whether these group constants can be used to update the infinite-lattice group constants that were originally used by the NK/TH code system for the transient simulation.

The following section provides an overview of the current methods applied for the computational analysis of reactor transients. Afterwards, the nuclear data and their uncertainties are briefly described to provide background information for the uncertainty and sensitivity analysis with respect to nuclear data uncertainties.

1.1 Computational analysis of reactor transients

The accurate prediction of the reactor dynamic behaviour in case of a reactor transient event requires coupled neutron-kinetic and thermal-hydraulic calculations. For this purpose various coupling schemes have been established over the last decades. A review is given by Wang et al. (2020). Often the individual codes already existed and were then coupled in a loosely manner. This means that each code applies its own solver and data are exchanged through an interface. Either the time step integrated result of one code forms the input for the time step integration of the other code (operator splitting method) or, at every time step, both codes first iterate a converged solution before the next time step is integrated (Picard iteration). In contrast, a tight coupling scheme is, for example, the Jacobian-free Newton-Krylov method as is implemented in the MOOSE framework (Gaston et al., 2009). All solution variables of the multi-physics problem are solved simultaneously via the formation of a large algebraic system.

A simple method to compute the change of the neutron flux level due to a positive or negative reactivity insertion is the point kinetic (PK) method. It is based on a factorisation of the neutron flux into a time-dependent amplitude function and a space- and energy-dependent, but time-independent shape function. Therefore, its applicability is limited to transients in small reactors and to transients in large reactors if the transient is caused by a uniform perturbation of the reactor conditions. It fails in case of localised perturbations, for example, if a control rod withdrawal occurs at an asymmetrical position in the reactor core (Stacey, 2007). The PK method is often one

1.1. Computational analysis of reactor transients

of the possible options in thermal-hydraulic system codes such as ATHLET (Lerchl et al., 2016b) to predict the neutron flux change. More accurate variants of the PK method exist that are outside of the scope of the present work. For an overview, it is referred to Betzler (2014).

Due to the limited applicability of the PK method, coupled calculations with a three-dimensional neutron-kinetic code and a thermal-hydraulic system code have been state-of-the-art for the analysis of reactor transients for many years. The neutron-kinetic code solves the neutron diffusion equation in few energy groups on a coarse spatial mesh; the mesh cells (commonly named *nodes*) often correspond to the size of a fuel assembly. The thermal-hydraulic system code simulates the thermal-hydraulics in the reactor core or even in the primary and secondary loop. Different mapping schemes between the neutron-kinetic core model and the thermal-hydraulic core model are possible: one thermo-fluiddynamic channel covers either one or several fuel assemblies. An example of such a coupled NK/TH code system is QUABOX/CUBBOX-ATHLET consisting of the thermal-hydraulic system code ATHLET and the nodal diffusion code QUABOX/CUBBOX (Langenbuch and Velkov, 2005). Its capability for the simulation of reactor transients has been demonstrated on, for example, a main steam line break transient in a PWR (Langenbuch et al., 2003) and a control rod ejection accident in a PWR (Pasichnyk et al., 2013).

In a preceding step to the coupled calculation, lattice physics calculations are performed for each fuel assembly type to provide the neutron-kinetic code with group constants. Figure 1.1 illustrates this conventional two-step approach consisting of the generation of group constants in a first step and the subsequent full-core calculation in the second step. In the lattice physics calculations, a neutron transport calculation is performed on the fuel assembly model with reflective boundary conditions. The resulting detailed neutron flux distribution is used to calculate the energy-collapsed and spatially-homogenised cross sections (hereinafter referred to as *group constants*). Since the thermal-hydraulic conditions change during a reactor transient and affect the cross sections, group constants are usually determined for many combinations of thermal-hydraulic state points (fuel temperature, moderator density and temperature, boron concentration) that are expected during the transient.

Within this two-step approach, pin power distributions are often determined through superposition of intranodal neutron fluxes with assembly-wise form factors obtained in the lattice physics calculation. Some neutron-kinetic codes are even equipped with a pin-by-pin neutron diffusion solver to calculate the pin power distribution directly. However, this requires the generation of group constants on the pin-cell level and is not pursued in this work.

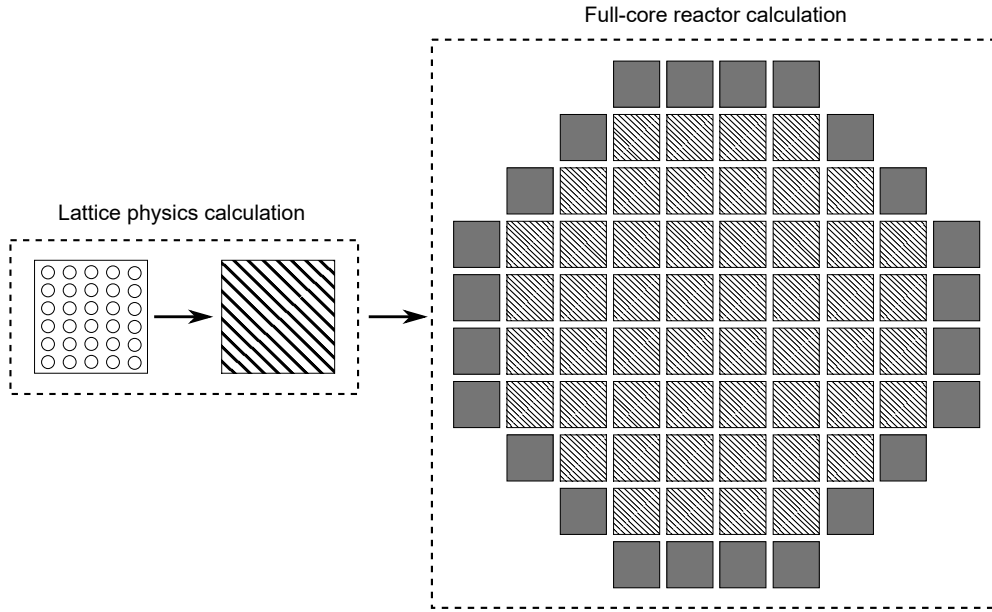


Figure 1.1: Conventional two-step approach for full-core reactor calculations.

Over the last years, there has been an ongoing trend to apply more sophisticated methods in both domains—neutron-kinetics and thermal-hydraulics—to obtain more accurate and highly resolved results.

Deterministic neutron transport codes allow for a finer spatial grid, a finer discretisation of the energy variable, and an explicit treatment of the angular dependence. In contrast, the neutron diffusion equation as the simplest approximation of the neutron transport equation exhibits no angular dependence and is usually solved only for a few energy groups. For these reasons, the application of a transport code is advantageous over a neutron diffusion code if the nuclear system exhibits strong gradients in the neutron flux. For example, the codes DORT-TD (two-dimensional) and TORT-TD (three-dimensional) apply the Discrete Ordinates method to model the neutron transport. Both codes coupled with the thermal-hydraulic system code ATHLET have already been successfully applied for the analysis of reactor transients (Pautz and Birkhofer, 2003; Seubert et al., 2008). Direct whole core neutron transport codes, such as DeCART and MPACT, apply a 2D-1D methodology for the three-dimensional neutron transport. The Method of Characteristics is used for the heterogeneous planar problem and a lower order solver is applied in the axial direction. These codes use MG neutron data libraries; thus the generation of group constants is not required. The simulation of various reactor transients were demonstrated with DeCART (Hursin, 2010) and MPACT (Zhu et al., 2015).

In many studies, thermal-hydraulic sub-channel codes are applied instead of thermal-

hydraulic system codes for the analysis of reactor transients (Knebel et al., 2016; García-Herranz et al., 2017). Thermal-hydraulic sub-channel codes can model the thermal-hydraulics on a pin-by-pin level. For the simulation of a large core, this method remains difficult because of the required computing resources. Therefore, the calculations are often performed with one thermo-fluiddynamic channel per fuel assembly. In case the results from the thermal-hydraulic sub-channel calculation are not relevant for the neutron-kinetic feedback, the calculation can be performed offline based on the results from the NK/TH code system. This allows, for example, the analysis of pin-wise DNB (departure from nucleate boiling) ratios for the fuel assembly experiencing the highest power during a loss of feedwater transient under ATWS (Anticipated Transient without SCRAM) conditions in a PWR (Périn et al., 2011). In other studies, the thermal-hydraulics are modelled with CFD codes in order to predict particular flow phenomena (coolant mixing or recirculation) more accurately as it would be possible with thermal-hydraulic system or sub-channel codes (Grahm et al., 2017; Henry et al., 2018).

Recently, high-fidelity coupled multi-physics calculations on a pin-by-pin level with time-dependent Monte Carlo neutron transport and sub-channel thermal-hydraulics were performed for different RIA events (Ferraro et al., 2020a,b). However, such calculations require extensive computational resources: for example, the simulation of a 1 s long transient required a walltime of 5–10 h on a high performance computing cluster with 1,000 processors.

1.2 Nuclear data and their uncertainty

Nuclear data form the basis for neutron transport calculations. In this context, relevant quantities are, for example, microscopic cross sections, the number of released neutrons per fission reaction, energy and angle distributions, decay constants. The nuclear data—determined from measurements and evaluations—are typically provided in evaluated nuclear data libraries (see Section 2.1). Over the last years, the amount of uncertainty data accompanying the nominal data in the evaluated nuclear data libraries became more comprehensive. In the following, the relevant nuclear data and their uncertainties are briefly described.

Cross sections

The microscopic cross section¹ $\sigma_i(E)$ is a measure for the probability that a neutron with the energy E undergoes a reaction i with the nucleus of a nuclide. It is dependent

¹The microscopic cross section is commonly expressed in the unit barn (b) with $1 \text{ b} = 10^{-24} \text{ cm}^2$.

on the nuclide, the reaction type, and the neutron energy. As an example, Figure 1.2 shows the microscopic fission cross section of ^{235}U in dependence of the neutron energy along with an indication of the different energy regions (thermal region, resolved resonance region, unresolved resonance region, fast region) that are commonly used to identify the cross section range.

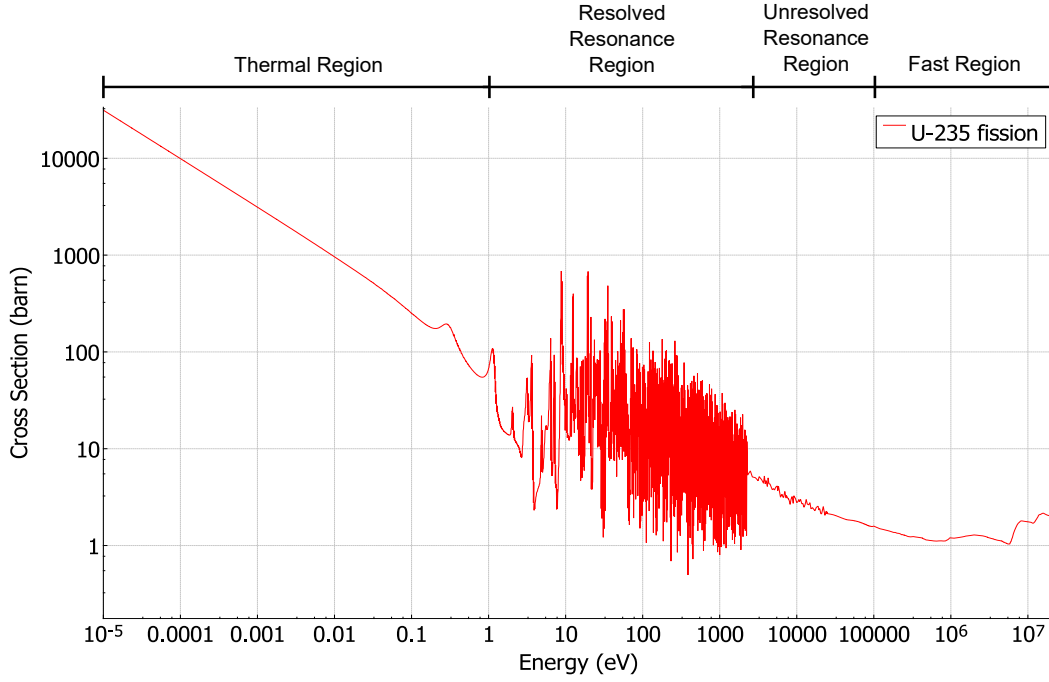


Figure 1.2: Microscopic fission cross section of ^{235}U ; data based on the ENDF/B-VII.1 nuclear data library at 293 K.

It is common practice to define the macroscopic cross section $\Sigma_i(E)$ as the product of the nuclide number density N (nuclides per unit volume with the unit cm^{-3}) and the microscopic cross section $\sigma_i(E)$:

$$\Sigma_i(E) = N \cdot \sigma_i(E). \quad (1.1)$$

The macroscopic cross section² can be interpreted as the probability for a reaction i between a neutron and a nucleus per unit path length travelled by the neutron (Duderstadt and Hamilton, 1976). If a target material was formed by a homogeneous mixture of different nuclide types, the macroscopic cross section would be determined from summation over the different number densities and the corresponding microscopic cross sections of the different nuclides.

²The macroscopic cross section is usually given in the unit cm^{-1} .

Neutron multiplicity

The average number of neutrons (both prompt and delayed) emitted in a fission reaction is given by the total neutron multiplicity $\bar{\nu}$ (also referred to as nubar). It is dependent on the nuclide and the energy of the neutron inducing the fission reaction. As an example, Figure 1.3 shows the total neutron multiplicities of ^{233}U and ^{235}U .

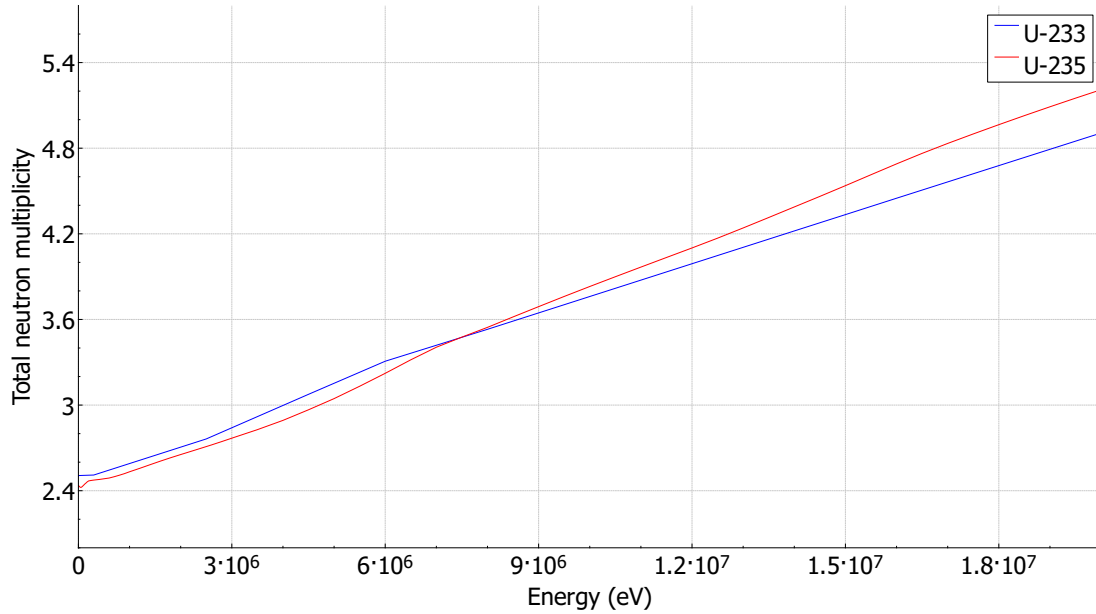


Figure 1.3: Total neutron multiplicity of both ^{233}U and ^{235}U as a function of the neutron energy; data based on the ENDF/B-VII.1 nuclear data library.

The fraction of the delayed neutrons appearing in a fission reaction is given by β . It is defined as $\beta = \bar{\nu}_d / \bar{\nu}$ with $\bar{\nu}_d$ as the average number of delayed neutrons emitted from the decay of radioactive fission products subsequent to a fission reaction. The variety of the different radioactive fission products, commonly referred to as delayed neutron precursors, is often represented by six effective time-groups where each time-group is characterised by a decay constant λ_i and a delayed neutron fraction β_i . The six time-groups are provided for every fissionable nuclide and, often, for different neutron energies. As an example, Table 1.1 lists the parameters of the six time-groups for both ^{233}U and ^{235}U for thermal neutrons inducing the fission reaction.

Nuclear data uncertainties

The nuclear data uncertainties are provided as covariance matrices in the evaluated nuclear data libraries. The covariance entries on the diagonal of such a covariance matrix are the variance—or the standard deviation by taking the square root of the

Chapter 1. Introduction

Table 1.1: Delayed neutron parameters given in the six time-group representation for ^{233}U and ^{235}U for thermal neutron-induced fission (Stacey, 2007).

	^{233}U			^{235}U		
	$\beta = 0.0026$			$\beta = 0.0067$		
Time group	β_i	$\lambda_i [\text{s}^{-1}]$	$T_{1/2} [\text{s}]$	β_i	$\lambda_i [\text{s}^{-1}]$	$T_{1/2} [\text{s}]$
1	$2.24 \cdot 10^{-4}$	$1.26 \cdot 10^{-2}$	55.012	$2.21 \cdot 10^{-4}$	$1.24 \cdot 10^{-2}$	55.899
2	$7.77 \cdot 10^{-4}$	$3.37 \cdot 10^{-2}$	20.568	$1.47 \cdot 10^{-3}$	$3.05 \cdot 10^{-2}$	22.726
3	$6.55 \cdot 10^{-4}$	$1.39 \cdot 10^{-1}$	4.987	$1.31 \cdot 10^{-3}$	$1.11 \cdot 10^{-1}$	6.245
4	$7.23 \cdot 10^{-4}$	$3.25 \cdot 10^{-1}$	2.133	$2.65 \cdot 10^{-3}$	$3.01 \cdot 10^{-1}$	2.303
5	$1.33 \cdot 10^{-4}$	1.13	0.613	$7.71 \cdot 10^{-4}$	1.14	0.608
6	$8.84 \cdot 10^{-5}$	2.5	0.277	$2.81 \cdot 10^{-4}$	3.01	0.23

variance—of the nominal values for the individual energy groups. The off-diagonal entries of a covariance matrix represent the joint variability between the nominal values at different energy groups. As examples, Figure 1.4 shows the covariance matrix of the ^{235}U fission cross section in a 44-group structure, and Figure 1.5 illustrates the standard deviations for the ^{235}U total neutron multiplicity, the ^{235}U fission cross section, and the ^{238}U capture cross section.

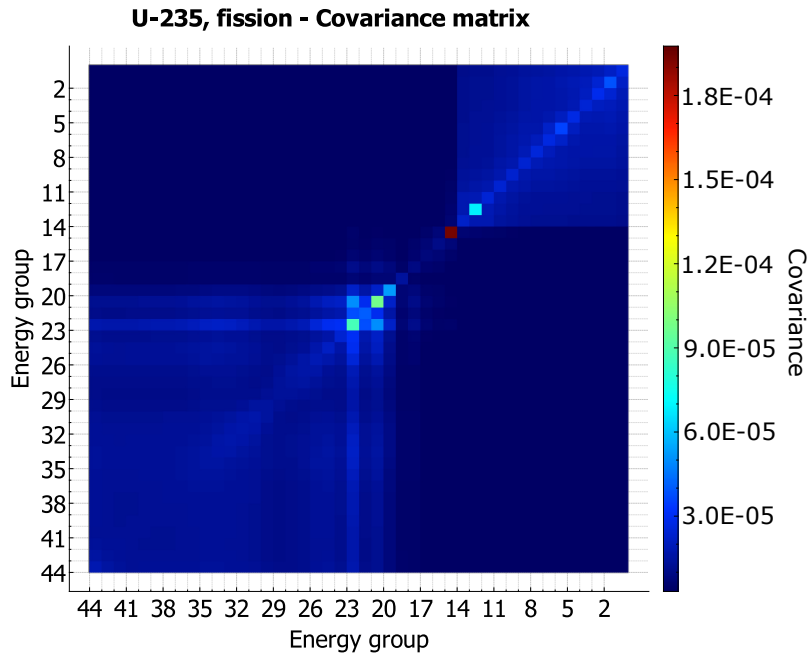


Figure 1.4: Covariance matrix of the ^{235}U fission cross section in a 44-group structure.

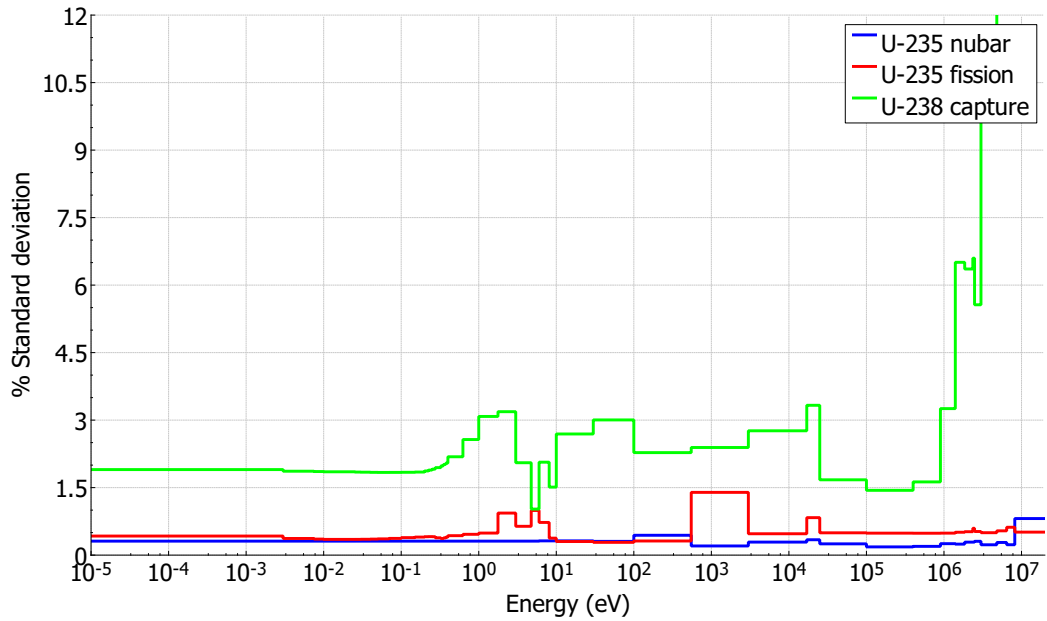


Figure 1.5: Standard deviations for the ^{235}U total neutron multiplicity (nubar), the ^{235}U fission cross section, and the ^{238}U capture cross section in a 44-group structure.

1.3 Objectives of this thesis

The objectives of this thesis are summarised in the following:

- Assess the applicability of the calculation sequence Serpent/DYN3D-ATHLET for the analysis of reactor transients in small reactor cores by coupled NK/TH calculations.
- Propagate nuclear data uncertainties via the random sampling approach through the coupled NK/TH calculations of reactor transients.
- Apply appropriate uncertainty measures to assess the impact of the nuclear data uncertainties on the outcome of the reactor transient simulations.
- Perform sensitivity analyses to determine the major contributors to the calculated reactor power uncertainty in terms of individual nuclide reactions as a function of the transient time.
- Investigate the applicability of group constants determined with a Monte Carlo full-core model for steady-state nodal diffusion calculations.
- Explore a novel approach where group constants determined with a Monte Carlo full-core model at selected times during a reactor transient simulation

using a NK/TH code system can be used to improve the NK/TH calculation, for example, via an update of the infinite-lattice group constants that are originally used by the NK/TH code system.

RIA tests performed at the SPERT III E-core research reactor with reactivity insertions in the range from delayed supercritical to prompt supercritical at two different reactor states are calculated with the calculation sequence Serpent/DYN3D-ATHLET. This sequence follows the conventional two-step approach for full-core reactor calculations. Thus, group constants are generated first with Serpent on the basis of infinite-lattice models of the different fuel assembly types. Afterwards, time-dependent NK/TH calculations are performed with DYN3D-ATHLET. In addition, static nuclear core characteristics (critical control rod positions, reactivity worths of control rods, point kinetic parameters) are determined with both Serpent/DYN3D and Serpent full-core models, and compared with experimental data.

The impact of the nuclear data uncertainties on the outcome of reactor transient calculations is investigated for two control rod withdrawal transients in a PWR mini-core. The transient calculations also follow the two-step approach. By application of the random sampling-based approach XSUSA in combination with the TRITON sequence of the SCALE code package, the nuclear data uncertainties are propagated through the lattice calculations to generate varied two-group constants libraries. With these libraries, the NK/TH calculations are carried out. Appropriate uncertainty measures, in particular non-parametric tolerance limits, are applied for the statistical analysis of the time series of the response values. The nuclide reactions contributing most to the reactor power uncertainty are identified via sensitivity analyses.

The applicability of group constants determined with a three-dimensional Serpent full-core model in subsequent steady-state DYN3D nodal diffusion calculations is assessed. Furthermore, a transient calculation with DYN3D-ATHLET is performed and at selected times during the transient, a Serpent full-core calculation is performed with the actual distribution of the thermal-hydraulic parameters and the current position of the control rod. From these Serpent calculations, group constants are determined for every node and it is investigated whether these group constants can be used to improve the NK/TH calculation.

1.4 Thesis outline

Chapter 2 provides an overview of the nuclear data libraries and the various processing steps of the nuclear data that are necessary for the application in neutron transport

codes. Furthermore, the various simulation codes used for the calculations in this thesis are described.

In Chapter 3, the SPERT III E-core RIA tests are analysed with the calculation sequence Serpent/DYN3D-ATHLET. The generation of the group constants of the different fuel assembly types with Serpent is presented. Calculated static nuclear core characteristics as well as the transient results are compared with experimental data.

Chapter 4 presents the uncertainty analysis of the two control rod withdrawal transients in a PWR mini-core with respect to nuclear data uncertainties. The generation of the varied two-group constants libraries and the execution of the sample NK/TH calculations are outlined. The applied statistical measures, in particular the non-parametric tolerance limits based on the approach of Wilks, are described. Finally, results of the sensitivity analysis with respect to the reactor power uncertainty are given.

In Chapter 5, first group constants are generated on the basis of a three-dimensional Serpent full-core model of a PWR mini-core and subsequently applied in static DYN3D nodal diffusion calculations. The performance of these group constants is assessed by comparison of the multiplication factor and the core power distribution with the Serpent full-core solution. Afterwards, a control rod withdrawal transient is calculated with DYN3D-ATHLET on the basis of infinite-lattice group constants. At selected time steps during the transient, Serpent calculations of the full-core model are performed under consideration of the actual distribution of thermal-hydraulic parameters and the current position of the control rod. From these Serpent full-core calculations, group constants are obtained for the individual nodes of the model. It is investigated whether these full-core group constants can be used to update the infinite-lattice group constants and thus improve the outcome of the transient calculation.

2 Nuclear data, methods, and computational tools

This chapter provides an overview about nuclear data libraries and how the data are processed for the possible application by the different neutron transport codes. Furthermore, the various simulation codes that were applied throughout this thesis are introduced.

2.1 Nuclear data in neutron transport

2.1.1 Evaluated nuclear data libraries

An evaluated nuclear data library (NDL) comprises nuclear reaction data required for the computational analysis of nuclear applications. The most commonly used multipurpose NDLs are the US Evaluated Nuclear Data File (ENDF/B) (Brown et al., 2018), the Japanese Evaluated Nuclear Data Library (JENDL) (Shibata et al., 2011), the TALYS-based Evaluated Nuclear Data Library (TENDL) (Koning et al., 2019), and the Joint Evaluated Fission and Fusion File (JEFF) (Plompen et al., 2020) which is compiled by the collaborating member countries of the NEA Data Bank. The principal focus of these NDLs is to provide neutron cross section data for an energy region of typically 10^{-5} eV to $2 \cdot 10^7$ eV, for some nuclide reactions with an upper limit of $1 \cdot 10^9$ eV (Brown et al., 2018). In addition, the NDLs include sublibraries with data on, for example, radioactive decay, fission yields, and charged particles. At regular intervals, updated revisions of the NDLs are released. Within the scope of this thesis, the ENDF/B libraries ENDF/B-VII.0 (Chadwick et al., 2006) and ENDF/B-VII.1 (Chadwick et al., 2011) were applied. Meanwhile, the ENDF/B-VIII.0 library (Brown et al., 2018) was released.

Chapter 2. Nuclear data, methods, and computational tools

On the basis of theoretical models and experimental nuclear reaction data as provided by, for example, the EXFOR library (Otuka et al., 2014), the nuclear reaction data in the NDLs are produced with nuclear reaction model codes, such as the EMPIRE code (Herman et al., 2007) or the TALYS code system (Koning and Rochman, 2012). Figure 2.1 shows the ^{241}Am (n, γ) CE cross section from the ENDF/B-VIII.0 library along with various experimental data sets provided by the EXFOR library.

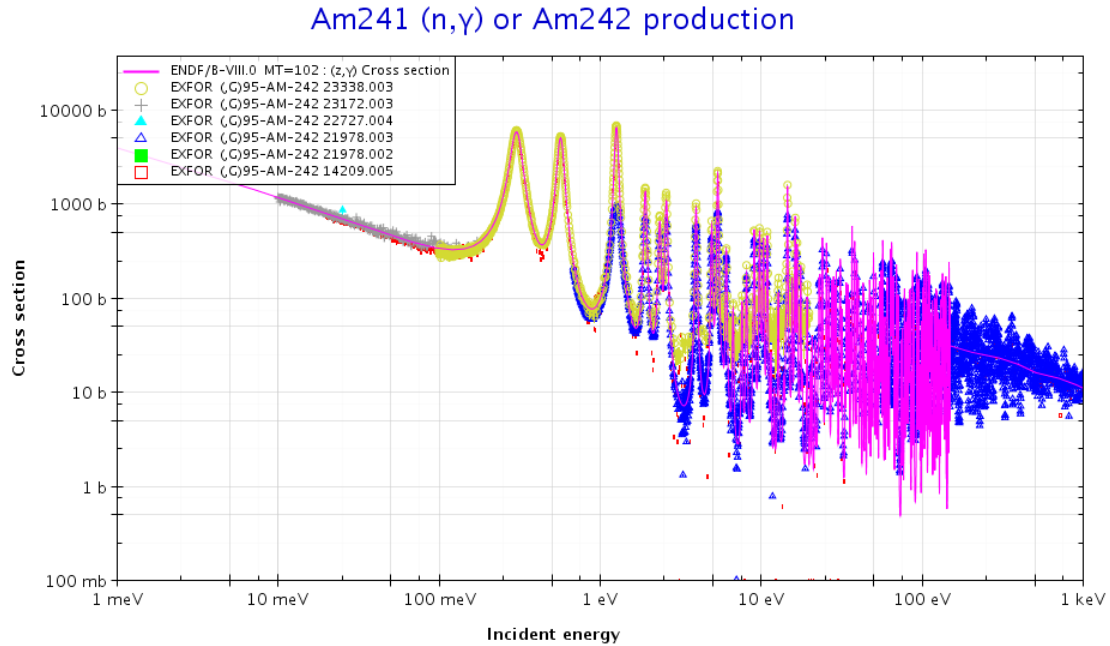


Figure 2.1: ^{241}Am (n, γ) cross section from ENDF/B-VIII.0 and various experimental data sets from the EXFOR library, plotted with the interactive version of JANIS Books from the OECD/NEA (JANIS, 2020).

A NDL provides nuclear data in the Evaluated Nuclear Data File (ENDF) format – a format used across the various NDLs. The latest version is ENDF-6 (CSEWG, 2018). A lot of data is given as tabulated values on a grid together with information on the interpolation law to be used for the calculation of values between the grid points. As an example, cross section values are tabulated over incident neutron energies for particular energy regions. In the case of heavier isotopes, however, it is impractical to provide tabulated cross sections for the resonance energy range. For this reason, a NDL provides resonance parameters and information on the resonance formulas (resolved resonance region) or the statistical models from resonance theory (unresolved resonance region) to be applied for the calculation of the actual cross section values. Angular distributions for scattering reactions are most commonly represented as a Legendre polynomial series, and energy distributions of emitted particles are derived from particular probability distributions (e.g. General Evaporation Spectrum,

Simple Maxwellian Fission Spectrum, Energy-dependent Watt Spectrum etc.). The corresponding input parameters for both are provided. A lot more data than described here is given in the NDLs, such as decay and fission product yields, multiplicities of radioactive products, photon production data, covariance data, but a detailed description is beyond the scope of this thesis. Further information on the data and its representation can be found in MacFarlane (2000); CSEWG, 2018.

In recent years a new format called the Generalized Nuclear Data (GND) structure has been developed for future releases of nuclear data libraries. The ENDF-6 format exhibits a general lack of extensibility and has certain limitations concerning, for example, the numerical precision and the support for correlated particle emission (Mattoon et al., 2012). The latest version of the ENDF/B library, ENDF/B-VIII.0 (Brown et al., 2018), was released in both the legacy ENDF-6 format and the new GND structure.

The NDLs must be processed before they can be used in transport codes. In brief, typical steps of a cross section processing sequence are:

- reconstruction of resonances into a pointwise representation, i.e. cross sections are tabulated on an energy grid for the entire energy region to allow for linear interpolation of values between the grid points to within a specified tolerance,
- Doppler broadening of resonances for specified temperatures,
- computation of probability tables for self-shielding effects of unresolved resonances,
- computation of thermal scattering cross sections,
- computation of heat and gas production cross sections, and
- either the preparation of MG cross sections or the conversion of the cross sections from the pointwise format into a CE format suitable for Monte Carlo neutron transport calculations.

Details on the individual processing steps are found in the documentations of the processing codes, which are, for example, NJOY (MacFarlane and Kahler, 2010), PREPRO (Cullen, 2019), or AMPX of the SCALE 6.2 code package (Wiarda et al., 2016). As an example, Figure 2.2 shows Doppler broadened resonances of the ^{238}U (n, γ) cross section in the pointwise representation for 300 K and 1200 K, respectively.

A major part of the validation of a NDL is carried out by first processing the NDL into CE representation and then performing hundreds of Monte Carlo calculations of

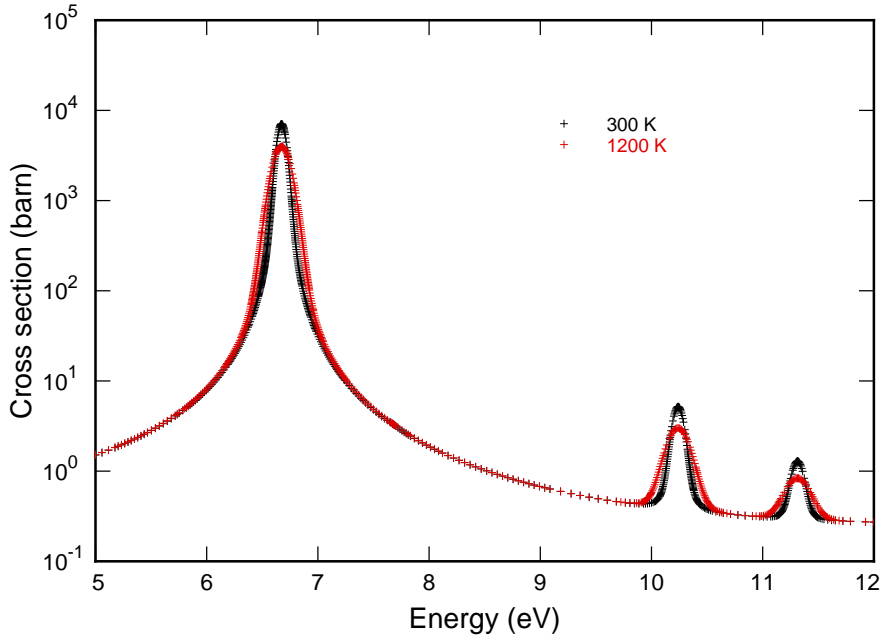


Figure 2.2: Pointwise ^{238}U (n,γ) cross section, reconstructed and Doppler broadened (300 K, 1200 K) with NJOY from the corresponding ENDF file of the JEFF-3.2 NDL.

criticality benchmarks. A resource for such criticality benchmarks is, for example, the International Handbook of Evaluated Criticality Safety Benchmark Experiments (ICS-BEP Handbook) (NEA, 2015). Besides criticality calculations, shielding benchmarks are also analysed and calculated neutron fluxes are compared with measured ones. (Chadwick et al., 2006)

2.1.2 Continuous-energy cross section data

Continuous-energy libraries are commonly used by Monte Carlo codes, such as MCNP (Werner et al., 2018), Serpent 2 (Leppänen et al., 2015), and KENO of the SCALE code package (Rearden and Jessee, 2018). Since Monte Carlo codes do not rely on approximations with respect to the energy dependence, the CE libraries retain all the details on the neutron and photon data given in the NDL (MacFarlane and Kahler, 2010). The CE cross sections for each reaction are tabulated on a dense energy grid so that cross section values between energy grid points can be linearly interpolated by the Monte Carlo code to within a demanded tolerance. Therefore, the energy grid may consist of up to 100,000 energy grid points, especially if a cross section has

resolved resonances. Moreover, the CE data allow the Monte Carlo code to sample the energy and angular distributions for every neutron-nuclide interaction. Because of this detailed representation of the interaction physics, the results of a Monte Carlo neutron transport calculation based on a CE library are commonly considered as a reference. One of the formats for CE libraries is the ACE (A Compact ENDF) format, which is applied when NJOY is used for the preparation of the CE data.

2.1.3 Groupwise cross section data and spatial homogenisation

While the Monte Carlo codes KENO and MCNP can be applied with either CE or MG libraries, deterministic neutron transport codes rely exclusively on MG libraries. A MG library contains microscopic cross section data that are averaged over discrete energy groups. The SCALE 6.2 code package (Rearden and Jessee, 2018), for example, provides MG libraries with 56 energy groups and 252 energy groups, respectively.

The fact that a MG library is produced with a generic weighting function necessitates a correction of the MG cross sections for resonance self-shielding and spectral effects specific to the analysed system. Only then the MG library is suitable for the subsequent neutron transport calculation.

Often, in full-core reactor calculations, heterogeneous regions are replaced by approximately equivalent homogeneous regions. For each heterogeneous region, this requires the spatial homogenisation of the cross sections over all material zones within this region to obtain effective cross sections. This is, for example, the case with the conventional two-step approach of nodal diffusion reactor core calculations that rely on precalculated, spatially-homogenised cross sections for each fuel assembly type (see Section 1.1). In addition, the number of energy groups is often further reduced by collapsing the cross sections into a few-group structure. Nodal diffusion calculations of a LWR core are typically performed with the energy region (10^{-5} eV – $2 \cdot 10^7$ eV) discretised in only two energy groups usually separated at 0.625 eV.

The following sections cover the collapsing of cross sections into a MG structure, the self-shielding treatment of cross sections, and the preparation of few-group cross sections including spatial homogenisation.

Multigroup cross sections

In a MG library, the energy range is discretised into a number of energy groups and the microscopic cross sections are given as averages for each energy group. For an energy group with the index g and the energy boundaries E_g and E_{g-1} , a collapsed

microscopic cross section σ_g is in principle obtained with:

$$\sigma_g = \frac{\int_{E_g}^{E_{g+1}} \sigma(E) \phi(E) dE}{\int_{E_g}^{E_{g+1}} \phi(E) dE}, \quad (2.1)$$

where $\sigma(E)$ is the energy-dependent microscopic cross section and $\phi(E)$ is the energy-dependent neutron flux. The exact neutron flux $\phi(E)$, however, is not known before the actual neutron transport calculation and must therefore be approximated with an energy-dependent weighting function representative for the considered system.

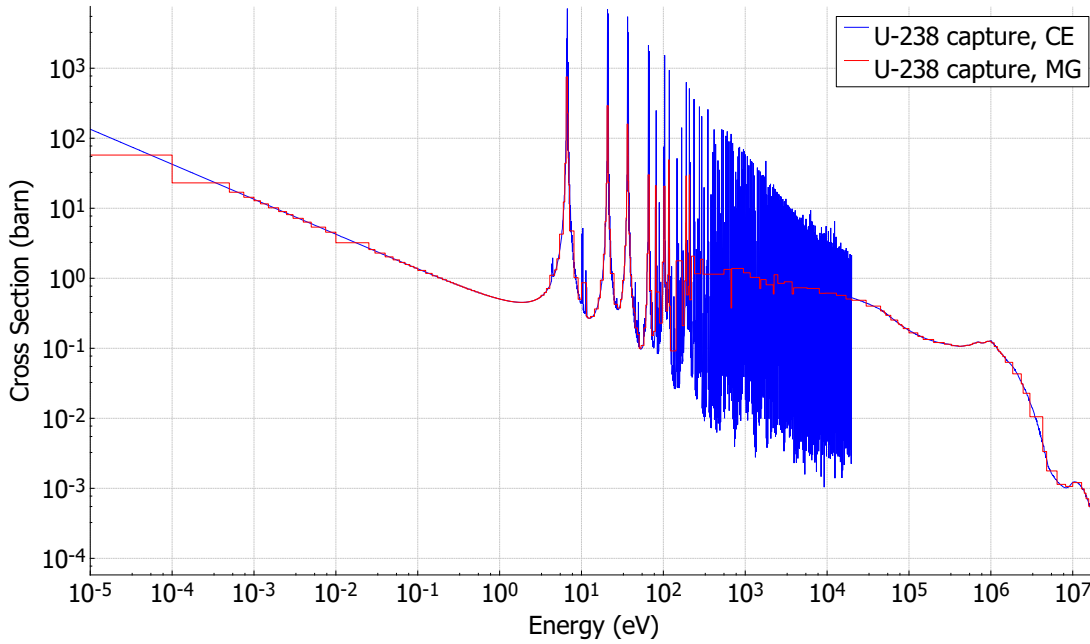


Figure 2.3: ^{238}U (n, γ) cross section based on ENDF/B-VII.1 in CE representation and 252-group representation for a temperature of 293 K.

The energy group structure, i.e. the number of energy groups and their boundaries, are chosen in a way that the resonances in the cross sections of the involved materials are appropriately captured. MG libraries applied for LWR analysis have therefore many energy groups in the resolved resonance region as is, for example, the case for the 56-group and 252-group libraries provided in SCALE 6.2. As an example, Figure 2.3 shows the ^{238}U (n, γ) cross section based on ENDF/B-VII.1 in CE representation and in the 252-group representation, both from SCALE 6.2. In contrast, the libraries used for the analysis of Sodium-cooled Fast Reactors (SFRs) must have a fine energy group structure in the higher energy region because the structural materials exhibit significant resonances there (Bostelmann et al., 2020).

Self-shielding treatment of cross sections

The neutron flux spectrum of the system to be simulated may differ from the generic energy-dependent weighting function used for generating the problem-independent MG library (see Section 2.1.3). The differences may arise, for example, from leakage effects in the fast energy region and from thermal absorption in the thermal energy region (Williams, 2011). In addition, if a nuclide with resonances in the absorption cross section is present in the system, localised depressions occur in the neutron flux spectrum corresponding to these resonances. According to Eq. 2.1, in which the cross sections are weighted with the neutron flux spectrum, these depressions may have a significant impact on the MG cross sections (Pautz, 2002). As a consequence, the problem-independent MG cross sections must be corrected for the resonance self-shielding effects and other spectral effects so that a problem-dependent MG cross section library is available for the subsequent neutron transport calculation of the system under consideration. A concrete example of a possible method for generating a problem-dependent MG library is given in Section 2.3.

Spatially-homogenised and energy-collapsed group constants

Spatially-homogenised and energy-collapsed group constants are determined with neutron transport calculations, often referred to as lattice physics calculations. In such a lattice physics calculation, the macroscopic cross sections are weighted by the neutron fluxes and the volumes of the individual material zones of the heterogeneous model, thus resulting in a preservation of the reaction rates. The formal definition of a spatially-homogenised and energy-collapsed macroscopic cross section Σ_g is given by:

$$\Sigma_g = \frac{\int_{E_g}^{E_{g-1}} \int_V \Sigma(\mathbf{r}, E) \phi(\mathbf{r}, E) dE d^3r}{\int_{E_g}^{E_{g-1}} \int_V \phi(\mathbf{r}, E) dE d^3r}, \quad (2.2)$$

where $\phi(\mathbf{r}, E)$ is the space- and energy-dependent neutron flux and $\Sigma(\mathbf{r}, E)$ is the space- and energy-dependent macroscopic cross section.

2.2 Monte Carlo reactor physics code Serpent

Serpent is a continuous-energy Monte Carlo particle transport code which has been developed at the VTT Technical Research Centre of Finland since 2004 (Leppänen et al., 2015). The current version, Serpent 2, which was used throughout this thesis, features a wide variety of possible applications, for example, criticality and burnup calculations, generation of homogenised group constants, multi-physics calculations

Chapter 2. Nuclear data, methods, and computational tools

by coupling with a thermal-hydraulic code or fuel performance code, and activation calculations with simulation of neutron and photon transport.

Serpent 2 tracks neutrons and photons in two- and three-dimensional geometries. Details on the implemented tracking routines are found in Leppänen (2010). The implemented geometry model (universe-based constructive solid geometry) allows the set up of complicated models using elementary and derived surface types, universes, transformations, and different kinds of lattices. Additionally, CAD (computer-aided design) and unstructured mesh based geometries can be employed. For burnup calculations, Serpent solves the Bateman depletion equations with the CRAM matrix exponential method (Pusa, 2011). Various predictor-corrector methods are available to reduce the discretisation error with respect to the time integration (Leppänen and Isotalo, 2012).

Serpent utilises CE libraries in the ACE format. The libraries provided with Serpent are based on, for example, the ENDF/B-VII.0 library (Chadwick et al., 2006) or the JEFF-3.1.1 library (Santamarina et al., 2009). The temperature dependence of the cross sections can be treated by a Doppler-broadening preprocessor routine (Viitanen, 2009) or on-the-fly using the implemented target motion sampling (TMS) method (Viitanen and Leppänen, 2014).

The multi-physics interface of Serpent 2 allows the coupling with CFD codes, thermal-hydraulic system codes, and fuel performance codes. Different interface formats are available. The choice of a particular interface format depends on the application. In this way, temperatures and densities can be locally adjusted without changing the general input (Leppänen et al., 2015).

Serpent 2 applies the iterated fission probability (IFP) method for the calculation of effective point kinetics parameters: the effective delayed neutron fraction, the effective generation time, and the precursor decay constants. It should be noted that these parameters are always determined for the entire model. (Leppänen et al., 2014, 2016)

Another feature of Serpent 2 is the lattice physics analysis for the generation of energy-collapsed, spatially-homogenised group constants which serve as input for nodal diffusion or other deterministic neutron transport codes. These group constants encompass, for example, few-group cross sections, diffusion coefficients, poison cross sections, inverse velocities, assembly discontinuity factors (ADFs) and pin-power form factors (Leppänen et al., 2016).

In Serpent 2, the group constants generation proceeds in two stages (Leppänen et al.,

2016). Instead of solving Eq. 2.1 directly, the neutron fluxes and the cross sections are first energy-collapsed and volume-averaged into a MG structure. Thereafter, the MG cross sections are collapsed into the few-group structure. The MG neutron flux ϕ_h is defined as:

$$\Phi_h = \int_{E_h}^{E_{h-1}} \int_V \phi(\mathbf{r}, E) dE d^3r \quad (2.3)$$

where $\phi(\mathbf{r}, E)$ is the neutron flux and h is the index of the MG structure. A MG cross section Σ_h is defined as:

$$\Sigma_h = \frac{\int_{E_h}^{E_{h-1}} \int_V \Sigma(\mathbf{r}, E) \phi(\mathbf{r}, E) dE d^3r}{\int_{E_h}^{E_{h-1}} \int_V \phi(\mathbf{r}, E) dE d^3r}, \quad (2.4)$$

where $\Sigma(\mathbf{r}, E)$ is the macroscopic cross section. In the second stage, the collapsing of the MG cross sections into the few-group structure is performed with:

$$\Sigma_g = \frac{\sum_{h \in g} \Sigma_h \Phi_h}{\sum_{h \in g} \Phi_h}. \quad (2.5)$$

This approach offers the possibility to use for Φ_h in Eq. 2.5 either the infinite neutron flux spectrum or the leakage-corrected critical spectrum (B1 approach, (Leppänen et al., 2016; Stamm'ler and Abbate, 1983)) for the collapsing of the cross sections from the MG structure into the few-group structure. Further details on the methodology and implementation can be found in Leppänen et al. (2016).

In terms of calculating group constants, the Monte Carlo method offers some advantages over deterministic lattice physics codes:

- with the application of CE cross sections, resonance self-shielding effects are automatically taken into account,
- group constants can be generated for models with a complex geometry and a high level of detail, and
- a Monte Carlo neutron transport calculation of the full-scale reactor core model with the same CE cross sections results in a reference solution that can be used for comparison with the nodal diffusion calculation of the reactor core.

However, a drawback results from the high computational effort immanent to the Monte Carlo method for obtaining statistically significant results. The generation of a group constant library suitable for reactor cycle analysis involving many fuel assembly

types and different reactor operating conditions entails a substantial computation time.

2.3 TRITON-NEWT of the SCALE code package

SCALE (Rearden and Jessee, 2018) developed by the Oak Ridge National Laboratory is a comprehensive code package applied for criticality calculations, depletion calculations, radiation shielding analysis, and uncertainty and sensitivity analysis. SCALE was used for the lattice physics calculations carried out in Chapter 4.

The TRITON sequence of SCALE allows for neutron transport and depletion calculations for one-, two-, and three-dimensional models. Depending on the type of analysis, TRITON automates all necessary calculations, such as the preparation of problem-dependent, i.e. self-shielded, MG cross section libraries, the neutron transport calculation, and the depletion calculation. Depending on the geometry of the considered model and the type of analysis, the modular approach facilitates the application of different neutron transport codes. In this thesis, TRITON was applied with the two-dimensional neutron transport code NEWT.

The MG cross section libraries provided with SCALE are problem-independent and must therefore be corrected for resonance self-shielding and spectral effects specific to the model under consideration. The self-shielding sequence applied in the present work encompasses the application of the SCALE functional modules BONAMI, CENTRM, and PMC. First, the BONAMI module multiplies precomputed Bondarenko self-shielding factors, also called f-factors, with the problem-independent (unshielded) MG cross sections over the entire energy region to obtain problem-dependent (shielded) MG cross sections. These self-shielding factors are dependent on the energy group, the Doppler broadening temperature, and a so-called background cross section, and they are provided for each nuclide in the SCALE library. In brief, the background cross section represents a cross section of all nuclides in the mixture except the one for which the self-shielding is actually performed. The smaller the background cross section the larger the resonance self-shielding effect. For several values of both the background cross section and the Doppler temperature, the f-factors are predetermined by the AMPX code system (Wiarda et al., 2016) of SCALE. In the self-shielding calculation, the BONAMI module determines background cross sections for every involved nuclide on the basis of the specified unit cell (a single fuel rod surrounded by coolant) and then uses these background cross sections besides the Doppler temperature for the interpolation of the tabulated f-factors.

In a next step, the CENTRM module determines pointwise neutron flux spectra with a

CE neutron transport calculation on the specified unit cell. These pointwise neutron flux spectra are then used by the PMC module to collapse CE cross sections into a MG structure. The collapsed MG cross sections then replace the BONAMI-shielded MG cross sections on the MG library up to an energy of 20 keV (SCALE, 2011). The reason is that the Bondarenko method is less suitable for the resolved resonance region and the thermal region (Williams, 2011).

The discrete ordinates neutron transport code NEWT enables MG neutron transport calculations in complex geometrical models. It allows for lattice physics analysis to generate group constants using either the infinite or a corrected critical neutron flux spectrum. The set of generated group constants encompasses all necessary values for subsequent nodal diffusion calculations, for example, homogenised few-group cross sections, delayed neutron data, fission energy spectra, and ADFs. (SCALE, 2011)

2.4 Reactor dynamics code DYN3D

The reactor dynamics code DYN3D (Rohde et al., 2016) developed at the Helmholtz-Zentrum Dresden-Rossendorf is used for steady-state and transient analysis of PWR, BWR and VVER type reactors. It was originally developed for the analysis of Russian VVER-type reactors and became recommended by the IAEA as a reference code for the analysis of the reactor type VVER-440/V213. Moreover, DYN3D has been further developed for the simulation of Generation IV type reactors, such as sodium-cooled fast reactors, molten salt reactors, and block-type gas-cooled high temperature reactors. The code consists of several neutron-kinetic solvers, a thermal-hydraulic model for the reactor core, and a thermo-mechanical fuel rod model.

The range of neutron-kinetic solvers includes solvers for the neutron diffusion equation in two-group and MG energy representation, respectively, and a solver for a simplified neutron transport equation (SP3 approach) (Rohde et al., 2016). In a transient calculation, the time-integration is performed using an implicit difference scheme (Grundmann et al., 2005). The neutron-kinetic calculation is performed based on group constants that are determined in lattice physics analyses. The group constants are provided in the form of library files to DYN3D and different library types are available: (1) group constants can be given for a reference state and their dependencies on the thermal-hydraulic variables are represented by polynomials, or (2) group constants can be provided explicitly of anticipated thermal-hydraulic conditions. By providing also nodal pin power form factors from the lattice physics calculations, DYN3D can determine a pin-wise power distribution.

During a transient calculation, DYN3D allows for calculating the dynamic reactivity.

The dynamic reactivity is based on the derivation of the point kinetics equations from the weighted integration of the time-dependent neutron diffusion equations. The steady-state adjoint flux¹ is used as the weighting function. In addition, DYN3D calculates the individual contributions to the dynamic reactivity. These contributions arise from the Doppler feedback, the movement of control rods, and changes in the moderator density, moderator temperature, and boron concentration, respectively. (Rohde et al., 2016)

Thermal-hydraulic feedback in steady-state and transient calculations can be taken into account by the application of the internal thermal-hydraulic solver or by coupling with an external thermal-hydraulic code, such as a thermal-hydraulic system code (see Section 2.5), a sub-channel code, and a CFD code. By imposing an external perturbation on the system, for example, the movement of control rods, a change in the mass flow rate or in the boron concentration, the reactor dynamic behaviour under transient conditions can be analysed. (Rohde et al., 2016)

2.5 Thermal-hydraulic system code ATHLET

ATHLET (Analysis of THERmal-hydraulics of LEaks and Transients) (Lerchl et al., 2016b) is a thermal-hydraulic system code developed by the Gesellschaft für Anlagen- und Reaktorsicherheit gGmbH (GRS). It allows the simulation of operational conditions, design basis and beyond design basis events (without core degradation) of LWRs (e.g. PWR, BWR, RBMK, VVER) and Small Modular Reactors. Light water and heavy water can be used as working fluids. Moreover, ATHLET's capability to simulate helium, liquid sodium, lead and lead-bismuth eutectic as working fluids enables the simulation of future Generation IV reactors (GIF, 2002), but these developments are still subject of validation (Austregesilo et al., 2016). The version ATHLET 3.1A was used throughout this thesis. In the following, an overview of ATHLET is provided.

ATHLET consists of various modules for the simulation of the phenomena related to the thermal-hydraulics in a nuclear reactor:

- the Thermo-Fluid dynamics (TFD) module,
- the Heat Conduction and Heat Transfer (HECU) module,
- the Neutron Kinetics (NEUKIN) module, and

¹The adjoint flux can be considered as a “neutron importance function”. If a perturbation, e.g. change of cross section, is introduced at a given point in the reactor, the adjoint function at this point depicts the magnitude of change of the reactivity. Details are found in Duderstadt and Hamilton (1976).

- the General Control Simulation Module (GCSM).

The TFD module provides basic fluiddynamic elements which are called thermo-fluiddynamic objects (TFOs). By connecting TFOs, the thermal-hydraulic system of a nuclear reactor can be set up. Different types of TFOs are available. The differential equations underlying the thermo-fluiddynamic model are based on the general conservation equations of mass, energy, and momentum for the liquid phase and the vapor phase, respectively. The different TFO types can be divided into the following categories: a *pipe object* consists of one or more control volumes and it models the one-dimensional fluid transport. A *branch object* consists of one control volume and allows for modelling of branches, i.e. coupling of several pipe objects. The application of *Cross Connection Objects* or *Single Junction Pipes* allows for the simulation of multi-dimensional flows via cross-coupling of the aforementioned pipe objects. In addition to these basic TFOs exists a number of *special objects* that allow for modelling of the thermal-hydraulic phenomena of a particular reactor component, for example, a valve, a pressuriser or a water-steam separator (Austregesilo et al., 2016; Lerchl et al., 2016b). The application of the thermo-fluiddynamic models yields a system of ordinary differential equations; the time integration is performed implicitly using the FEBE (Forward-Euler, Backward Euler) solver. The implemented error control mechanisms ensure an adequately chosen time step size for the integration of each time step (Austregesilo et al., 2016).

The HECU module enables the simulation of one-dimensional heat conduction in solid structures, such as plates (heat conduction normal to the surface), hollow cylinders, full cylinders, and spheres (heat conduction in radial direction). For this, Heat Conduction Objects (HCOs) are assigned to TFOs. An HCO can comprise three material zones, each of which can be further subdivided into temperature layers. The material properties—mass density, heat conductivity, and heat capacity—are either determined from built-in correlations or from tabulated data input by the user. Additionally, between each pair of adjacent material zones, a gap can be implemented which is defined by a width and a heat transfer coefficient. Heat generation can be enabled within the material zones of a HCO. Thus, HCOs allow for modelling of, for example, heat exchangers, fuel rods, electrical heaters, and spherical fuel elements of a pebble-bed reactor. The temperatures in the layers are implicitly integrated in time. (Austregesilo et al., 2016)

Heat generation from nuclear fission is simulated with the NEUKIN module (Austregesilo et al., 2016). For this task, the NEUKIN module provides different options. One of these options is the solution of the built-in point kinetics equations system to model the time-dependent amplitude of the power generated by nuclear fission. In this case,

adequate point kinetics parameters (delayed neutron fractions, decay constants, and generation time) for the studied nuclear reactor core must be provided by the user. Reactivity feedback from the Doppler effect of the fuel and from changes of the moderator density as well as of the moderator temperature is taken into account from either reactivity coefficients or input tables. These input tables depict the dependency of the reactivity of the reactor core on the thermal-hydraulic conditions. Another option provided by the NEUKIN module is the coupling of a three-dimensional neutron-kinetic code with ATHLET. Details on this option are provided in Section 2.5.1 with the example of the neutron-kinetic code DYN3D coupled with ATHLET.

The GCSM module (Austregesilo et al., 2016) is used to set up control circuits that represent the control systems, auxiliary systems, and protection systems of a nuclear reactor. For this purpose, functional blocks, for example, logical AND, logical OR, signal adder, integrator, differentiator, can be combined to a control circuit. Switches and function generators enable the conversion of continuous signals to boolean signals or vice versa. In this way, system variables of the various ATHLET modules serve as process variables to the control circuits. The output of these control circuits serve then as control signals for hardware actions, such as changing a valve position or the insertion of a control rod. In addition, the GCSM module enables the simulation of nuclear power plant components in a simplified way and the modelling of boundary conditions. The latter is applied, for example, in a so-called “open core” model (Périn, 2016), which is a model of only the reactor core with the inlet and outlet conditions (mass flow and enthalpy) defined through GCSM signals.

The goal of ATHLET is the simulation of the realistic system behaviour. For this reason, ATHLET has been subject to an extensive validation procedure comprising mainly the calculation of separate effect tests, integral system tests, and real plant transients. For details on the validation procedure and the validation tests, it is referred to the validation manual of ATHLET (Lerchl et al., 2016a).

2.5.1 Coupling of the neutron-kinetic code DYN3D with the thermal-hydraulic system code ATHLET

ATHLET’s various code coupling interfaces enable multi-scale and multi-physics simulations. One of these coupling interfaces allows for coupling with a three-dimensional neutron-kinetic code. The plug-in concept of ATHLET requires that the neutron-kinetic code must be given as a plug-in binary to ATHLET. The data transfer between ATHLET and the plug-in binary, in this case the neutron-kinetic code, is realised by providing pointers to exported ATHLET variables. In this way, the ATHLET variables

can be accessed by the plug-in binary (Austregesilo et al., 2016).

Since the interface for the code coupling with a three-dimensional neutron-kinetic code is predefined by ATHLET, the description given in the following applies not only to the coupling with DYN3D but also to the coupling with other neutron-kinetic codes, for example, QUABOX/CUBBOX (Langenbuch and Velkov, 2003) or TORT-TD (Seubert et al., 2008). Minor differences may result from peculiarities specific to the applied neutron-kinetic code.

The currently applied coupling method for DYN3D-ATHLET is the *internal* method. With this method, the thermal-hydraulics of the analysed system is entirely modelled with ATHLET and the neutron-kinetics are modelled with DYN3D (DYN3D's internal thermal-hydraulic solver is not used). In this way, DYN3D uses the thermal-hydraulic results from ATHLET, and ATHLET applies the power distribution computed by DYN3D. For completeness, it should be mentioned that also two other coupling methods were used in the past: the *external* method and the *parallel* method. These methods apply the internal thermal-hydraulic solver of DYN3D in addition to ATHLET. (Périn, 2016; Rohde et al., 2016)

Coupling scheme for time-dependent calculations

For coupled time-dependent calculations, the staggered time synchronisation scheme (Périn, 2016) is applied. Basically, it consists of the following steps that are conducted for every time step (Figure 2.4):

1. DYN3D calculates the power distribution in the reactor core region at time t_i and provides it to ATHLET,
2. ATHLET performs the time-integration with the time step size Δt_i ,
3. the resulting distributions of the thermal-hydraulic variables at $t_i + \Delta t$ are provided to DYN3D,
4. DYN3D performs the time-integration with the time step size Δt_i .

The fact that the neutron-kinetic calculation at time t_i is performed on the basis of the thermal-hydraulic results at time t_{i+1} necessitates the choice of a small time step size Δt to achieve an accurate solution and to avoid numerical instabilities. (Périn, 2016)

The time step size for the integration is determined by each code individually under observance of the respective defined limits. Due to this fact, the situation may arise

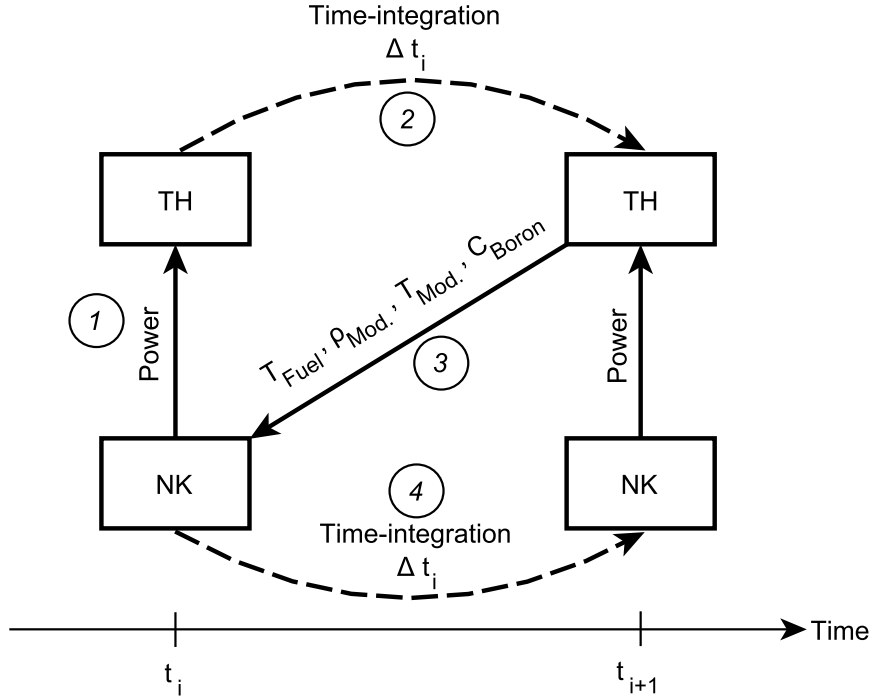


Figure 2.4: Scheme for coupled time-dependent neutron-kinetic (NK) and thermal-hydraulic (TH) calculations for the analysis of reactor transients. *Numbers in circles depict the order of the individual calculation steps for the integration of one time step.*

that the time step integrated by ATHLET is larger than the maximum permissible neutron-kinetic time step. Then, in contrast to the representation in Figure 2.4, multiple neutron-kinetic calculations with the maximum permissible neutron-kinetic time step are carried out during one ATHLET time step. However, to enable synchronisation between both codes at the end of the ATHLET time step, the last of these neutron-kinetic calculations is performed with a possibly reduced time step. In this procedure, the neutron-kinetic code uses at each smaller time step linearly interpolated values of the thermal-hydraulic variables. (Périn, 2016; Grundmann et al., 2005)

Spatial coupling scheme

In terms of space, DYN3D is a three-dimensional code, which means that the positions of the control volumes, i.e. nodes, that form a fuel assembly in the DYN3D neutron-kinetic model are defined through all three spatial dimensions. In contrast, ATHLET specifies the positions of the control volumes that form a thermo-fluiddynamic channel only in the axial direction. Hence, the spatial coupling for the exchange of data—

power distribution from DYN3D to ATHLET and distribution of the thermal-hydraulic parameters from ATHLET to DYN3D—between both codes requires some additional measure.

In the axial direction, the spatial coupling can be realised easily in case both models have the same axial nodalisation. If the axial nodalisations do not match, the data to be exchanged are linearly interpolated in the axial direction by the coupling interface.

In the radial direction, the fuel assemblies of the DYN3D neutron-kinetic model are assigned to the thermo-fluiddynamic channels of the ATHLET model with a mapping scheme. This mapping scheme is given as a user input in the DYN3D input. Besides a one-to-one mapping, in which each fuel assembly is covered by an individual thermo-fluiddynamic channel, it is also possible that one thermo-fluiddynamic channel covers several fuel assemblies. In this case, the thermo-fluiddynamic channel gains the power of all covered fuel assemblies and, in turn, the same thermal-hydraulic parameters apply to the covered fuel assemblies, i.e. they are subject to the same thermal-hydraulic feedback. Coupled NK/TH calculations with a one-to-one mapping are more accurate, but also require longer computation times. (Périn, 2016)

2.6 Core simulator KMACS

The nodal core simulator KMACS (Kernsimulator – a Modular Adaptable Core Simulator) (Zilly and Bousquet, 2019) developed by GRS can be used for the reactor cycle analysis of PWRs with a quadratic or hexagonal fuel assembly design. Like many other nodal core simulators, KMACS is based on the conventional two-step approach: i) lattice physics calculations for the generation of group constants under a priori expected thermal-hydraulic conditions for all fuel and reflector assemblies involved in the operation cycle, ii) the reactor cycle calculation by iteratively performing the nodal diffusion/thermal-hydraulic calculations and the depletion calculations.

For the various calculations involved in the analysis of an operation cycle, KMACS relies both on inhouse codes from GRS and on external codes. The execution of these codes and the pre- and postprocessing is performed by the different KMACS modules. The modules are designed in a way that different simulation codes can be used for the same function. KMACS uses a generic input from which the inputs for the individual codes are generated. A central data base stores results and allows the exchange of data between the different simulation codes.

KMACS allows the use of TRITON-NEWT and HELIOS (Studsvik Scandpower, 2012) for lattice physics calculations. Within the scope of this thesis, KMACS was extended

to allow lattice physics calculations with Serpent 2 (see Section 2.2).

KMACS allows coupled nodal diffusion/thermal-hydraulic calculations with either the coupled NK/TH code system QUABOX/CUBBOX-ATHLET or DYN3D with its internal thermal-hydraulic solver. In addition, nodal diffusion calculations without thermal-hydraulic feedback can also be performed with QUABOX/CUBBOX or DYN3D. Currently, KMACS is not capable of automatically performing coupled NK/TH calculations with DYN3D-ATHLET. Therefore, both the DYN3D inputs and the ATHLET inputs, which were both generated automatically by the KMACS modules, had to be modified manually for the DYN3D-ATHLET calculations performed in this thesis.

KMACS provides two methods for the determination of the fuel assembly-wise burnup: the burnup is either calculated from the assembly power and a specified time interval, or it is calculated using a coupling to the inventory code VENTINA (Liu, 2014; Zilly et al., 2018).

KMACS with both calculation sequences TRITON-NEWT – QUABOX/CUBBOX-ATHLET – trivial burnup and TRITON-NEWT – QUABOX/CUBBOX-ATHLET – VENTINA have been validated by the analysis of multiple cycles of 4-loop PWRs of type KWU Pre-Konvoi with a 16x16 fuel lattice (Zilly and Périn, 2018).

2.7 Random sampling-based method XSUSA

In the context of neutron transport calculations, the XSUSA (Cross Section Uncertainty and Sensitivity Analysis) method (Zwermann et al., 2009) developed by GRS enables the quantification of result uncertainties that arise from uncertainties in the nuclear data. XSUSA applies random sampling on the uncertain nuclear data, thereby taking correlations between energy-dependent cross sections of the same nuclide reaction and cross correlations between different reactions or even nuclides into account. The same neutron transport calculation is then performed a number of times with always a different realisation of the varied nuclear data. A statistical analysis of the results reveals the output uncertainties of interest as well as the most contributing nuclide reactions to the observed uncertainties.

The uncertainty information of the nuclear data is provided to XSUSA in the form of energy-dependent covariance matrices (see Section 1.2). Since no information about the distribution is available in the covariance libraries, the random sampling is performed with the assumption of a normal distribution. In the case of large relative uncertainties, the distribution must be truncated to avoid sampling of negative values. When truncation is performed, it is ensured that the mean value is not changed.

2.7. Random sampling-based method XSUSA

Furthermore, other dependencies between nuclide reactions must be considered in the sampling procedure to maintain consistency in the varied nuclear data. Examples for these dependencies are: a summation cross section such as the total cross section must be reconstructed from the varied partial cross sections, and the varied fission spectrum must be renormalised to one after every variation.

Within the XSUSA approach, the relative variations obtained from the sampling procedure are applied to the nuclear data after the self-shielding calculations. In this way, so-called implicit effects are not considered. This simplification is justified because in many comparisons with models of different neutron flux spectra it was observed that the uncertainties of the integral results are only barely affected by the negligence of the implicit effects (Bostelmann et al., 2015). The advantage of this simplification is a substantial reduction in computation time.

XSUSA is most commonly applied with the criticality codes of the SCALE code package (see Section 2.3) (Aures et al., 2017b). Moreover, XSUSA was also used to prepare varied MG libraries for the subsequent application with the Monte Carlo code MCNP executed in MG mode (Aures et al., 2017a). The current version of XSUSA utilises the covariance libraries provided with SCALE for the determination of the relative variations. If covariance data for a particular quantity are not available in this library, additional data can be taken from other sources, for example, JENDL-4.0 (Shibata et al., 2011).

The results of the sample calculations are statistically analysed. Basic uncertainty measures, such as the mean value and the standard deviation, are determined. When XSUSA is used in combination with a lattice physics code, varied group constant libraries can be generated that can be used to extend uncertainty calculations to nodal diffusion calculations.

XSUSA allows several options for sensitivity analysis of the output in order to identify the major contributors of the varied nuclear data to the output variance of a particular quantity of interest (QOI) (see Chapter 4).

3 Applicability of Serpent/DYN3D-ATHLET for the analysis of SPERT III experiments

This chapter demonstrates that the calculation sequence Serpent/DYN3D-ATHLET is suitable for the simulation of reactor transients in small reactor cores. For this purpose, the reactivity initiated accident tests carried out at the SPERT III E-core research reactor were taken as validation basis. Due to the uniqueness of available experimental data, the static core tests as well as the reactivity accident tests performed at the SPERT III E-core research reactor are frequently used for validation purposes (Knebel et al., 2016; Zoia and Brun, 2016; Cao et al., 2015; Aoki et al., 2009; Grandi and Moberg, 2012; Olson, 2012; IAEA, 2015; Dokhane et al., 2018a).

Compared to commercial LWRs, research reactors are smaller in size, often have a more complex geometry, and they are often operated with other fuel assembly types. As a consequence, the neutron flux distribution in space can be characterised by strong gradients and pronounced angular dependences. These characteristics are a particular challenge for the steady-state and transient analysis with codes that apply the MG neutron diffusion approximation as it has been demonstrated by Pautz (2002). In general there are further challenges for the computational analysis of transients: the response time of a reactor core becomes very small, namely in the range of milliseconds, when the reactor core undergoes a prompt supercritical reactivity insertion. If the reactor dynamic behaviour is analysed, an additional difficulty is the correct modelling of the reactivity feedback mechanisms in terms of timing and size.

Seven reactivity initiated accident tests carried out at the SPERT III E-core research reactor were analysed in this study. The reactivity insertions of the considered tests are in the range from delayed supercritical to prompt supercritical. To cover different reactor conditions, four of these tests are low-initial power tests performed under cold-startup conditions, and three of these tests are high-initial power tests performed

Chapter 3. Applicability of Serpent/DYN3D-ATHLET for the analysis of SPERT III experiments

under hot-standby conditions. The code sequence Serpent/DYN3D-ATHLET was applied in the conventional two-step approach for this analysis: in the first step, Serpent was used for the generation of group constants parameterised with respect to thermal-hydraulic parameters; and in the second step, DYN3D-ATHLET was applied for coupled NK/TH calculations of the selected reactivity accident tests.

First, an overview is provided about the SPERT III E-core research reactor and the reactivity accident tests studied. Afterwards, the models used for the computational analysis are introduced. These include Monte Carlo full-core models and nodal diffusion models for the steady-state analysis, and coupled NK/TH models for the transient analysis. Moreover, the models for the generation of the group constants are outlined. Results of the steady-state analyses are presented, and compared with available experimental data (McCardell et al., 1969) or recent studies (Zoia and Brun, 2016; Knebel et al., 2016). Finally, the results from the coupled NK/TH simulations of the reactivity accident tests are outlined and compared with experimental data.

Some methods and results studied in this chapter have been published as a conference paper (Aures et al., 2020b).

3.1 SPERT III experiments

The Special Power Excursion Reactor Test III (SPERT III) E-core reactor was a small, UO_2 -fueled pressurised water research reactor (Figure 3.1) operated at the National Reactor Testing Station in Idaho, USA (Heffner and Wilson, 1961).

In the 1960's, 80 non-damaging reactivity accident tests were performed under operating conditions similar to those of a commercial PWR in order to gather experimental power excursion data and to investigate the dynamic reactivity feedback mechanisms (Olson, 2012; McCardell et al., 1969). By rapid ejection of a central transient rod, reactivities ranging from 0.5 \$ to 1.3 \$¹ were inserted into the core, causing power excursions with reactor periods in the range of about 1,000 ms to 10 ms (McCardell et al., 1969). Tests with low initial power ($5 \cdot 10^{-5}$ MW) and with high initial power (1 and 20 MW) were performed under the initial reactor conditions given in Table 3.1, respectively.

The core was essentially free of fission products and no boron was used in the moderator. The criticality was controlled by four groups of two control rod assemblies each (Figure 3.2a). Every control rod assembly consisted of an absorber section, a fuel section, and flux suppressors between these sections (Figure 3.2b).

¹ Reactivity worth in the units of the total effective delayed neutron fraction β_{eff} , see Sec. 3.3.1.

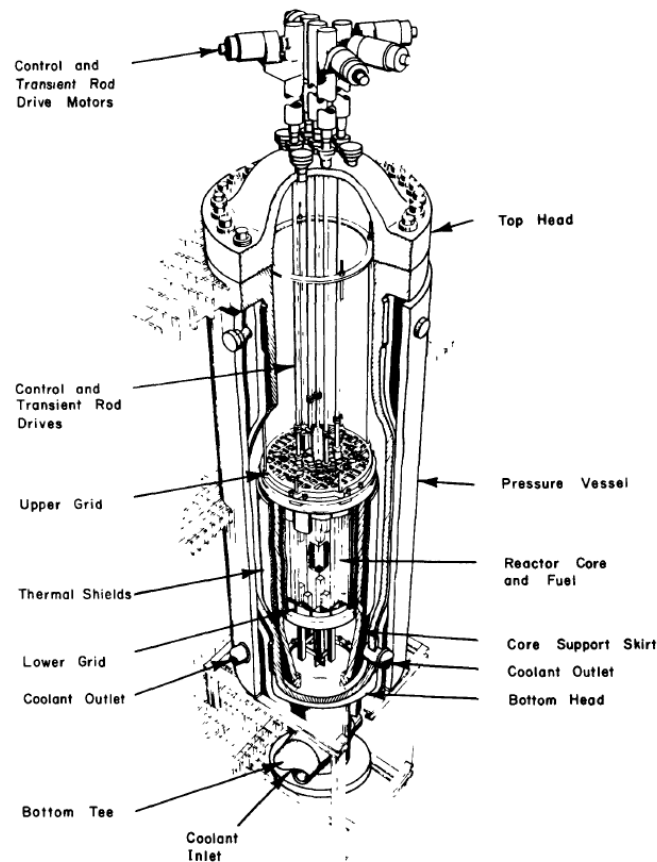


Figure 3.1: Cutaway view of the SPERT III reactor pressure vessel (McCardell et al., 1969).

The experiments were analysed with calculational models to gain more data about the reactor kinetic behaviour as could be observed during the experiments alone. In this way, the performance of the calculational models in predicting the reactor behaviour could also be assessed. For example the PARET code (Obenchain, 1969) was used. It modelled the neutron-kinetic behaviour with the point kinetics equations and the reactivity feedback effects with heat transfer and hydrodynamic calculational models. (McCardell et al., 1969)

The reactor power was measured using five ^{10}B lined ion chambers that were installed at different distances from the reactor core. The standard deviation in reactor power was determined by means of different calibration experiments of the detectors which were performed at different system temperatures. An average moderator inlet temperature was obtained from thermocouples installed at the bottom tee. From thermocouples installed near the upper grid, an average moderator outlet temperature was obtained. (McCardell et al., 1969)

Chapter 3. Applicability of Serpent/DYN3D-ATHLET for the analysis of SPERT III experiments

Table 3.1: Initial reactor conditions under which reactivity accident tests were performed (McCardell et al., 1969).

Conditions	Coolant inlet temperature ¹ [K]	System pressure ^{1,2} [MPa]	Average coolant flow rate ¹ [m/s]	Initial reactor power [MW]
Cold-startup	294	0.1013	0.0	$5 \cdot 10^{-5}$
Hot-startup	400	10.43	4.2672	$5 \cdot 10^{-5}$
	533	10.43	4.2672	$5 \cdot 10^{-5}$
Hot-standby	533	10.43	4.2672	1
Operating-power	533	10.43	4.2672	20

¹ Values converted to SI units.

² System pressure of 10.43 MPa determined from 1500 psig and an atmospheric pressure at 1500 m altitude (IAEA, 2015).

With the assumption of an initial exponential rise in power, the reactor period was determined from the measured power data. In case of the low-initial power tests, the reactivity insertion was calculated by the inhour equation (Lewis, 2008). By propagating the uncertainties of the input parameters of the inhour equation, namely reactor period, reduced prompt neutron generation time, and delayed neutron parameters, the uncertainty of the reactivity was obtained. Since no asymptotic development of the power occurred in the high-initial power tests, the inhour equation could not be applied for these cases. Instead, the reactivity insertion was derived from a control rod worth curve, and the corresponding standard deviation was calculated from the variance of a least-square fitted curve to the control rod worth data. The reactivity compensation was calculated with the point kinetic equations. The standard deviation therefore resulted from the standard deviations of the individual input parameters of the point kinetic equations. (McCardell et al., 1969)

A three-dimensional distribution of fuel rod cladding surface temperatures was obtained with 38 fine-wire, Chromel-Alumel thermocouples installed in the core (McCardell et al., 1969). The standard deviations of the various result quantities are given in Table 3.2.

3.2. Models for steady-state and transient analysis

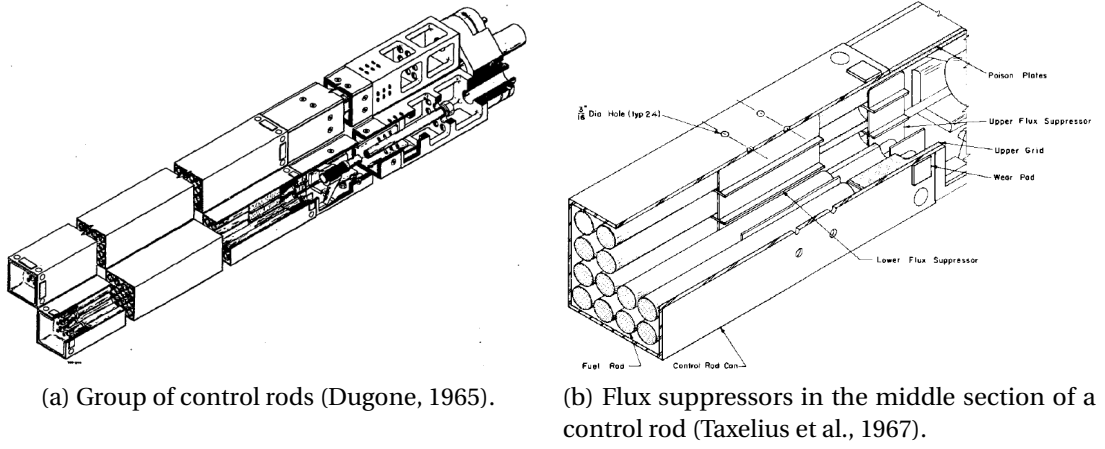


Figure 3.2: Cutaway views of a control rod group and of the flux suppressors in the middle section of a control rod assembly.

Table 3.2: Standard deviations of the reactivity accident test results at different system temperatures and initial power levels (McCardell et al., 1969).

Quantity	Standard deviation
Power	$\pm 15\%$ (at 294, 394, 478 K)
	$\pm 10\%$ (at 533 K)
Energy release at max. power	$\pm 17\%$ (at 294, 394, 478 K)
	$\pm 13\%$ (at 533 K)
Reactor period	$\pm 2\%$
Reactivity insertion	$\pm 4\%$ (at $5 \cdot 10^{-5}$ MW)
	$\pm 4\%$ (at 1 and 20 MW)
Reactivity compensation at max. power	$\pm 11\%$

3.2 Models for steady-state and transient analysis

This section provides an overview of the models built for the steady-state analyses as well as for the transient analyses of the SPERT III experiments.

Two full-core models were developed for Serpent: (1) a detailed reference model, and (2) a model exhibiting various simplifications with respect to the control rod geometries. The second model is consistent with the static DYN3D nodal diffusion model.

Infinite-lattice models of the various assembly types and reflector models were built for Serpent for the generation of group constants libraries. Two libraries were created, one for the cold-startup conditions and one for the hot-standby conditions.

Chapter 3. Applicability of Serpent/DYN3D-ATHLET for the analysis of SPERT III experiments

DYN3D nodal diffusion models and ATHLET thermal-hydraulic models were developed. A static variant of the DYN3D model was used in standalone nodal diffusion calculations for further steady-state analysis in addition to the Serpent full-core calculations. The transient analyses were done with transient variants of the DYN3D model in combination with ATHLET thermal-hydraulic models.

The following subsections provide additional details on the various models.

3.2.1 Serpent full-core models

In the following, the Serpent full-core models are described. Unless otherwise stated, the Serpent calculations with these models were carried out with 50,000 neutrons per cycle, 5,000 active cycles, and 150 inactive cycles. A CE cross section library based on the ENDF/B-VII.1 nuclear data library (Chadwick et al., 2011) was applied.

Serpent reference model

The Serpent reference model consists of the active core and the following structural components confining the active core: a bottom and a top grid, a core skirt, four thermal shields and a vessel wall (Figures 3.3 and 3.4).

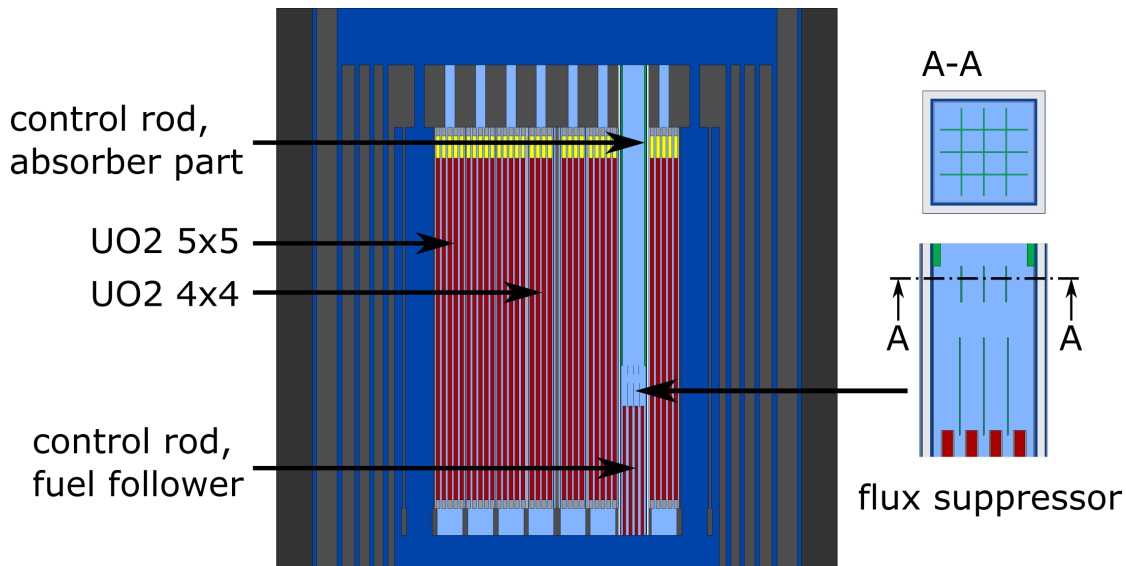


Figure 3.3: Vertical view of the Serpent reference model of the SPERT III E-core with the fuel assembly types UO2 5x5 and UO2 4x4, and a control rod consisting of the three sections: absorber, flux suppressors, and fuel follower. Detail: Horizontal and vertical view of the flux suppressors.

3.2. Models for steady-state and transient analysis

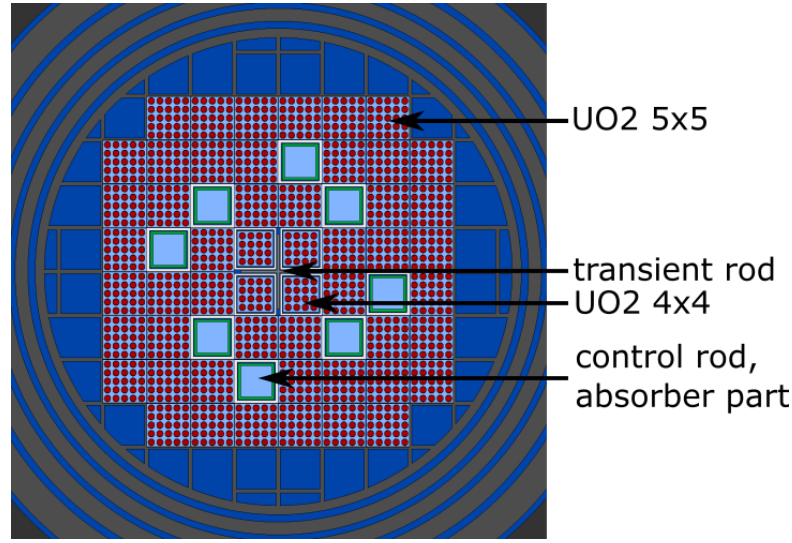


Figure 3.4: Horizontal view (detail) of the Serpent reference model of the SPERT III E-core with the fuel assembly types UO2 5x5 and UO2 4x4, the transient rod, and the control rods.

Selected dimensions used to model the parts described in the following are provided in Table 3.3. Both the bottom grid and the top grid are modelled with type SS304L stainless steel (IAEA, 2015). The original grids had a variety of through holes for cooling with water, holding the fuel assemblies and filler pieces in place, guiding the transient rod and control rods etc. The holes are modelled in a simplified way: only one type of hole was modelled in each grid. The holes are positioned below and above each assembly position, respectively. The core skirt, four thermal shields, and the vessel wall are modelled as concentric steel shells that are separated by water annuli (IAEA, 2015). The space between the cylindrical core skirt and the square shaped core is filled with differently shaped stainless steel filler pieces. Their hollow space is filled with water.

The core is composed of 60 fuel assemblies in total (Figure 3.4). 48 fuel assemblies (UO2 5x5) consist of a 5×5 fuel rod lattice which is confined by a square can. The original can was made from type SS348 stainless steel and provided holes with a total area of 774 cm^2 to allow cross flow of the coolant (Dugone, 1965). Instead of an explicit modelling of the holes, a homogenised mixture of steel and water is applied for the can in the model. Four fuel assemblies (UO2 4x4) with a 4×4 fuel rod lattice are located around the transient rod. Each of the four fuel assemblies is encased by a stainless steel can and separated from the transient rod by means of a Zircaloy-2 guide tube (IAEA, 2015; Zoia and Brun, 2016). Eight positions in the core lattice are occupied by movable control rods.

Chapter 3. Applicability of Serpent/DYN3D-ATHLET for the analysis of SPERT III experiments

Each movable control rod consists of three sections in the axial direction. The lower section is a fuel follower with a 4×4 fuel rod lattice encased in a stainless steel can. The upper section is a hollow, square box made from the neutron absorbing material 1.35 wt.% ^{10}B in type SS304 stainless steel (1.35 wt.% ^{10}B / SS304) (IAEA, 2015). The middle section contains flux suppressors. These are twelve small absorber plates of which six are arranged in a group. These plates consist of 1.35 wt.% ^{10}B / SS304 and are arranged in a rectangular grid. The control rods are guided in square tubes modelled with Zircaloy-2 (Dugone, 1965).

All fuel assembly types use the same fuel rod type and the same fuel rod pitch. The fuel — in the form of pellets — is UO_2 with a mass density of 10.5 g/cm^3 and an ^{235}U enrichment of 4.8 %. The cladding is modelled with type SS348 stainless steel. Both ends of the fuel rods are equipped with stainless steel end plugs. The expansion space above the upper fuel pellet is modelled as a homogenised material mixture composed of helium and the compression spring (Dugone, 1965).

The cruciform transient rod used for initiating the transient is located at the core centre and is axially divided into two sections. The lower section is made of the neutron absorbing material 1.35 wt.% ^{10}B / SS304. The upper section consists only of type SS304 stainless steel. (IAEA, 2015)

Serpent simplified model

The Serpent simplified model is the same as the Serpent reference model except that the flux suppressors in the control rods were replaced by the fuel follower part. In this way, the Serpent simplified model served as a suitable comparison model to the nodal diffusion model (Section 3.2.3) because the flux suppressors were not modelled in the nodal diffusion model.

3.2. Models for steady-state and transient analysis

Table 3.3: Selected dimensions used in the Serpent full-core models as well as in the Serpent infinite-lattice and reflector models.

Parameter	Dimension
Bottom grid thickness	7.62 cm
Top grid thickness	17.78 cm
Hole diameter (bottom grid)	6.36 cm
Hole diameter (top grid)	2.54 cm
Active core lattice pitch (x- and y-dimension)	7.62 cm × 7.62 cm
Fuel rod (IAEA, 2015)	
Pitch	1.486 cm
Active length	97.282 cm
Cladding outer diameter	1.184 cm
Cladding inner diameter	1.082 cm
Fuel pellet outer diameter	1.067 cm
Absorber part of control rods (Heffner and Wilson, 1961; Dugone, 1965)	
Length	116.84 cm
Width	6.29 cm
Thickness	0.473 cm
Flux suppressor plates – upper group (Dugone, 1965)	
Length	5.547 cm
Height	2.54 cm
Thickness	0.076 cm
Flux suppressor plates – lower group (Dugone, 1965)	
Length	5.944 cm
Height	6.906 cm
Thickness	0.076 cm
Transient rod (IAEA, 2015)	
Width	13.018 cm
Thickness	0.476 cm
Lower absorber section length	96.52 cm
Upper section length	142.24 cm

3.2.2 Serpent infinite-lattice models and reflector models for the generation of group constant libraries

Libraries with two-group constants were applied in the static and transient calculations with the DYN3D nodal diffusion models. The group constants were determined from various Serpent models that were deduced from the Serpent simplified model described above.

Two-dimensional infinite-lattice models with reflective boundary conditions were built for the different fuel assembly types (Figure 3.5a, c, d, e). To determine group constants for the absorber part of a control rod, a supercell model was created in which the absorber part was surrounded by fuel assemblies in order to provide a representative neutron flux spectrum (Figure 3.5b). The absorber part and the surrounding fuel assemblies of type UO₂ 5x5 were modelled with half width and thus reflective boundary conditions could be applied.

In order to account for the strong gradients in the spatial neutron flux distribution in the calculation of the reflector group constants, larger models were built for the radial and axial reflectors. In case of the radial reflector, a two-dimensional model was created that consisted of a row of eight UO₂ 5x5 fuel assemblies and of two non-multiplying regions at both ends. The non-multiplying regions next to the fuel assemblies were mainly filled with water, whereas the outer non-multiplying regions contained a significant amount of steel representing the core skirt and a thermal shield (Figure 3.6a). The radial reflector group constants were determined in one of the outer non-multiplying region so that the neutron-physical properties of the stainless steel were taken into account. The boundary conditions were vacuum in the direction of the x-axis and reflective in the direction of the y-axis.

The axial reflector group constants were determined using a fully expanded three-dimensional fuel assembly model of the type UO₂ 5x5 fuel assembly (Figure 3.6b). The assembly foot was chosen as the homogenisation region to obtain group constants that represent the neutron-physical properties of water and steel structures. The boundary conditions are vacuum in the direction of the x-axis and reflective in the direction of the y- and z-axis.

The Serpent calculations were performed with 10,000 neutrons per cycle, 5,000 active cycles, and 20 inactive cycles, and the ENDF/B-VII.1 CE cross section library (Chadwick et al., 2011) was applied. The group constants were calculated using the infinite neutron flux spectrum. Assembly discontinuity factors were not determined. The group constants were generated at the thermal-hydraulic conditions as listed in Table 3.4 and combined in a cold-startup library and a hot-standby library, respectively.

3.2. Models for steady-state and transient analysis

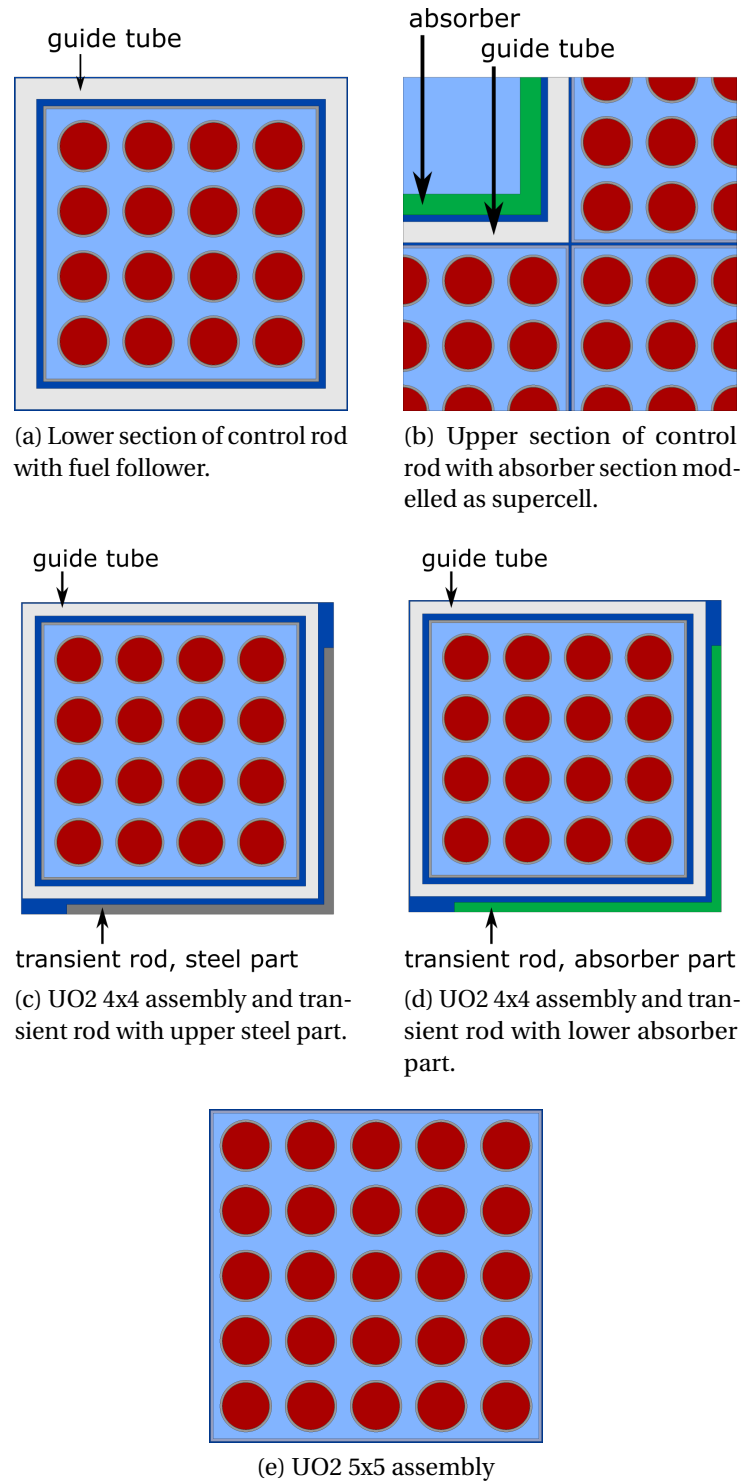


Figure 3.5: Infinite-lattice models used for the generation of two-group constants libraries with Serpent.

Chapter 3. Applicability of Serpent/DYN3D-ATHLET for the analysis of SPERT III experiments

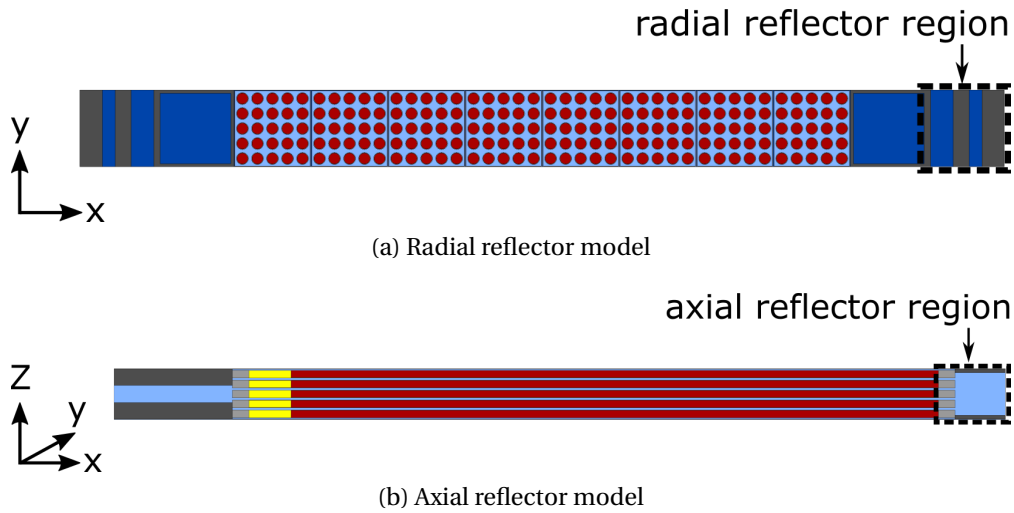


Figure 3.6: Reflector models used for the generation of two-group constants libraries with Serpent.

Table 3.4: Thermal-hydraulic parameter ranges of the two-group constants libraries for the cold-startup tests and the hot-standby tests.

Cold Startup		Hot Standby	
System pressure: 1.013 bar		System pressure: 104.3 bar	
Fuel temperature [K]	Moderator density [g/cm ³]	Fuel temperature [K]	Moderator density [g/cm ³]
294	0.99803	500	0.791
500	0.99189	700	0.762
700	0.98276	900	0.732
900	0.97126	1100	0.683
1100	0.95863	1300	
1300		1500	

3.2.3 DYN3D steady-state models and DYN3D-ATHLET models

The DYN3D nodal diffusion models and the ATHLET thermal-hydraulic models were generated by means of the core simulator KMACS. For this purpose, appropriate KMACS inputs of the SPERT III E-core for cold-startup and hot-standby conditions, respectively, were compiled. KMACS was also used to parse the group constants from the output files of the Serpent infinite-lattice and reflector calculations and to write this data into appropriately formatted library files for DYN3D.

The DYN3D nodal diffusion model consists of 60 fuel assemblies, a top and a bottom reflector, and two rows of radial reflector assemblies. The mesh size in radial direction is $7.62\text{ cm} \times 7.62\text{ cm}$, which corresponds to one node per assembly. In the axial direction, the mesh of the active core consists of 40 layers, each with a height of 2.43205 cm . The axial reflector nodes have a height of 9.7282 cm . The control rods consist of an absorber section and a fuel follower section; the flux suppressors are not modelled. All eight control rods are grouped together in a bank, so that they are moved up and down simultaneously. In the static nodal diffusion calculations, values for the fuel temperature, moderator density, and moderator temperature were fixed and applied to all nodes. In the kinetic variant of the DYN3D model, a time step size of $1.0 \cdot 10^{-4}\text{ s}$ was chosen for the neutron flux integration. The Doppler temperature in each node, i.e. the fuel temperature required for the interpolation of the group constants from the library, was determined by taking the average over the fuel temperatures of the radial layers of a fuel pin modelled in the ATHLET thermal-hydraulic model. The kinetic parameters were taken from the Serpent calculation with the full-core simplified model (see Section 3.3.1).

The ATHLET thermal-hydraulic model simulates only the thermal-hydraulics of the core. Every fuel assembly is represented by an individual thermo-fluiddynamic channel, while all reflector assemblies are represented by one channel. Cross connections between the channels are not modelled, thus cross flows are not considered. An axial discretisation of 40 layers for the active core as in the nodal diffusion model was set. The fuel rod objects are modelled with four radial layers of equal volume for the fuel pellet and of two radial layers of equal volume for the cladding. Depending on the simulated reactivity accident test, inlet temperature and system pressure were set according to the initial reactor conditions under which the tests were carried out. A coolant mass flow rate of 0.0 kg/s was set for the cold-startup tests. In the case of the hot-standby tests, a coolant mass flow rate of 596 kg/s was applied which was derived from the measured volume flow rate of $12,000\text{ gpm}$ (gallons per minute) (McCardell et al., 1969). The ATHLET integration module adapts the time step size automatically but does not exceed a maximum time step size defined by the user. This maximum

Chapter 3. Applicability of Serpent/DYN3D-ATHLET for the analysis of SPERT III experiments

time step size was set to $1.0 \cdot 10^{-4}$ s.

ATHLET has a built-in correlation for the calculation of the heat capacity of UO_2 fuel which is valid in a temperature range from 533.15 K to 3023.15 K (Austregesilo et al., 2016). Since the initial fuel temperature of the cold-startup tests was 294 K — which is far below the lower temperature limit of the built-in correlation — the ATHLET model was extended by tabulated values for the heat capacity for a temperature range from 298.15 K to 3120 K. The tabulated values were taken from IAEA (2006). For intermediate fuel temperatures, ATHLET determines the heat capacity via linear interpolation. If the fuel temperature is below the lower temperature limit or exceeds the upper temperature limit, ATHLET uses the heat capacity at the respective temperature limit. Therefore, it is considered acceptable that the initial fuel temperature of the cold-startup tests is 4.15 K lower than the lower temperature limit of the tabulated heat capacity values.

The initial positions of both the control rods and the transient rod are different for each SPERT III test, as described below. Therefore, discrete positions of the transient rod as a function of time were calculated with a uniform acceleration rate of 50.8 m/s^2 (McCardell et al., 1969). The positions at intermediate time steps are linearly interpolated by DYN3D-ATHLET.

Initial positions of the control rods and the transient rod

The experimental reports of the reactivity accident tests provide the inserted reactivity in each test, but lack information about the initial positions of both the control rods and the transient rod. To overcome this issue, the travel distance of the transient rod necessary to achieve the demanded reactivity was estimated by means of a static reactivity difference between two criticality calculations: one with the transient rod partially inserted and the other with the transient rod fully withdrawn. Another requirement was that the transient starts from the critical state, which is achieved by adjusting the insertion of the control rod bank. Similar approaches have already been applied by Knebel et al. (2016) and Dokhane et al. (2018a). In this study, the following scheme was applied, in which criticality calculations with DYN3D at constant thermal-hydraulic conditions were performed. The starting situation is a critical core, and the control rod bank and the transient rod are partially inserted.

1. DYN3D criticality calculation with transient rod and control rod bank partially inserted.
2. DYN3D criticality calculation with transient rod fully withdrawn and control

3.2. Models for steady-state and transient analysis

rod bank partially inserted.

3. If the reactivity difference between the calculations of the 1st and the 2nd step exceeds the demanded reactivity insertion, the scheme is stopped; if not, the scheme is continued.
4. The transient rod is repositioned to the insertion from the 1st step and it is further inserted by a small amount (0.025 cm)—more absorber is inserted; a DYN3D criticality calculation is performed.
5. The control rod bank is further inserted by a small amount (0.00125 cm)—more fuel follower is inserted—and a DYN3D criticality calculation is carried out.
6. Repeat the 5th step until the core has reached a critical state again.
7. Repeat this scheme by starting at the 1st step again.

It turned out that in most cases the applied scheme led to useful results for the rod positions, although static reactivity differences obtained by criticality calculations were considered. In the transient calculations, the reactivity inserted by the transient rod withdrawal was actually determined from the calculation of the dynamic reactivity. In most cases, especially the cold-startup tests, the static reactivity difference was in agreement with the dynamic reactivity, although their calculation methods are different. However, for *Test 81* and *Test 82*, which are prompt supercritical tests at hot-standby conditions, the dynamic reactivity resulting from the transient rod withdrawal was substantially larger than the previously determined static reactivity difference. As a consequence, transient rod positions and control rod positions that correspond to lower static reactivity differences were applied. A possible reason for this behaviour could be that the dynamic reactivity is impacted by the distribution of the thermal-hydraulic parameters. In the transient calculations of the hot-standby cases, the distribution is in fact three-dimensional due to the initial power of 1 MW; but in the static criticality calculations, the same thermal-hydraulic parameters were applied in all nodes. The initial positions of both the control rod bank and the transient rod used in the DYN3D-ATHLET calculations of the different reactivity accident tests are listed in Table 3.5.

Chapter 3. Applicability of Serpent/DYN3D-ATHLET for the analysis of SPERT III experiments

Table 3.5: Calculated initial positions of both the control rod bank and the transient rod for the simulations of the reactivity accident tests with DYN3D-ATHLET. The positions are measured from the bottom of the active core.

Test	Initial position [cm]	
	Control rods	Transient rod
<i>Test 18</i>	30.38875	11.25
<i>Test 43</i>	31.22625	14.025
<i>Test 48</i>	31.0525	13.1
<i>Test 49</i>	30.91625	12.45
<i>Test 79</i>	59.3725	18.425
<i>Test 81</i>	60.57375	21.925
<i>Test 82</i>	61.1575	23.225

3.3 Results

In this section, first the results of the static core calculations under cold-startup conditions are outlined, and then the results of the transient analyses of the selected reactivity accident tests are presented.

3.3.1 Static nuclear core characteristics under cold-startup conditions

Static core calculations under cold-startup conditions were performed with the Serpent reference model, the Serpent simplified model, and the static DYN3D model, respectively. If possible, results were compared with values given in the experimental report (McCardell et al., 1969) to investigate the performance of the Serpent full-core models as well as the performance of the DYN3D nodal diffusion model in combination with the cold-startup group constant library.

Critical position of the control rod bank

For all models, the critical position of the control rod bank was determined by moving it up and down in order to achieve a multiplication factor k_{eff} of 1.0. In case of the Serpent reference model, the position describes the distance between the bottom of the active core and the upper edge of the flux suppressors. In contrast, the critical position of the Serpent simplified model and the DYN3D model is the distance between the bottom of the active core and the upper edge of the fuel follower because the flux suppressors were not modelled. Table 3.6 lists the calculated positions and the measured position from the experiment.

Table 3.6: Critical position of the control rod bank at cold-startup conditions.

	Experiment (McCardell et al., 1969)	Serpent reference	Serpent simplified	DYN3D static
Critical Position [cm]	37.084	38.248	29.046	28.879

The critical control rod bank position of the Serpent reference model overestimates the measured critical position by 1.164 cm. When positioning the control rod bank at the measured critical position, the Serpent reference model yields a multiplication factor of 0.99422. Since the flux suppressors were replaced with fuel in both the Serpent simplified model and the DYN3D model, they show necessarily a much lower critical position of the control rod bank. The critical position of the DYN3D model is in good agreement with the one of the Serpent simplified model. This indicates a good performance of the DYN3D model together with the cold-startup group constant library.

Point kinetics parameters

Effective point kinetic parameters of both the Serpent reference model and the Serpent simplified model were determined with criticality calculations where the control rod banks were positioned at their respective critical positions (see Table 3.6). Serpent has different methods to calculate effective point kinetic parameters. In this study, the parameters obtained with the IFP method were considered (Leppänen et al., 2014). In Table 3.7, the total effective delayed neutron fraction β_{eff} and the effective mean generation time Λ_{eff} obtained for both Serpent full-core models are compared with the parameters that were used in the computational analyses during the experiments (McCardell et al., 1969).

Table 3.7: Effective point kinetic parameters.

Quantity	Serpent reference model	Serpent simplified model	Experiment (McCardell et al., 1969)
β_{eff}	0.00743(3) ¹	0.00748(3)	0.00718
Λ_{eff} [μ s]	17.084(8)	16.936(8)	15.55
$\Lambda_{eff} / \beta_{eff}$ [ms]	2.30(1)	2.26(1)	2.15

¹ Values in parentheses are the 1σ statistical uncertainty associated with the Monte Carlo result.

In addition, the values for β_{eff} and Λ_{eff} determined by Serpent were used to calculate

Chapter 3. Applicability of Serpent/DYN3D-ATHLET for the analysis of SPERT III experiments

the reduced mean generation times through: $\Lambda_{eff}/\beta_{eff}$. These are also compared with the reduced mean generation time found in the experimental report (McCardell et al., 1969). It is observed that the point kinetic parameters determined with both Serpent full-core models overestimate the computed values used during the experiments. However, the point kinetic parameters from Serpent are in good agreement with results found in other publications, for example, the IFP based parameters obtained by Zoia and Brun (2016) ($\beta_{eff} = 761 \pm 4.6$ pcm, $\Lambda_{eff} = 17.3 \pm 0.01$ μ s, $\Lambda_{eff}/\beta_{eff} = 2.27 \pm 0.01$ ms).

Moreover, delayed neutron fractions β_i , decay constants λ_i , and lifetimes τ_i , were determined with both Serpent full-core models in the commonly used representation of six time groups with $i = 1, \dots, 6$. The values are listed in Table 3.8.

Table 3.8: Serpent results of the effective delayed neutron fractions β_i , decay constants λ_i , and lifetimes τ_i , in the six-time group representation at cold-startup conditions.

	Serpent reference model			Serpent simplified model		
Time group	β_i	λ_i [s ⁻¹]	τ_i [s]	β_i	λ_i [s ⁻¹]	τ_i [s]
1	$2.40 \cdot 10^{-4}$	$1.34 \cdot 10^{-2}$	74.88	$2.37 \cdot 10^{-4}$	$1.34 \cdot 10^{-2}$	74.88
2	$1.28 \cdot 10^{-3}$	$3.26 \cdot 10^{-2}$	30.67	$1.28 \cdot 10^{-3}$	$3.26 \cdot 10^{-2}$	30.67
3	$1.26 \cdot 10^{-3}$	$1.21 \cdot 10^{-1}$	8.26	$1.26 \cdot 10^{-3}$	$1.21 \cdot 10^{-1}$	8.26
4	$2.85 \cdot 10^{-3}$	$3.06 \cdot 10^{-1}$	3.27	$2.86 \cdot 10^{-3}$	$3.06 \cdot 10^{-1}$	3.27
5	$1.26 \cdot 10^{-3}$	$8.62 \cdot 10^{-1}$	1.16	$1.31 \cdot 10^{-3}$	$8.62 \cdot 10^{-1}$	1.16
6	$5.36 \cdot 10^{-4}$	2.89	0.35	$5.35 \cdot 10^{-4}$	2.89	0.35

Multiplication factors and power distributions at the all rods out state

Power distributions at assembly level and multiplication factors were determined with criticality calculations for the all rods out state, i.e. the absorber parts of both the transient rod and the control rod bank were fully withdrawn. The upper edge of the fuel follower was aligned with the active core height. While DYN3D automatically outputs radially as well as axially integrated power distributions, appropriate tallies were defined in the Serpent models.

Differences between multiplication factors are expressed in terms of the reactivity difference:

$$\Delta\rho = \rho - \rho_{ref} = \frac{1}{k_{ref}} - \frac{1}{k}, \quad (3.1)$$

where k_{ref} and k are the multiplication factors of, for example, different models or reactor states. The reactivity difference is given in the unit pcm (1 pcm is equivalent to 10^{-5}).

The multiplication factors of the Serpent reference model and of the Serpent simplified model are $1.11724(6)$ and $1.11708(6)^2$, respectively. The small reactivity difference of -13 pcm is explained by the close similarity between the Serpent full-core models in the all rods out state. The DYN3D model yields a multiplication factor of 1.11292 which is -347 pcm smaller than the Serpent reference model and -334 pcm less than the Serpent simplified model. These deviations are considered acceptable.

The radial assembly power distribution from DYN3D was compared with the radial assembly power distributions from both Serpent full-core models (Figure 3.7).

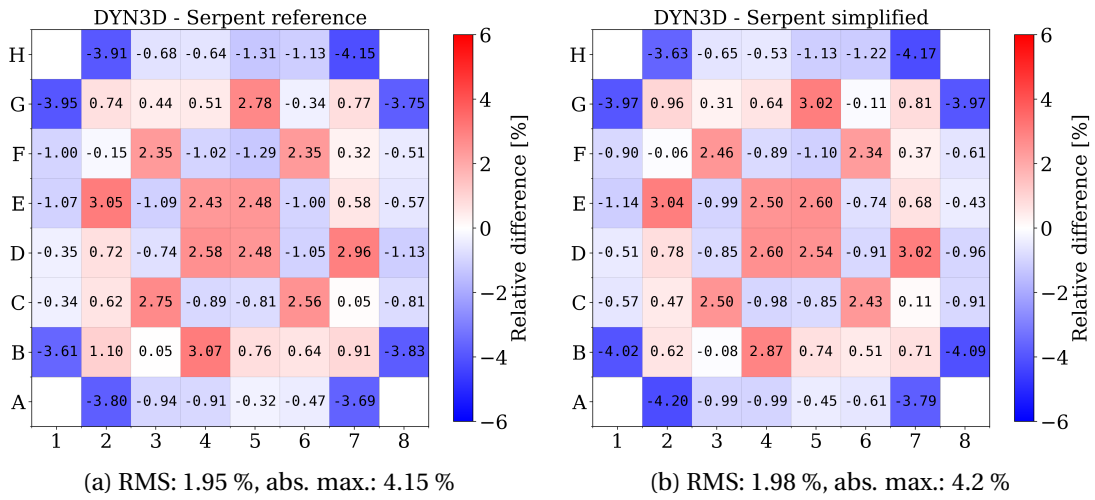


Figure 3.7: Relative differences of assembly powers between DYN3D and the Serpent reference model, and between DYN3D and the Serpent simplified model, of the SPERT III E-core under cold-startup conditions and the all rods out state.

While the radial power distribution from DYN3D has rotational symmetry with respect to 90° , the radial power distributions of the Serpent models are subject to variations due to the Monte Carlo method although a large number of neutron histories was used. Since the Serpent models are very close in this state, the distributions of the relative differences of the assembly powers are similar. A good agreement is generally observed. The maximum differences occur at corner positions where DYN3D underestimates the assembly powers. The assembly powers of the eight fuel followers and the four fuel assemblies surrounding the transient rod are overestimated by DYN3D. This observation may indicate that the complex geometrical layout of the assemblies containing neutron absorbers cannot be represented with sufficient accuracy by two-group constants when the focus is on local results such as assembly power distributions. In Knebel et al. (2016), relative differences from -2.87 % to 3.39 % between a

²The value in parentheses is the 1σ statistical uncertainty associated with the Monte Carlo result.

Chapter 3. Applicability of Serpent/DYN3D-ATHLET for the analysis of SPERT III experiments

Serpent full-core calculation and a nodal diffusion/sub-channel thermal-hydraulic calculation with the code DYNSUB were found.

The axial power distributions of the different models are in good agreement (Figure 3.8). A slight tilt is observed between the DYN3D calculation and both Serpent calculations.

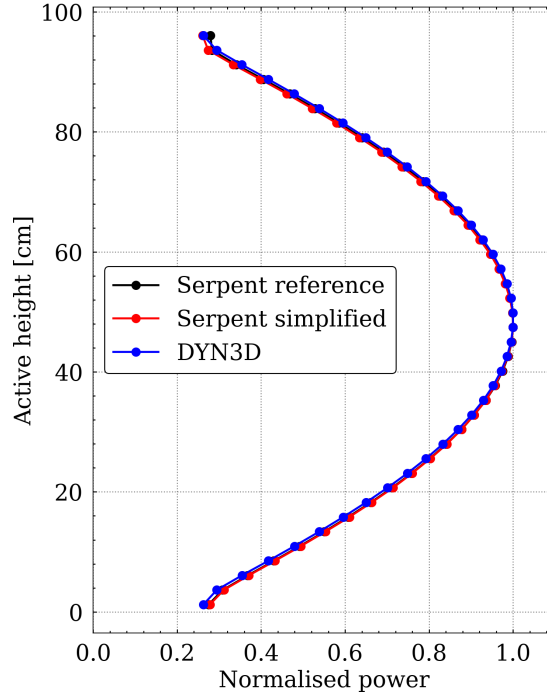


Figure 3.8: Normalised axial power distribution of the SPERT III E-core under cold-startup conditions and the all rods out state.

Excess reactivity and transient rod worth

The excess reactivity of the core is the inserted positive reactivity when the control rod bank is fully withdrawn. It is expressed with the normalised reactivity worth which is computed as follows:

$$\widetilde{\Delta\rho} = \frac{\rho_u - \rho_r}{\beta_{eff}} = \frac{\left(\frac{1}{k_r} - \frac{1}{k_u}\right)}{\beta_{eff}}, \quad (3.2)$$

where k_u and k_r are the multiplication factors of the unrodded and rodded state, respectively, and β_{eff} is the total effective delayed neutron fraction used as a normalisation constant to express the reactivity worth in the units of β_{eff} . A reactivity worth of $\Delta\rho = \beta_{eff}$ is designated as one dollar [\$].

For all models, the excess reactivity was then calculated on the basis of the following two control rod bank positions: the all rods out state and the critical state in both of which the transient rod was fully withdrawn. The total effective delayed neutron fractions determined for the two Serpent models with the control rod banks in the critical positions and the transient rods fully withdrawn were used as normalisation constants (see Table 3.7). In case of the DYN3D model, β_{eff} of the Serpent simplified model was used.

Similarly, the reactivity worth of the transient rod was determined. For each model, two additional criticality calculations were performed, one with the transient rod fully withdrawn and the other with the transient rod fully inserted. In both states the control rod bank was set on the critical position.

Table 3.9 compares the calculated reactivity worths with the values from the experimental report (McCardell et al., 1969). A very good agreement is observed between the calculated reactivity worths and the experimental values. The largest deviation is found for the excess reactivity obtained by the DYN3D model. This is considered acceptable when comparing few-group nodal diffusion methods against CE Monte Carlo calculations.

Table 3.9: Calculated and measured absolute excess reactivity and transient rod worth under cold-startup conditions.

Model	Excess reactivity [\$]	Transient rod worth [\$]
Experiment (McCardell et al., 1969)	14	4.8
Serpent Reference	14.12(6) ¹	4.67(2)
Serpent Simplified	14.03(6)	4.59(2)
DYN3D	13.58(5)	4.65(2)

¹ Values in parentheses are the 1σ statistical uncertainty associated with the Monte Carlo result. In case of DYN3D, the statistical uncertainty of β_{eff} was considered.

Control rod worth and transient rod worth

To gain not only the total reactivity worths of the control rod bank and the transient rod as described in Section 3.3.1, but also the reactivity worths as a function of insertion, additional criticality calculations were performed in which the control rod bank or the transient rod were set on intermediate positions. Due to the large number of calculations, the Serpent calculations were performed with a reduced number of neutron histories: 50,000 neutrons per cycle, 2,500 active cycles, 50 inactive cycles. The average Monte Carlo uncertainty of the obtained multiplication factors is 9 pcm. It should be noted that the insertion of the transient rod actually results in negative

Chapter 3. Applicability of Serpent/DYN3D-ATHLET for the analysis of SPERT III experiments

reactivity worths and is presented in absolute values.

Figure 3.9 shows the integral reactivity worth of the control rod bank as a function of insertion. Very good agreement is observed between the DYN3D model and the Serpent simplified model. The average difference is 0.28\$, and the largest difference is 0.4\$ at an insertion of 68 cm. When comparing these results to the Serpent reference model, the negligence of the flux suppressors is clearly visible, especially at the critical position.

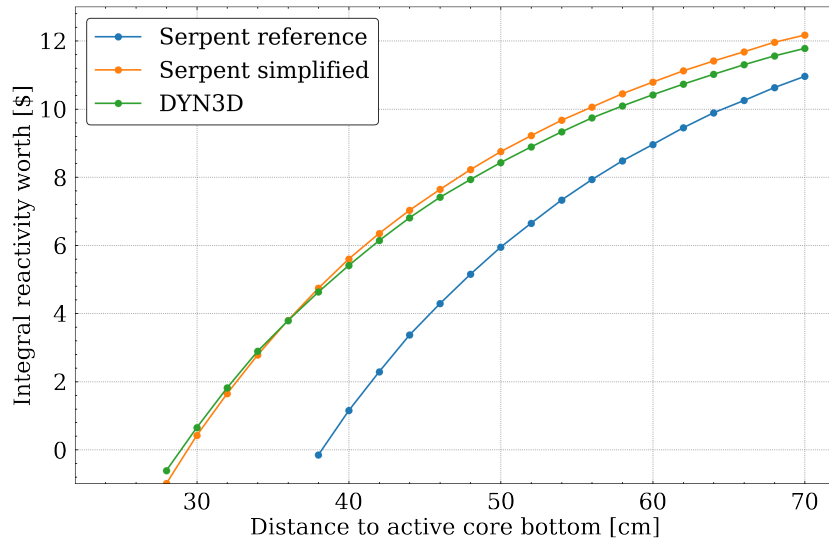


Figure 3.9: Calculated integral reactivity worth of the control rod bank.

The absolute integral reactivity worths of the transient rod obtained by the different models are compared in Figure 3.10. Very good agreement is observed between all models. The Serpent reference model and the Serpent simplified model have an average difference of 0.04\$; the maximum deviation is 0.1\$ at 24 cm. The DYN3D model slightly overestimates the transient rod worth of both Serpent full-core models in the range between 3 cm and 30 cm. When comparing the transient rod worth of the DYN3D model with the one of the Serpent simplified model, the average deviation is 0.06\$ and the maximum deviation is 0.16\$ at 15 cm.

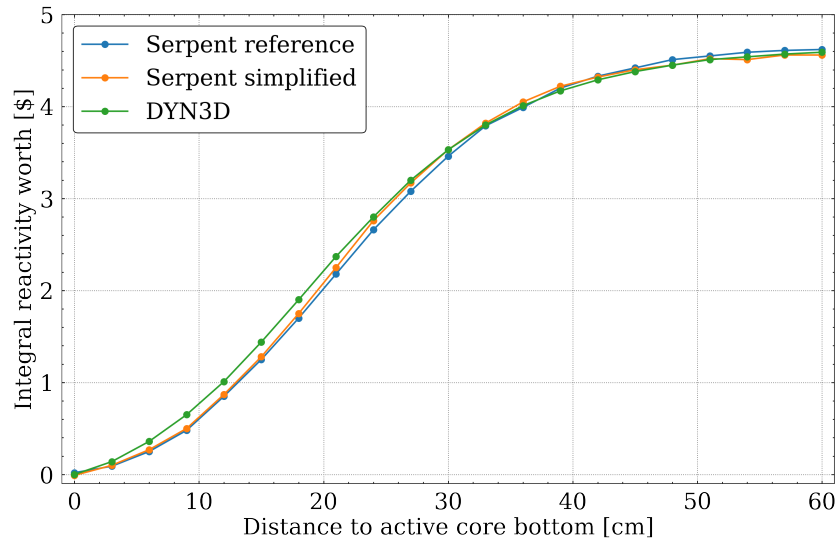


Figure 3.10: Calculated absolute integral reactivity worth of the transient rod.

3.3.2 Reactivity accident tests

In this section calculational results of the reactivity accident tests *Test 18*, *Test 43*, *Test 48*, *Test 49*, *Test 79*, *Test 81*, and *Test 82*, are presented. While *Test 18*, *Test 43*, *Test 48*, and *Test 49*, belong to the category low-initial power tests under cold-startup conditions, *Test 79*, *Test 81*, and *Test 82*, are from the category high-initial power tests at hot-standby conditions.

The reactivity accident tests were analysed with the coupled NK/TH code system DYN3D-ATHLET in combination with two-group constants libraries generated with Serpent for the cold-startup and hot-standby conditions, respectively.

The following calculational results were examined:

- power over time,
- maximum power,
- occurrence time of maximum power,
- energy release until maximum power,
- total reactivity and individual reactivity contributions,
- reactivity compensation at maximum power,
- stable reactor period (only for cold-startup tests).

Chapter 3. Applicability of Serpent/DYN3D-ATHLET for the analysis of SPERT III experiments

The stable reactor period is examined only for the cold-startup tests. In case of the hot-standby tests, significant reactivity feedback during and after the reactivity insertion prevented the formation of a stable reactor period (McCardell et al., 1969).

From the solution of the point kinetic equations in combination with the inhour equation for a neutron-kinetic problem with a step reactivity change, and without reactivity feedback, it can be derived that the neutron population $n(t)$ first undergoes a prompt change and then adopts an asymptotic behaviour. The asymptotic behaviour is represented by an exponential growth or decay depending on whether the change in reactivity is positive or negative. It has the form (Lewis, 2008):

$$n(t) \simeq A_1 \exp(t/\tau), \quad (3.3)$$

where A_1 is a constant and τ is the reactor period. Thus, the reactor period describes the time interval in which the neutron population increases or decreases by a factor of $e \approx 2.718$ (Lewis, 2008). Since such an asymptotic behaviour of the reactor power was observed in case of the cold-startup tests during a certain time interval, the stable reactor period was determined by fitting a one-term exponential model to values of the reactor power within this time interval. The assumption was made that the reactor power is proportional to the neutron population. The time interval for the fit is selected by visual inspection of the power over time.

Results over time are presented in the following for the selected reactivity accident tests. In addition, Table 3.10 summarises key figures from the calculated transient results and compares them with experimental results. The experimental results including their corresponding standard deviations are taken from (IAEA, 2015).

Test 43 - low initial power under cold-startup condition

The prompt supercritical experiment *Test 43* was performed with a reactivity insertion of 1.21 ± 0.05 \$. A maximum power of 280 ± 42 MW was measured at 0.23 ± 0.006 s.

The DYN3D-ATHLET result for the reactor power over time is shown in Figure 3.11a. After a rapid increase, the power approaches a maximum of 286 MW at an occurrence time $t_{P_{max}}$ of 0.219 s. Then, the power decreases to an asymptotic value that is larger than the initial power. The calculated maximum power is in very good agreement with the experimental value and the occurrence time $t_{P_{max}}$ lies within two standard deviations of the experiment.

The total reactivity and the individual reactivity contributions calculated by DYN3D-ATHLET are shown in Figure 3.11b. The total reactivity is first dominated by the

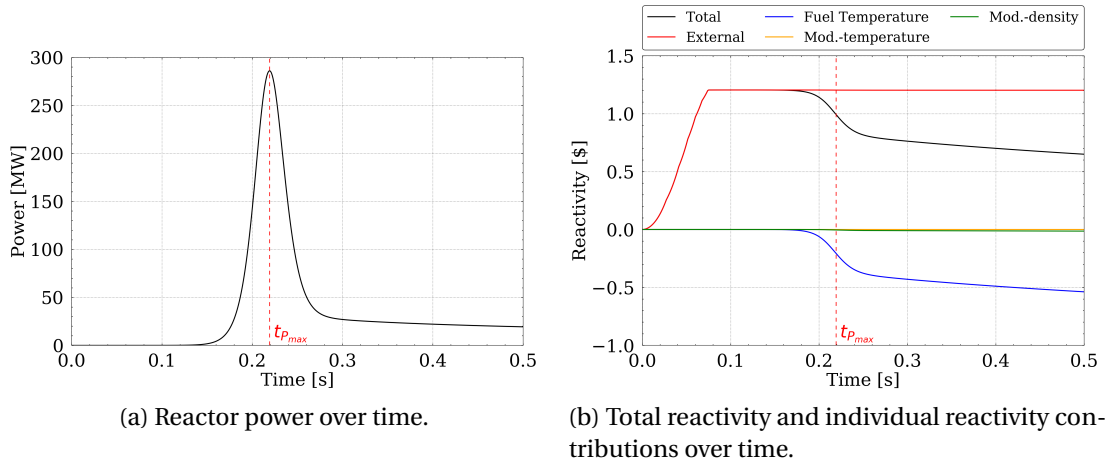


Figure 3.11: DYN3D-ATHLET results of *Test 43* under cold-startup conditions.

external reactivity insertion from the transient rod withdrawal. An asymptotic value of 1.20\$ is reached when the transient rod is fully withdrawn. Later, with a rise in the fuel temperature and thus an increase in the resonance absorption (Doppler effect), a negative reactivity contribution occurs. At $t_{P_{max}}$, the calculated reactivity compensation is 0.212\$. Both the inserted reactivity and the reactivity compensation determined from the calculation match the experimental values well. The reactivity compensation determined in the experiment was 0.22 ± 0.02 \$. No significant reactivity contribution from either a change in the moderator density or a change in the moderator temperature is observed.

The reactor period determined from the calculated power decreases during the withdrawal of the transient rod and reaches a minimum value of 8.6 ms at 0.075 s (Figure 3.12a) which is the same time when the transient rod is fully withdrawn. From the oscillations of the reactor period at the beginning of the transient it is observed that the power does not increase steadily. After the reactor period has reached its minimum, it takes on an asymptotic value indicating that the power rises exponentially (Figure 3.12b). With the occurrence of reactivity feedback, the reactor period increases. At the occurrence time $t_{P_{max}}$ of the maximum power, the reactor period has a pole. Afterwards, during the power decrease, the reactor period takes on a negative value.

The one-term exponential model (Eq. 3.3) was fitted to power values that lie within the time interval 0.12 s – 0.16 s (indicated by t_1 and t_2 in Figure 3.12b), resulting in a value of 10.52 ms for the stable reactor period. The stable reactor period determined in the experiment is 10.0 ± 0.3 ms; thus, the fitted value agrees well with the measured value within two standard deviations. The time interval for the fit was selected by visual inspection of the plots in Figure 3.12.

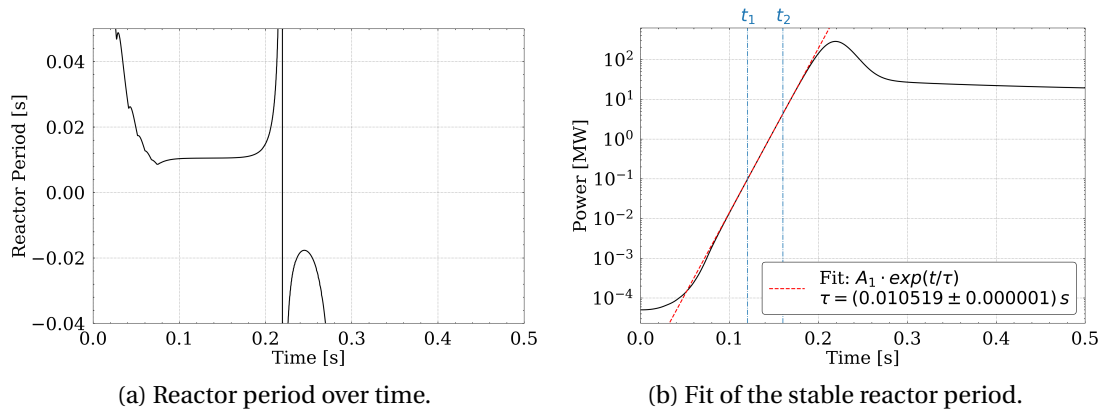


Figure 3.12: Reactor period calculated from reactor power and determination of the stable reactor period by fit of the one-term exponential model to the reactor power between t_1 and t_2 of Test 43.

The impact of the selected time interval on the fit result was assessed with repeating the fit with other time intervals. A shorter time interval did not improve the fit result. A larger time interval, such as 0.08 s - 0.17 s, resulted in a reactor period of 10.6 ms. A significant deviation occurred by extending the time interval beyond 0.18 s. With the observation that a reasonable value for the stable reactor period was obtained by visual inspection of the fit interval and that this value hardly changed as long as the fit interval was in the period of the exponential rise, this approach has been adopted for the other cold-startup tests.

Test 18 - low initial power under cold-startup condition

Test 18 was a delayed supercritical test with a reactivity insertion of $0.9 \pm 0.4 \text{ \$}$ and a maximum power of $4.3 \pm 0.6 \text{ MW}$ measured at $5.3 \pm 0.1 \text{ s}$.

Figure 3.13a shows the reactor power over time calculated by DYN3D-ATHLET. Since the inserted reactivity is below 1 \$, the core is not prompt supercritical. Thus, the response time of the reactor is mainly determined by the decay times of the precursors (see Table 3.8). As a consequence, the rise in power is significantly smaller and slower. The calculated maximum power of 4.83 MW is in good agreement with the measured maximum power. The occurrence time of the calculated maximum power, which is 5.33 s, also agrees well with the measured time in the experiment.

The total reactivity and the individual reactivity contributions determined by DYN3D-ATHLET are presented in Figure 3.13b. The total reactivity approaches a value of 0.88 \$ which agrees well with the experiment. Reactivity feedback results first from

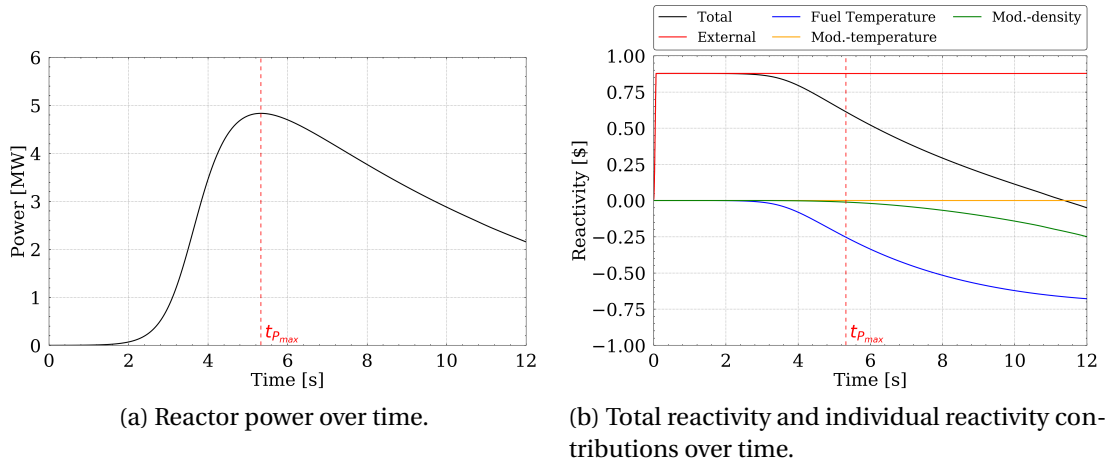


Figure 3.13: DYN3D-ATHLET results of *Test 18* under cold-startup conditions.

the Doppler broadening, and later from a decrease of the moderator density.

The fit of the one-term exponential model for the determination of the stable reactor period is shown in Figure 3.14. The fit yields a stable reactor period of 381 ms which is 30 ms larger than the measured reactor period of 351 ± 7 ms.

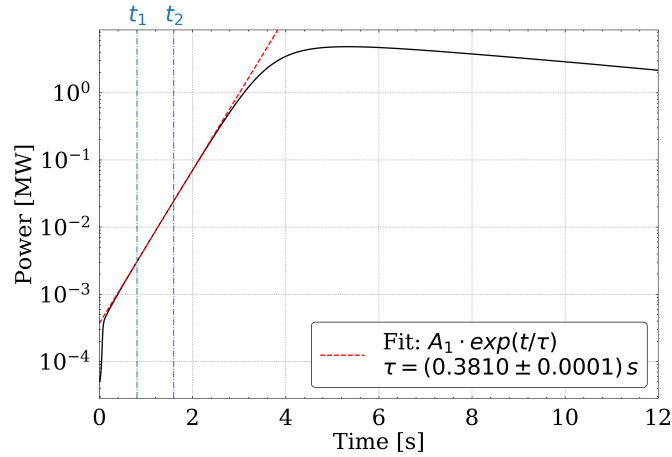


Figure 3.14: Determination of the stable reactor period by fit of an one-term exponential model to the reactor power between t_1 and t_2 of *Test 18*.

Test 48 - low initial power under cold-startup condition

In this test, a maximum power of 63 ± 9 MW was detected at 0.37 ± 0.01 s. The reactivity insertion was prompt supercritical with 1.09 ± 0.04 \$.

The maximum power calculated by DYN3D-ATHLET is 68.8 MW (Figure 3.15a) which

Chapter 3. Applicability of Serpent/DYN3D-ATHLET for the analysis of SPERT III experiments

is in very good agreement with the measured value. The calculated maximum occurs slightly earlier than in the experiment, namely at 0.35 s, but lies within two standard deviations of the experimental time. When comparing this test with *Test 43*, which is also a prompt supercritical test, it is observed that the maximum power is about one-fourth of the maximum power of *Test 43* and that the occurrence time of the maximum power is about 0.14 s later than in *Test 43*. The calculated reactivity insertion is 1.091\$ and the reactivity compensation at $t_{P_{max}}$ is 0.111\$ (Figure 3.15b). Both results are in excellent agreement with the experimental values.

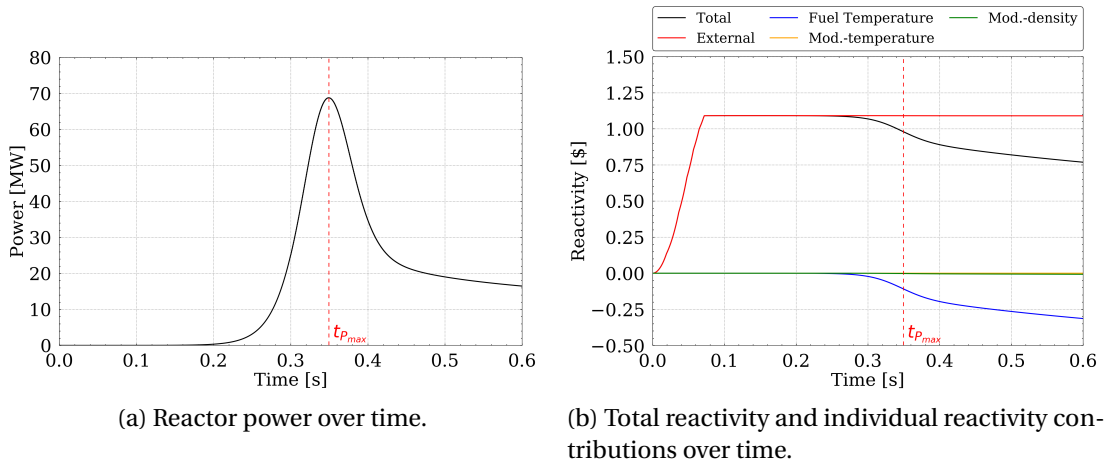


Figure 3.15: DYN3D-ATHLET results of *Test 48* under cold-startup conditions.

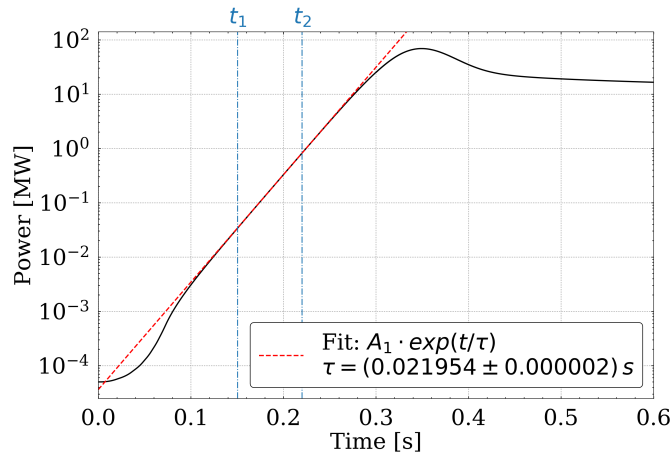


Figure 3.16: Determination of the stable reactor period by fit of an one-term exponential model to the reactor power between t_1 and t_2 of *Test 48*.

Figure 3.16 illustrates the power over time and the fit of the one-term exponential model in the time interval between t_1 and t_2 . The fit results in a stable reactor period

of 21.95 ms which agrees well with the stable reactor period from the experiment, namely 21.1 ± 0.4 ms.

Test 49 - low initial power under cold-startup condition

Test 49 was a prompt critical transient with a reactivity insertion of 1.00 ± 0.04 \$ and a measured maximum power of 11 ± 2 MW, which occurred at 0.97 ± 0.04 s.

The analysis of this transient with DYN3D-ATHLET led to a maximum power of 12.3 MW at $t_{P_{max}}$ of 0.854 s (Figure 3.17a). The calculated reactivity insertion is 1.005\$ (Figure 3.17b); the reactivity compensation at $t_{P_{max}}$ is 0.081\$ which matches the experimental value. After a problem time of 2 s, a negative reactivity contribution also arises from the decrease of the moderator density.

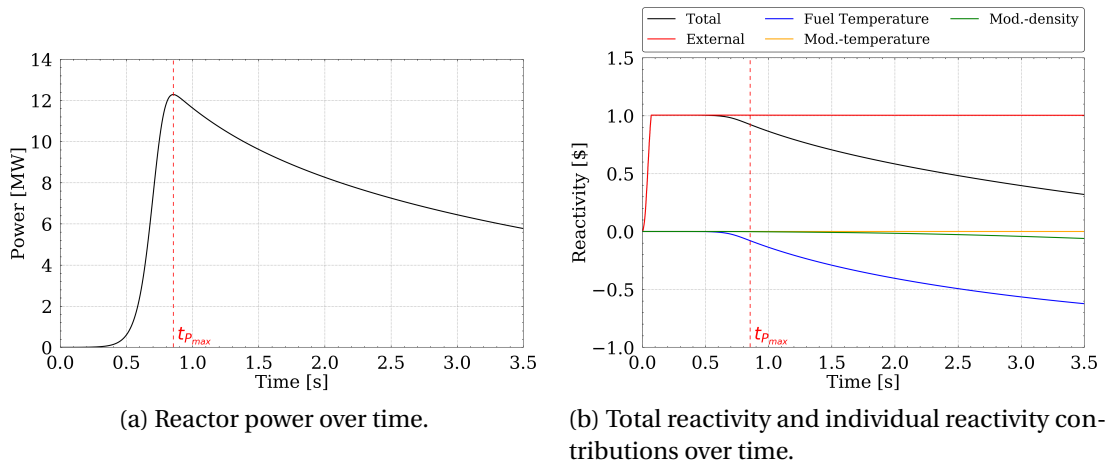


Figure 3.17: DYN3D-ATHLET results of Test 49 under cold-startup conditions.

The deviations between the experiment and the calculation in terms of the maximum power and the occurrence time of the maximum power can be explained by the fact that the time response of a reactor core becomes very sensitive when the inserted reactivity approaches 1\$. Below 1\$, the reactor period is mainly determined by the half-lives of the precursors. If the reactivity insertion exceeds 1\$, the reactor is supercritical on the prompt neutrons alone and the reactor period is mainly determined by the substantially shorter prompt neutron generation time rather than the half-lives of the precursors (Emendörfer and Höcker, 1993). In case of the Serpent simplified model, the prompt neutron generation time is $1.636 \cdot 10^{-5}$ s and the average half-life of the precursors³ is 10.506 s (Section 3.3.1).

³Calculation of the average half-life by weighting with delayed neutron fractions: $\tau = \sum_i (\beta_i \tau_i) / \beta$ (Emendörfer and Höcker, 1993)

Chapter 3. Applicability of Serpent/DYN3D-ATHLET for the analysis of SPERT III experiments

The fit of the one-term exponential model to the power over time between t_1 and t_2 (Figure 3.18) led to a stable reactor period of 68.1 ms which matches the stable reactor period from the experiment, namely 68.4 ± 1.4 ms.

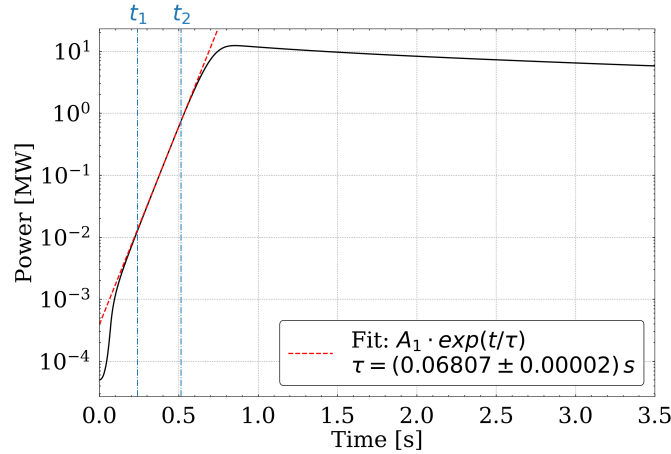


Figure 3.18: Determination of the stable reactor period by fit of an one-term exponential model to the reactor power between t_1 and t_2 of *Test 49*.

Test 81 - high initial power under hot-standby condition

The prompt supercritical reactivity accident test *Test 81* had a reactivity insertion of 1.17 ± 0.04 \$ and a maximum power of 330 ± 30 MW, which was detected at 0.135 ± 0.003 s.

The maximum power obtained by DYN3D-ATHLET is 330 MW. It is in excellent agreement with the measured maximum power (Figure 3.19a). It occurs 0.0054 s later than in the experiment which is in the range of two standard deviations of the experimental occurrence time.

The inserted reactivity in the calculation is 1.157\$ (Figure 3.19b). In contrast to the cold-startup tests, reactivity feedback coming from the Doppler effect already occurs at the end of the transient rod withdrawal. Thus, an asymptotic value of the total reactivity is prevented. When the transient rod is fully withdrawn and therefore no more external reactivity is inserted, the total reactivity has a maximum and then declines because of the Doppler effect. A further difference with the cold-startup tests is that even at $t_{p_{max}}$ the decrease of the moderator density is already an important contributor to the reactivity feedback.

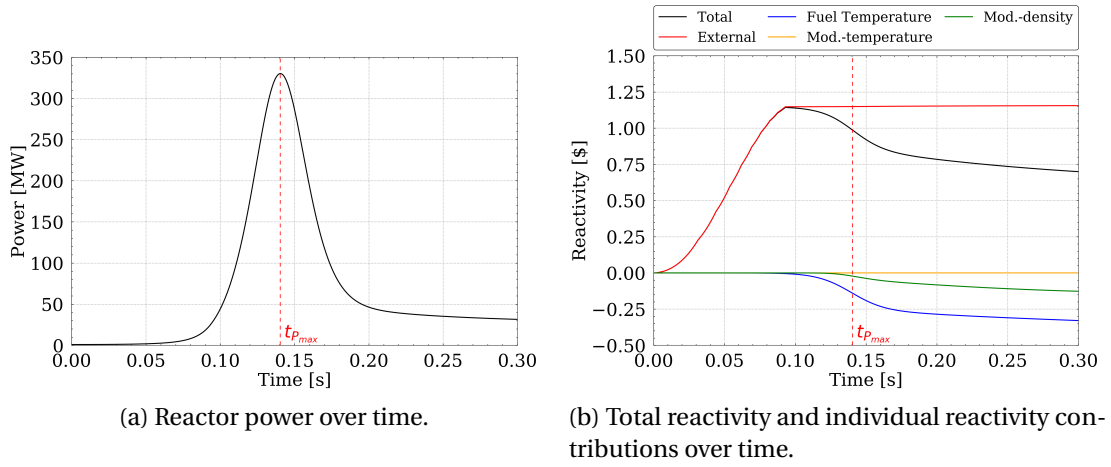


Figure 3.19: DYN3D-ATHLET results of *Test 81* under hot-standby conditions.

Test 79 - high initial power under hot-standby condition

Test 79 was a delayed supercritical test characterised by a reactivity insertion of 0.86 ± 0.03 \$. The maximum power was 13 ± 1 MW and it occurred at 0.68 ± 0.08 s.

The calculated power over time approaches a maximum of 13.5 MW at a time $t_{P_{max}}$ of 0.841 s (Figure 3.20a). The calculated and the experimental maximum power agree well, and the calculated maximum power occurs 0.161 s later than in the experiment. This is a deviation of slightly more than two standard deviations of the experimental time.

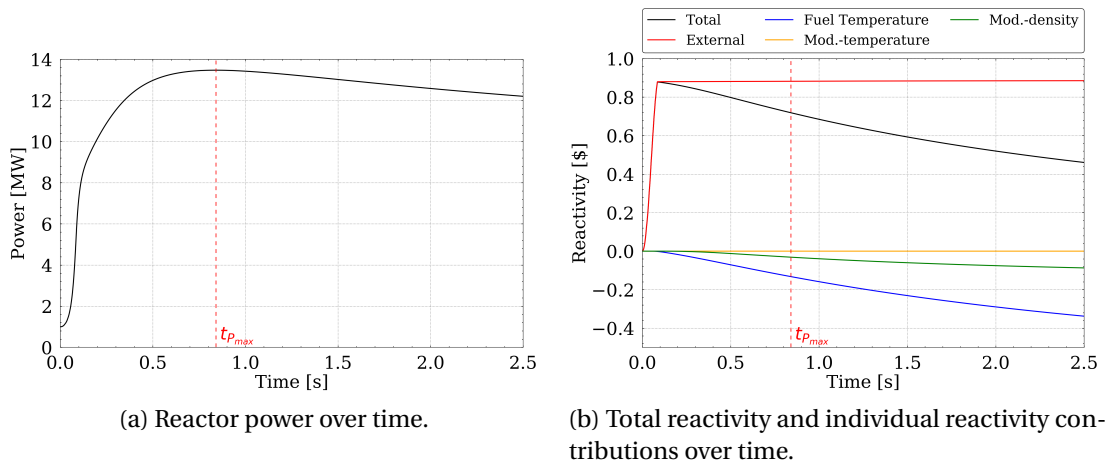


Figure 3.20: DYN3D-ATHLET results of *Test 79* under hot-standby conditions.

The calculation yields a reactivity insertion of 0.886\$ which is within one standard

Chapter 3. Applicability of Serpent/DYN3D-ATHLET for the analysis of SPERT III experiments

deviation of the experiment (Figure 3.20b). The calculated reactivity compensation of 0.164\$ at $t_{P_{max}}$ is significantly larger than the experimental value of 0.09\$. A possible explanation for this deviation may be that $t_{P_{max}}$ in the calculation is later than in the experiment and therefore the reactivity feedback from the Doppler effect has increased further and, in addition, that the decrease of the moderator density has then become an important contributor to the reactivity feedback.

Test 82 - high initial power under hot-standby condition

Test 82 had a reactivity insertion of 1.29 ± 0.04 \$ which was close to the upper permitted limit of 1.3\$ during this experimental programme. This limit was established to prevent mechanical damages to the fuel (McCardell et al., 1969). A maximum power of 880 ± 90 MW was measured at 0.118 ± 0.002 s.

The DYN3D-ATHLET calculation yielded a maximum power of 877 MW at 0.1246 s (Figure 3.21a). While the maximum power agrees well with the experimental value, the occurrence time of the maximum power is later than in the experiment.

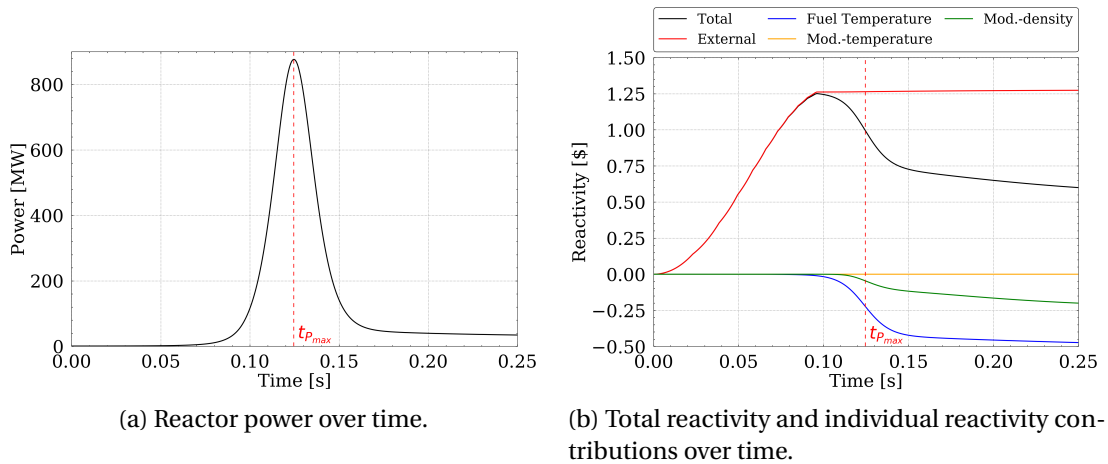


Figure 3.21: DYN3D-ATHLET results of Test 82 under hot-standby conditions.

The computed reactivity insertion is 1.276\$ (Figure 3.21b). At $t_{P_{max}}$, significant contributions to the reactivity feedback are observed from the Doppler effect and the moderator density decrease.

As an example for the course of the reactor period for a high-initial power test performed under hot-standby conditions, Figure 3.22 shows the reactor period derived from the calculated reactor power over time. The reactor period approaches a minimum value of 7.6 ms when the transient rod is fully withdrawn, which is at 0.096 s.

After this point, due to the presence of reactivity feedback, the reactor period increases instead of approaching an asymptotic value. At the occurrence time of the maximum power, the reactor period has a pole. It then becomes negative during the power decline. As has already been observed in *Test 43*, the reactor period shows oscillations during the power increase.

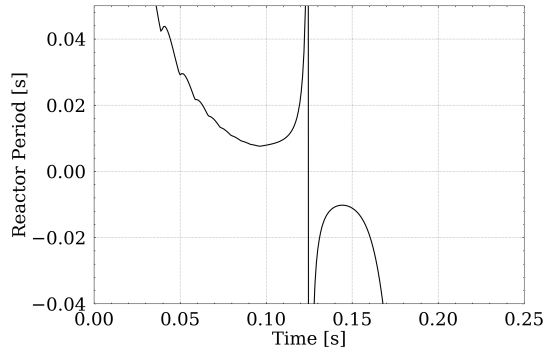


Figure 3.22: Reactor period calculated from reactor power over time of *Test 82*.

3.4 Summary and discussion

To prove the applicability of the code sequence Serpent/DYN3D-ATHLET for the analysis of transients in small reactor cores, four cold-startup and three hot-standby reactivity accident tests of the SPERT III E-core experimental programme were analysed. The selection of tests included delayed supercritical tests, prompt critical tests, and prompt supercritical tests. Parameterised two-group constants libraries generated from Serpent infinite-lattice and reflector models were used in transient calculations with the coupled NK/TH code system DYN3D-ATHLET. In addition, static nuclear core characteristics of the SPERT III E-core at cold-startup conditions were analysed with a detailed Serpent reference model, a static DYN3D nodal diffusion model, and with a simplified Serpent model that is consistent with the static DYN3D nodal diffusion model.

The static results from the Serpent reference model for the critical position of the control rod bank, the excess reactivities of both the control rod bank and the transient rod, and the effective point kinetic parameters are generally in very good agreement with the experimental values. The static DYN3D nodal diffusion model and the Serpent simplified model also match the experimental excess reactivities of both rod types well. In the static DYN3D model, the flux suppressors were replaced by an additional fuel follower part because of their complex structure. Therefore, the critical position of the control rod bank is much lower. It is in very good agreement with the critical position of the Serpent simplified model. Because of the fact that consistent results

Chapter 3. Applicability of Serpent/DYN3D-ATHLET for the analysis of SPERT III experiments

between the static DYN3D model and the Serpent simplified model were obtained, a good performance was also attributed to the Serpent infinite-lattice and reflector models.

The time-dependent behaviour of the DYN3D-ATHLET results—reactor power, total reactivity, individual contributions to the total reactivity—were analysed for the selected reactivity accident tests. Key figures were extracted from the DYN3D-ATHLET results and compared with experimental values (Table 3.10). For all tests, an excellent agreement for both the inserted reactivity and the maximum power with the respective experimental values was observed. The occurrence time of the maximum power lies for the majority of the tests within two standard deviations of the experimental time. It is notable that in case of the cold-startup tests (with the exception of the delayed supercritical test), the maximum power occurs earlier than in the experiment, while the opposite is observed for the hot-standby tests. A very good agreement was generally found between the calculated and the experimental reactivity compensation. The energy release until the occurrence time of the maximum power (not discussed for the individual tests) is for most of the prompt supercritical tests in very good agreement with the experimental value. For the delayed supercritical tests a deviation of up to three standard deviations was observed. In case of the cold-startup tests, the stable reactor period was determined by fitting a one-term exponential model to the calculated power over time. A good agreement was observed for the prompt critical and prompt supercritical tests, while for the delayed supercritical test a larger discrepancy of more than three standard deviations of the experimentally determined stable reactor period is found.

The general good agreement between the calculated and the experimental results proves the applicability of DYN3D-ATHLET in combination with two-group constants obtained with Serpent for the analysis of the reactor dynamic behaviour in the event of delayed supercritical, prompt critical, and prompt supercritical reactivity initiated accidents even for small reactor cores.

Table 3.10: Calculated and measured reactivity accident test results for cold-startup and hot-standby conditions. Values marked with * are reported as approximate due to uncertainties in initial reactivity insertions and occurrence times of maximum power (Olson, 2012).

Test		Inserted reactivity [\$]	Maximum power [MW]	Time at max. power [s]	Energy release [MJ]	Reactivity compensation [\$]	Reactor period [ms]
Test 18	Experiment	0.9 ± 0.04	4.3 ± 0.6	5.3 ± 0.1	6.7 ± 1.1	0.23 ± 0.03	351 ± 7
	DYN3D-ATHLET	0.88	4.83	5.33	8.2	0.265	381
Test 43	Experiment	1.21 ± 0.05	280 ± 42	0.23 ± 0.006	6.0 ± 1.0	0.22 ± 0.02	10.0 ± 0.2
	DYN3D-ATHLET	1.20	286	0.219	6.1	0.212	10.52
Test 48	Experiment	1.09 ± 0.04	63 ± 9	0.37 ± 0.01	2.8 ± 0.5	0.11 ± 0.01	21.1 ± 0.4
	DYN3D-ATHLET	1.091	68.8	0.35	3.10	0.111	21.95
Test 49	Experiment	1.00 ± 0.04	11 ± 2	0.97 ± 0.04	2.1 ± 0.4	0.08 ± 0.01	68.4 ± 1.4
	DYN3D-ATHLET	1.005	12.3	0.854	2.27	0.081	68.1
Test 79	Experiment	0.86 ± 0.03	13 ± 1	0.68 ± 0.08	6.7 ± 0.9	0.09 *	N/A
	DYN3D-ATHLET	0.886	13.5	0.841	9.46	0.164	N/A
Test 81	Experiment	1.17 ± 0.04	330 ± 30	0.135 ± 0.003	7.8 ± 1	0.18 *	N/A
	DYN3D-ATHLET	1.157	330	0.1404	8.2	0.162	N/A
Test 82	Experiment	1.29 ± 0.04	880 ± 90	0.118 ± 0.002	15 ± 2	0.3 *	N/A
	DYN3D-ATHLET	1.276	877	0.1246	12.9	0.27	N/A

4 Impact of nuclear data uncertainties in transient analysis

For stationary states, three-dimensional calculation models—neutron-kinetics and thermal-hydraulics—of a reactor core are commonly validated with measured data from a nuclear power plant. For example, the power distribution is measured using in-core power distribution detectors or the aeroball neutron flux measuring system. Reactivity worths of control rods are determined in the startup physics tests after refueling of a reactor core.

The situation is different when it comes to transient events that happen within a short period of time, i.e. milliseconds to minutes. Measured data are either non-existent or scarcely available, i.e. only for a particular type of both reactor and event, such as the reactivity accident tests performed during the SPERT III E-core experimental programme (see Chapter 3). Therefore, validations of NK/TH code systems cannot be easily performed due to the lack of experimental data for comparison. However, code-to-code comparisons provide the opportunity to compare developed methods and models for transient analysis. A useful framework for a code-to-code comparison is commonly offered by benchmarks. The experience gained in such benchmark activities stimulated the idea to accompany best-estimate calculations of transients with systematic uncertainty and sensitivity analyses (D'Auria et al., 2007). Uncertainties in the calculations can arise from the numerical methods and physical models used in the applied analysis tools, and they can arise from the uncertainties in the input data such as nuclear data, material parameters and geometry parameters (Ivanov et al., 2016).

In recent years, uncertainty quantification and sensitivity analyses (UQ/SA) with respect to nuclear data uncertainties were performed for a variety of different reactor transient calculations. For example, I. Pasichnyk studied the influence of nuclear data

Chapter 4. Impact of nuclear data uncertainties in transient analysis

uncertainties on a control rod ejection transient for a reactor core loaded with UO_2 and MOX fuel (Pasichnyk et al., 2013), and A. Dokhane analysed several SPERT III transients in the presence of nuclear data uncertainties (Dokhane et al., 2018a,b). In particular, Phase II of the *Benchmarks for Uncertainty Analysis in Modelling (UAM) for the Design, Operation and Safety Analysis of LWRs* (LWR-UAM) of the OECD/NEA has defined various reactor kinetic and dynamic problems to assess the impact of the input uncertainties on the outcome of coupled multi-physics calculations (Hou et al., 2014).

This chapter focuses on the impact of nuclear data uncertainties on the time series of response values of reactor transient calculations. By application of a random sampling approach, nuclear data uncertainties were propagated through the conventional two-step calculation sequence—generation of group constants with subsequent coupled NK/TH calculations—for the analysis of reactor transients. The UQ/SA analyses were performed for two reactivity initiated transients characterised by different control rod movements of a PWR mini-core model. The nuclide reactions that were the major contributors to the calculated reactor power uncertainty were revealed using sensitivity analysis. Due to the fact that such an analysis involves a large number of uncertain input parameters, statistically significant results were ensured with the application of a large sample size. To limit the computational burden of this UQ/SA, the model used for the analysis in this chapter is the TMI-1 mini-core model. It has a simple design and resembles a PWR in terms of the fuel assembly design.

In general, by using the random sampling approach for a UQ/SA analysis, the output realisations usually follow a particular distribution. Often, the assumption of a normal distribution is valid for most output quantities of interest and the analysis of the output variance can be performed via classical uncertainty measures such as the sample mean and the sample standard deviation. In this study, complete time series for particular quantities of interest were analysed and it was found that the distributional patterns¹ of the output samples vary across the problem time. For this reason, the Wilks tolerance limits (WTLs) were applied as a non-parametric (aka distribution-free) approach for the analysis of the uncertainty patterns of the time series.

In the following, a description of the TMI-1 mini-core model is provided and the studied control rod withdrawal transients with nominal reactivity insertions of 0.5\$ and 0.97\$, respectively, are described. The successive steps involved in the UQ/SA analysis of the reactor transients are outlined, in particular the application of the random sampling-based method XSUSA for the generation of the varied two-group

¹The term distributional patterns refers to the potential change in the parameterisation of a distributional type or the change in the distributional type itself.

constants. The applied uncertainty measures as well as the sensitivity index R^2 are explained. Finally, the output uncertainties of both the reactivity and the reactor power are discussed. Sensitivity analysis results are provided for the reactor power uncertainty.

Some methods and results presented in this chapter have been published as a journal paper (Aures et al., 2020a).

4.1 TMI-1 mini-core model and reactor transients

The TMI-1 mini-core model is specified as Case II-2b in Phase II of the LWR-UAM benchmark (Hou et al., 2014). The benchmark exercise is a purely neutron-kinetic transient in which the control rod is moved by only 5 cm. In contrast to the benchmark exercise, the two transients analysed in this study have larger withdrawal distances of the control rod and reactivity feedback mechanisms from the core thermal-hydraulics are taken into account.

4.1.1 TMI-1 mini-core model

The active part of the core consists of a 3×3 lattice filled with nine UO_2 fuel assemblies of identical type (Figure 4.1). The active length is approximately 365 cm. One row of radial reflector assemblies surrounds the active core. These reflector assemblies consist of a stainless steel shroud and water. Axial reflectors are not modelled. The central fuel assembly can be controlled with a control rod cluster made up of 16 AgInCd control rods.

The UO_2 fuel assemblies consist of 204 UO_2 fuel rods, 4 $\text{UO}_2+\text{Gd}_2\text{O}_3$ fuel rods, 16 guide tubes, and 1 instrumentation tube. The ^{235}U enrichment of both the UO_2 fuel and the $\text{UO}_2+\text{Gd}_2\text{O}_3$ fuel is 4.12 %. Moreover, the $\text{UO}_2+\text{Gd}_2\text{O}_3$ fuel consists of 2.00 wt.-% Gd. The material of the cladding tubes, the guide tubes, and the instrumentation tube is Zircaloy-4.

4.1.2 Reactor transients

In the first transient, hereafter referred to as *Transient 1*, the control rod is moved by 54 cm, and in the second, hereafter referred to as *Transient 2*, by 60 cm. These particular choices of withdrawal distances allow the analysis of two characteristically different transient evolutions: with nominal nuclear data, the reactivity insertion of *Transient 1* is delayed supercritical whereas the reactivity insertion of *Transient 2* is

	Refl	Refl	Refl	Refl	Refl
C	Refl	UO ₂	UO ₂	UO ₂	Refl
B	Refl	UO ₂	UO ₂ CR	UO ₂	Refl
A	Refl	UO ₂	UO ₂	UO ₂	Refl
	Refl	Refl	Refl	Refl	Refl
		1	2	3	

Figure 4.1: Layout of the TMI-1 mini-core model composed of 'UO₂': uncontrolled fuel assemblies, 'UO₂ CR': controlled fuel assembly and 'Refl': reflector assemblies (Hou et al., 2014).

close to the prompt critical state. The transient calculations start with a 2 s long *zero-transient*. In this phase, the neutron-kinetics are fixed, so that the thermal-hydraulic calculation can reach a converged state first. The *zero-transient* is then followed by another phase of 2 s in which also the neutron-kinetics can change over time. After these two phases, the control rod is withdrawn from its fully inserted position within 10 s, and, within the next 20 s, it is moved back to the fully inserted position. The control rod positions as a function of time are shown for both reactor transients in detail in Figure 4.2.

The following initial conditions were set for both transients: a fuel temperature of 560 K, a moderator density of 0.75206 g/cm³, and a reactor power of 0.1409 MW. Furthermore, the critical boron concentration was evaluated as a prior step to the actual NK/TH calculation so that the reactor core model was critical in the initial state of the transients.

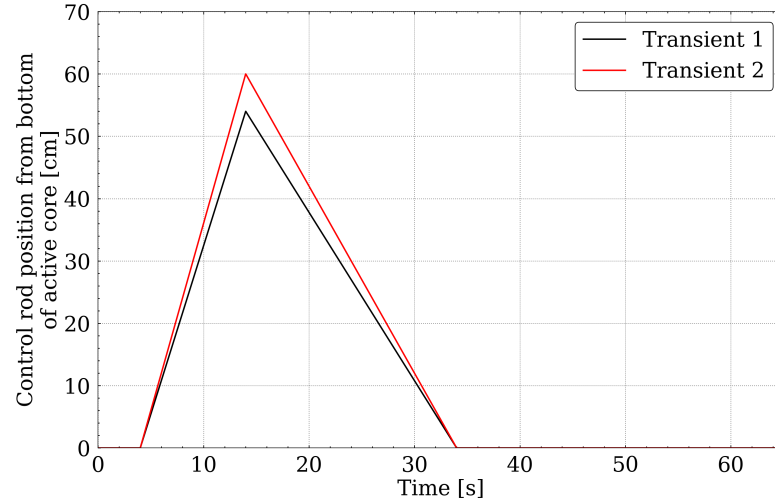


Figure 4.2: Control rod position as a function of time for the studied transients.

4.2 Methods and tools

The transient calculations in this study followed the conventional two-step approach, namely, first, the generation of group constants and, second, the coupled NK/TH calculations. Through the fact that this scheme consists of calculations that build on one another, the random sampling approach easily allows the propagation of nuclear data uncertainties through the transient calculations.

The overall analysis involved the following successive steps:

1. the generation of randomly sampled group constants sets along with kinetic parameters for the assembly types loaded in the core parameterised with respect to thermal-hydraulic parameters;
2. the execution of coupled NK/TH calculations on the basis of the randomly sampled group constants sets;
3. the uncertainty and sensitivity analysis on the resulting output data.

Details on the different steps are provided in the following sections. Beside the transient calculations with the varied group constants, both transients were also calculated with the nominal group constants.

4.2.1 Generation of randomly sampled two-group constants with XSUSA and SCALE

The generation of varied two-group constants along with kinetic parameters was carried out with the random sampling-based method XSUSA in combination with the lattice physics sequence TRITON/NEWT of the SCALE 6.1 code package. Correspondingly, the ENDF/B-VII.0 238-group cross section library and the 44-group covariance library of the SCALE 6.1 code package were used.

First, by means of the core simulator KMACS, two-dimensional TRITON/NEWT models were built for the UO_2 fuel assembly and for the reflector. While the UO_2 fuel assembly model is an infinite-lattice model, the reflector model consists of two regions: one region is the reflector consisting of water and the stainless steel shroud, and the other region contains the uncontrolled UO_2 fuel assembly. The purpose of the fuel assembly region is to establish a neutron flux in the reflector region, but the group constants are only generated for the reflector region. Except for the outer boundary of the reflector region, which is specified with a vacuum boundary condition, all other outer boundaries are reflective.

The individual steps for the generation of the varied group constants are shown in the flow diagram in Figure 4.3. Random sampling with a sample size of $N = 1,000$ was performed using covariance data to obtain relative variations for the cross sections, the prompt neutron multiplicities, the delayed neutron multiplicities (average number of delayed neutrons per fission), and the fission spectra. These relative variations were applied to the nominal self-shielded MG cross section libraries generated for the K assembly types with a parameterisation over L thermal-hydraulic conditions (Table 4.1). Finally, lattice calculations were performed on the basis of the varied self-shielded MG cross sections to obtain the varied group constants.

The fact that within the XSUSA approach the variations are applied after the self-shielding calculations (see Section 2.7) offers the advantage of a considerable saving in calculation time, particularly in such UQ/SA analyses at which the computational effort significantly increases with the sample size, the number of assembly types, and the number of thermal-hydraulic conditions.

The reactor dynamic behaviour is influenced by the delayed neutron fraction, which in turn depends on the delayed neutron multiplicities. Therefore, in UQ/SA analyses of reactor transients, the uncertainty of the delayed neutron multiplicity should also be taken into account in the generation of the group constants. The 44-group covariance library of the SCALE 6.1 code package used in this analysis, however, does not include individual uncertainties of both the prompt and the delayed neutron multiplicities,

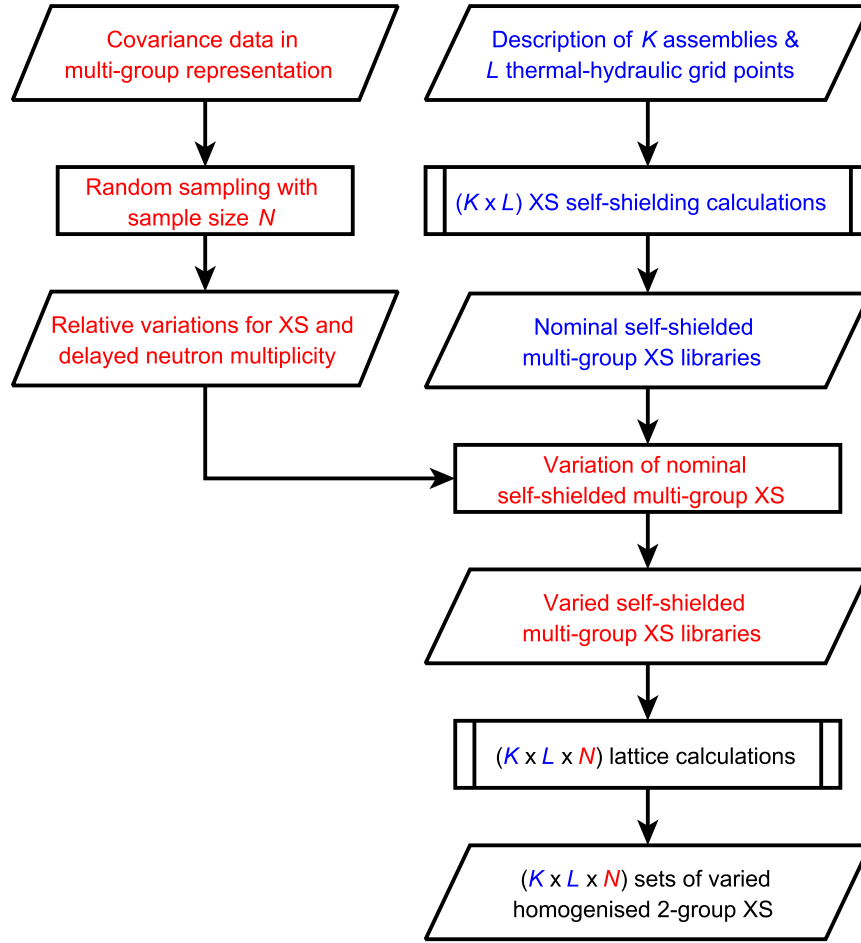


Figure 4.3: Generation of varied two-group constants (XS) sets by combination of the cross section random sampling-based method XSUSA (red) with the lattice calculation sequence TRITON/NEWT of SCALE 6.1 (blue), with K : number of assembly types, L : number of thermal-hydraulic conditions, and N : sample size.

but only of the total multiplicities. Because the total neutron multiplicity and the prompt neutron multiplicity have almost identical uncertainties, the uncertainties of the total neutron multiplicities were applied only to the prompt neutron multiplicities, and uncertainties for the delayed neutron multiplicities were additionally taken from the covariance data of the JENDL-4.0 (Shibata et al., 2011) library (Aures et al., 2017c). For this purpose, the covariance data were first processed with the nuclear data processing system NJOY (MacFarlane and Kahler, 2010) and then converted into a 44-group library with energy group boundaries according to the SCALE 6.1 covariance library.

It shall be noted that with SCALE 6.2 a more modern covariance library mainly based

Chapter 4. Impact of nuclear data uncertainties in transient analysis

Table 4.1: Thermal-hydraulic parameters used for the parameterisation of the group constants.

Fuel temperature [K]	Moderator density [g/cm ³]	Boron concentration [ppm]
560	0.66114	0
900	0.71187	1000
1320	0.75206	2000

on the ENDF/B-VII.1 nuclear data library with 56 energy groups is available. One of the main differences is a substantial reduction of the uncertainty of the ^{239}Pu neutron multiplicity. Recent studies showed that for a model without plutonium the differences between the UQ results obtained with the SCALE 6.2 library and UQ results obtained with the SCALE 6.1 library are minor (Aures et al., 2017b). Since the TMI-1 mini-core model does not contain plutonium, the application of the older 44-group covariance library is regarded as justified.

4.2.2 Transient analyses with DYN3D-ATHLET

For both reactor transients, N coupled NK/TH calculations were performed with DYN3D-ATHLET. As illustrated in Figure 4.4, the sample NK/TH calculations differ only in terms of the group constants library due to the variation of the cross sections, but not in terms of the NK/TH calculation model.

The core simulator KMACS was applied to generate the DYN3D nodal diffusion model, the ATHLET thermal-hydraulic model, and the appropriately formatted group constants libraries of the N sample cases.

The DYN3D nodal diffusion model has a radial mesh size that corresponds to the width of one fuel assembly. In the axial direction, the mesh is subdivided in 16 layers. The time step size for the neutron flux integration is automatically adapted in the range $10^{-5} \text{ s} - 10^{-2} \text{ s}$, but the time step size of the thermal-hydraulic calculation is not exceeded. The ATHLET thermal-hydraulic model simulates only the thermal-hydraulics of the core. Every fuel assembly is modelled with an individual fluid channel with fixed boundary conditions, i.e. the inlet temperature, the outlet pressure, and the mass flow are constant. The inlet temperature is 560 K, the outlet pressure is 15.5 MPa, and the core mass flow is 816.10 kg/s. Cross connections between the fluid channels are not modelled. The time step size for the integration is automatically adapted by the code but limited to a maximum of $5 \cdot 10^{-4} \text{ s}$ in the power excursion phase.

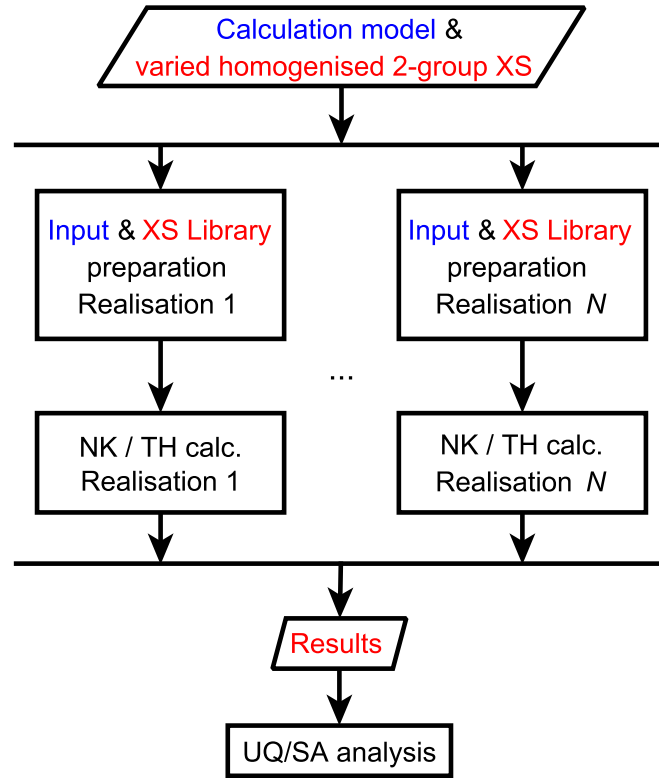


Figure 4.4: Performance of N NK/TH calculations with the varied two-group constants libraries (XS Library), followed by UQ/SA analysis of the N resulting data sets.

4.3 Uncertainty analysis

In order to quantify the impact of the nuclear data uncertainties on the transient calculations, the N resulting output data sets of the transient calculations are statistically analysed with respect to the quantities of interest reactor power and reactivity.

For the estimation of the uncertainties, two different approaches were followed: i) basic uncertainty measures—mean value, standard deviation, and median value—were determined, thereby assuming as a first order approach a normal distribution for the output data; ii) the determination of non-parametric (aka distribution-free) tolerance limits (TLs) because the assumption of a particular type of distribution underlying the output data is often not fulfilled for the entire problem time of such transient calculations.

Descriptions on the applied uncertainty measures are provided in the following.

4.3.1 Normally distributed data

If y_1, \dots, y_N form a sample of independent output values (i.e. realisations) determined for the uncertain output variable Y in N calculations, the sample mean \bar{y} as an indicator of the centrality and the sample standard deviation \bar{s} as an indicator of the dispersion can be calculated as follows:

$$\bar{y} = \frac{1}{N} \sum_{i=1}^N y_i \quad \text{and} \quad \bar{s} = \sqrt{\frac{1}{N-1} \sum_{i=1}^N (y_i - \bar{y})^2}. \quad (4.1)$$

If the output variable Y follows a normal distribution, it is possible to estimate the probability of output values lying within a certain interval symmetric around the sample mean. This empirical uncertainty interval is defined via

$$\bar{y} \pm k \cdot \bar{s}, \quad (4.2)$$

with the parameter k derived for a demanded probability from a standard normal distribution. For example, $k = 1.96$ for a probability of 95%, which means that 95% of the output realisations lie within the interval $\bar{y} - 1.96 \cdot \bar{\sigma} < \bar{y} < \bar{y} + 1.96 \cdot \bar{\sigma}$. Often, $k = 2$ is used which corresponds to a probability of slightly more than 95% (Arens et al., 2012). In this context the term proportion may be more appropriate than the term probability.

The sample median is the value that separates the output values of the sample in two halves, provided that the values have been ordered by increasing size before. It therefore indicates the middle of an output data set. The median of the ordered output values $y_{(1)}, \dots, y_{(N)}$ (index in parentheses indicates the ordered values) of a sample with the size N is defined as:

$$y_{med} = \begin{cases} y_{(\frac{n+1}{2})}, & \text{for odd } n, \\ \frac{1}{2} \left(y_{(\frac{n}{2})} + y_{(\frac{n}{2}+1)} \right), & \text{for even } n. \end{cases} \quad (4.3)$$

In contrast to the sample mean, the sample median is resistant against a small proportion of extreme outliers and therefore depicts a robust estimate of the centrality of the sample.

4.3.2 Non-parametric tolerance limits

In general, TLs characterise a lower limit L and an upper limit U of an interval $[L, U]$ that encloses a proportion of at least β percent of an output sample (y_1, \dots, y_N) of an uncertain variable Y at a confidence level of at least γ . A general definition for a two-sided TL (i.e. a tolerance interval enclosed by L and U) can be given by the nested probability expression (Kloos and Berner, 2017):

$$P(P(Y \in [L, U]) \geq \beta) \geq \gamma. \quad (4.4)$$

Since the sample size is finite, the TLs vary from sample to sample. This variability is considered by the statistical confidence level γ . In this way, the confidence level γ indicates the probability of all samples with the same sample size N for which the respective tolerance intervals enclose a proportion of at least β percent. The parameter β is called coverage probability or tolerance proportion. A one-sided upper TL can be defined by choosing $L \rightarrow -\infty$ for the lower TL, and analogously, a one-sided lower TL is defined by $U \rightarrow \infty$ for the upper TL (Krzykacz, 1990). Generally, TLs are dependent on the sample size N , the coverage probability β , and the confidence level γ .

TLs as uncertainty estimators for an uncertain variable can be derived by either making the assumption of a particular distribution underlying the output sample, for example, a normal distribution, or with approaches that do not require the assumption of a particular distribution (Glaeser et al., 2008). Since this study aims for the uncertainty analysis of time series of response values for which the assumption of a particular distribution may not be valid for the entire problem time, the approach of Wilks for the determination of non-parametric TLs was applied.

The Wilks TLs (WTLs) (Wilks, 1942; Wald, 1943; Porter, 2019) are based on the idea that calculations may be seen as independent trials of an experiment with an underlying unknown continuous distribution. With a given success probability, each trial results either in success or in failure as captured by the Binomial distribution. In the case of WTLs, a success is seen as a calculation output falling with a certain confidence level γ into an interval with a success probability related to the coverage probability β .

Let y_1, \dots, y_N be output values of an uncertain variable Y . When they are ordered by increasing size, the indication $y(l)$ with l as the index of the ordered values is used. The minimum and the maximum of the sample are then defined via:

$$y(1) = \min\{y_1, \dots, y_N\} \quad \text{and} \quad y(N) = \max\{y_1, \dots, y_N\}. \quad (4.5)$$

Chapter 4. Impact of nuclear data uncertainties in transient analysis

With the definition of the boundary values $y(0) = -\infty$ and $y(N+1) = +\infty$, the confidence level γ can be analytically determined through the Binomial distribution as given by

$$\gamma \leq \sum_{j=0}^{s-r-1} \binom{N}{j} \cdot \beta^j \cdot (1-\beta)^{N-j} \quad (4.6)$$

with ranking $0 \leq r \leq s \leq N$, and lower TL $L = y(r)$ and upper TL $U = y(s)$.

In a first approach, the WTLs offer the useful feature to determine the minimum sample size that is necessary to derive either one-sided or two-sided WTLs for a demanded set of (β, γ) . This feature is, for example, useful in the context of uncertainty analyses that rely on time-expensive calculations. If the parameters are set to $r = 1$ and $s = N$, Eq. 4.6 takes the form

$$1 - \beta^N - N(1 - \beta)\beta^{N-1} \geq \gamma, \quad (4.7)$$

from which the minimum sample size N can be computed so that $L = y(1)$ and $U = y(N)$, i.e. the sample extremes, form a two-sided WTL for a particular set of (β, γ) . In a similar manner, with $r = 0$ and $s = N$, Eq. 4.6 takes the form

$$1 - \beta^N \geq \gamma, \quad (4.8)$$

from which the minimum sample size for a one-sided, upper WTL given by $U = y(N)$ can be determined. (Krzykacz, 1990)

Another approach is offered by the WTLs in case the sample size N is fixed and a particular set (β, γ) is demanded. Then, either the indices r and s for a two-sided WTL with $L = y(r)$ and $U = y(s)$ or only the index s for a one-sided, upper WTL with $U = y(s)$ can be computed. In this study, a sample size of 1,000 was applied in the UQ/SA analyses of both transients. The two-sided (95 %, 95 %) WTL for $N = 1,000$ is then defined through the 19th lowest and the 982nd highest value of the ranked output values, i.e. $[y(19), y(982)]$, with an actual confidence level $\gamma = 0.957$. The one-sided, upper (95 %, 95 %) WTL is given by the 962nd highest value. It should be noted that when analysing the uncertainty pattern of time series by application of WTLs, the output values must be ranked at every time step.

The sample size of 1,000 used in this study is much larger than the sample sizes often found in the literature, for example, $N = 59$ for a one-sided, upper (95 %, 95 %) WTL or $N = 93$ for a two-sided (95 %, 95 %) WTL (Krzykacz, 1990). The sample size determines the degree of the variability of the WTLs, i.e. the conservativity or, conversely, the precision of the estimated WTL. This behaviour is illustrated in the following by means of the conservativity profiles of the WTLs, but it is also shown for different sample

sizes of the output sample of *Transient 2* in Appendix A. For a one-sided, upper WTL, the relationship between β and γ is given by

$$\gamma = 1 - \beta^N, \quad (4.9)$$

which depicts the conservativity profile and yields the respective complementary cumulative distribution function (ccdf) at the same time. The upper plot in Figure 4.5 shows conservativity profiles determined with Eq. 4.9 for selected WTLs that match $(\beta, \gamma) = (95\%, 95\%)$.

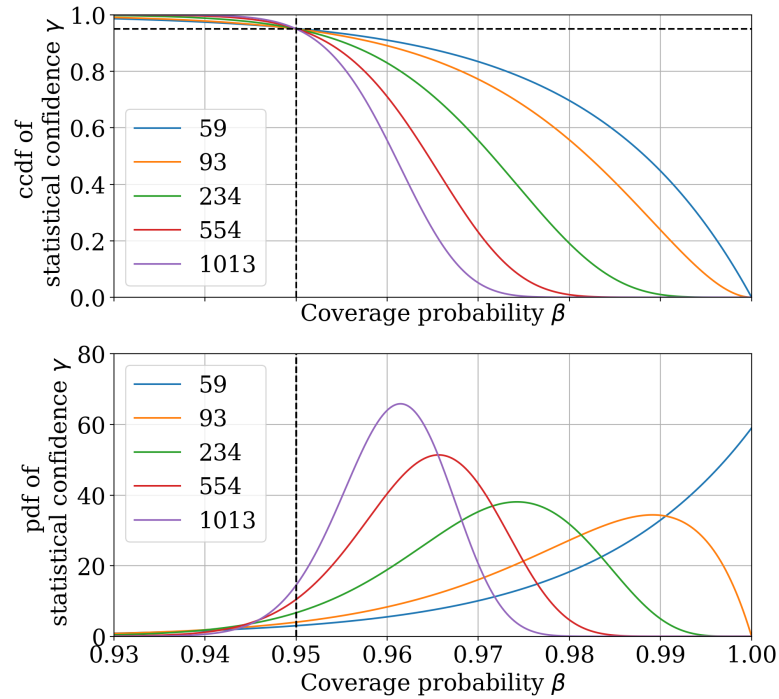


Figure 4.5: Conservativity profiles of the one-sided, upper Wilks Tolerance Limit of coverage probability $\beta = 0.95$ and statistical confidence level $\gamma = 0.95$ for varying sample sizes N . The profiles are presented via the complementary cumulative distribution function (ccdf) and via the probability density function (pdf).

From these conservativity profiles, it can be seen at which confidence level γ the WTL exceeds a certain proportion β . For instance, for $N = 59$, the WTL covers a proportion of at least 95% at a confidence level of at least 95%, but at the same time it covers also a proportion of at least 99% at a confidence level of at least 45%. In other words, in 45% of the cases, the WTL exceeds a proportion of 99% (Glaeser et al., 2008). Moreover, there is also a confidence of 5% (from $1 - \gamma$) that a proportion of less than 95% is covered by the WTL, and at the same time, the same is true for a confidence of 2.6% and a proportion of 94%. For a particular $\beta \geq 0.95$, the confidence level γ decreases as the sample size increases. This means that the estimate of the WTL becomes more

precise, i.e. less conservative. The probability density functions given in the lower plot of Figure 4.5 depict that the accuracy of estimating the target β on average increases with an increasing sample size.

4.4 Sensitivity analysis

The identification of the major contributors of the varied input parameters groups, i.e. varied nuclide cross sections, to the output variance, in this case the variance of the reactor power, can be performed by the determination of the squared multiple correlation coefficient R^2 . The R^2 coefficient of each parameter group is calculated from correlations between the output quantity and the sampled input parameters of the respective group, while taking into account correlations between these input parameters. In this way and under the assumption of linearity, the R^2 coefficient states the relative amount of the output variance resulting from uncertainties of an input parameter group including the fraction of uncertainties due to dependencies with other input parameter groups (Glaeser et al., 2008; Bostelmann et al., 2018). From the calculation of the R^2 coefficients for all possible input parameter groups and their ranking in size, the major contributors to the output variance can be found.

For instance, let an input parameter be represented as a cross section Σ_i in MG representation for $i = 1, \dots, k$. The parameter k is the number of independently sampled parameters of this group, i.e. $k \leq \text{number of energy groups}$. The reason why k may be smaller than the number of energy groups is the presence of dependencies between the parameters of a group. The R_j^2 for the variance of the reactor power P resulting from an input parameter group $\Sigma(j)$ is calculated as follows:

$$R_j^2 = (\rho(P, \Sigma_1), \dots, \rho(P, \Sigma_k)) \cdot C_{\Sigma(j)}^{-1} \cdot \begin{pmatrix} \rho(P, \Sigma_1) \\ \vdots \\ \rho(P, \Sigma_k) \end{pmatrix},$$

whereas $\rho(P, \Sigma_i)$ refers to the sample Pearson correlation coefficient between the reactor power P and the cross section Σ_i , and $C_{\Sigma(j)}^{-1}$ refers to the inverse of the sample correlation matrix with size $k \times k$ containing the sample Pearson correlation coefficients between the sampled input parameters Σ_i of the input parameter group $\Sigma(j)$.

The R^2 coefficient exhibits the following properties (Glaeser et al., 2008; Bostelmann, 2020):

- $0 < R_j^2 < 1$, the above given explanation applies,

4.5. Uncertainty and sensitivity analysis results

- $R_j^2 = 0$, if the uncertain variable, here P , is not linearly correlated to any of the sampled input parameters of the group $\Sigma(j)$,
- $R_j^2 = 1$, if the uncertain variable, here P , is fully linearly correlated to only the sampled input parameters of the group $\Sigma(j)$, and
- $R_j^2 = \rho(P, \Sigma(j))^2$, if the input parameter group $\Sigma(j)$ only consists of a single parameter; the R_j^2 coefficient then corresponds to the squared sample Pearson correlation coefficient.

The calculation of R^2 requires an input sample size that is significantly larger than the number of independent input parameters in the considered group.

Beside the determination of R_j^2 coefficients for each individual input parameter group $\Sigma(j)$, in principle a total R^2 coefficient can be determined from a parameter group that contains all the input parameters of the model under investigation. The total R^2 then allows the conclusion whether the output variance is influenced by non-linear effects: this applies if the total R^2 shows a significant deviation from 1.

However, in the case of nuclear data uncertainty propagation, the total number of input parameters can be very large. For example, in case the neutron transport calculations are performed with 50 or more nuclides and there are 2 to 10 reactions per nuclide, and the microscopic cross sections are discretised in 44 energy groups, the number of input parameters may be about 20,000 and the number of independent parameters may be in the order of 10,000. Consequently, the analysis of the total R^2 would require a sample size that may be impractical for computationally-intensive calculations.

4.5 Uncertainty and sensitivity analysis results

The UQ/SA analyses for both reactor transients *Transient 1* and *Transient 2* were performed with a sample size of 1,000. The results of the NK/TH calculations with the varied two-group cross sections were statistically analysed with respect to the quantities of interest reactivity and reactor power. Reactivity refers to the dynamic reactivity calculated by DYN3D (see Section 2.4). First, the uncertainty analysis results for the reactivity and the reactor power are presented. Afterwards, the results of the sensitivity analysis for the reactor power uncertainty are outlined.

4.5.1 Uncertainty analysis of the critical boron concentration

The NK/TH calculation of each input sample realisation started with the evaluation of the critical boron concentration to force the reactor model into the critical state before the transient is initiated. The application of the varied group constants resulted in a different critical boron concentration for each realisation. Figure 4.6 illustrates for *Transient 1* the distribution of the critical boron concentration of the complete sample, and the estimated normal distribution $\mathcal{N}(\hat{\mu}, \hat{\sigma}^2)$ characterised with the sample mean value $\hat{\mu} = 1252$ ppm and the sample standard deviation $\hat{\sigma} = 56$ ppm.

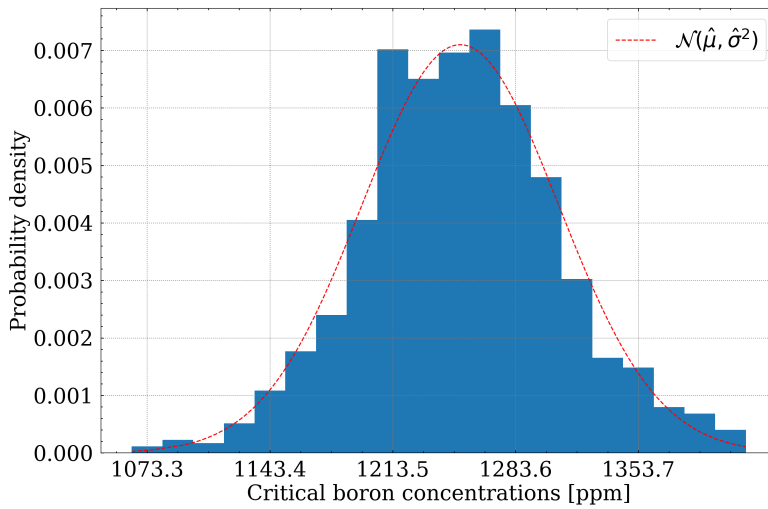


Figure 4.6: Distribution of the critical boron concentration at the initial state of *Transient 1* and the estimated normal distribution $\mathcal{N}(\hat{\mu}, \hat{\sigma}^2)$ with $\hat{\mu} = 1252$ ppm and $\hat{\sigma} = 56$ ppm.

A critical boron concentration of 1251 ppm was obtained by the nominal calculation. The results are identical for *Transient 2* because both transient scenarios differ only in terms of the removal distance of the control rod position.

4.5.2 Uncertainty analysis of Transient 1

Figure 4.7 shows the development of the reactivity over time for both the nominal calculation and the sample calculations. The maximum reactivity of the nominal calculation is 0.508\$ occurring at a time of 14.005 s. The mean of the sample calculations approaches a maximum of 0.51\$ with a relative 1σ -uncertainty of 8.26%. It occurs at the same time as in the nominal calculation.

The trends of the nominal reactor power, and of the mean and the median of the reactor power from the sample calculations are presented in Figure 4.8.

4.5. Uncertainty and sensitivity analysis results

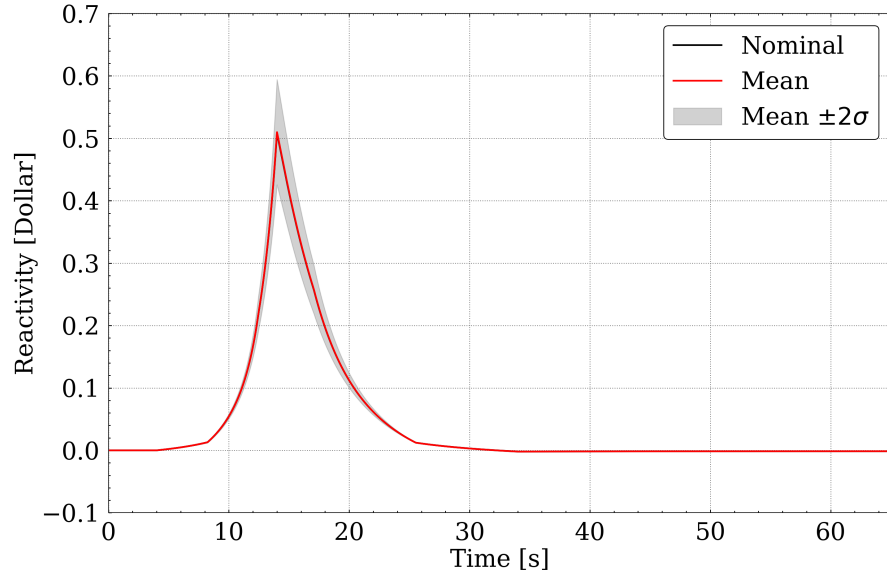


Figure 4.7: Nominal reactivity and sample mean reactivity with 2σ -uncertainty interval for *Transient 1*. It should be noted that the sample mean curve coincides with the nominal curve.

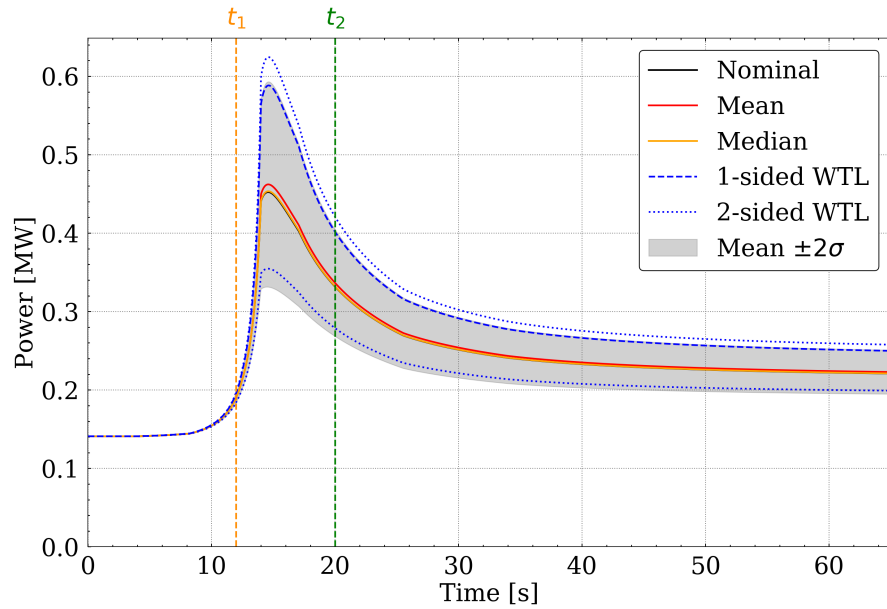


Figure 4.8: Nominal power, and mean, median, 2σ -uncertainty interval and the one-sided (95%,95%) WTL and the two-sided (95%,95%) WTL of the power output sample for *Transient 1*. The marked time points t_1 and t_2 are used for the investigation of the distributional patterns of the power output sample.

Chapter 4. Impact of nuclear data uncertainties in transient analysis

The nominal power encounters a maximum of 0.452 MW at 14.595 s, and afterwards, it gradually decreases and reaches a value of 0.221 MW at 65 s. The sample median has a trend very similar to the nominal output. The sample mean, in particular its maximum, lies above the sample median. The maximum of the sample mean is 0.462 MW and it occurs at the same time as the maximum of the nominal calculation. Afterwards, it shows a gradual decrease to a value of 0.223 MW.

For comparison purposes, Figure 4.8 shows also the trends of the 2σ -uncertainty interval for normally distributed output values, and the one-sided, upper (95%, 95%) WTL and the two-sided (95%, 95%) WTL as non-parametric TLs. The two-sided WTL encloses almost the same proportion as the 2σ -confidence interval, but it is shifted towards larger power values, particularly at the maximum. This behaviour of the two-sided WTL is in compliance with the conservativity profile (see Figure 4.5) indicating a relatively high conservativity of the applied non-parametric TLs. The one-sided WTL lies below the two-sided WTL, but still encloses the 2σ -uncertainty interval.

As can be seen from Figure 4.9, the distribution of the power output values from the sample calculations is subject to variability across the problem time. Visual inspection reveals that the power output values at t_1 appear to be normally distributed, whereas at t_2 the distribution of these values is obviously right-skewed.

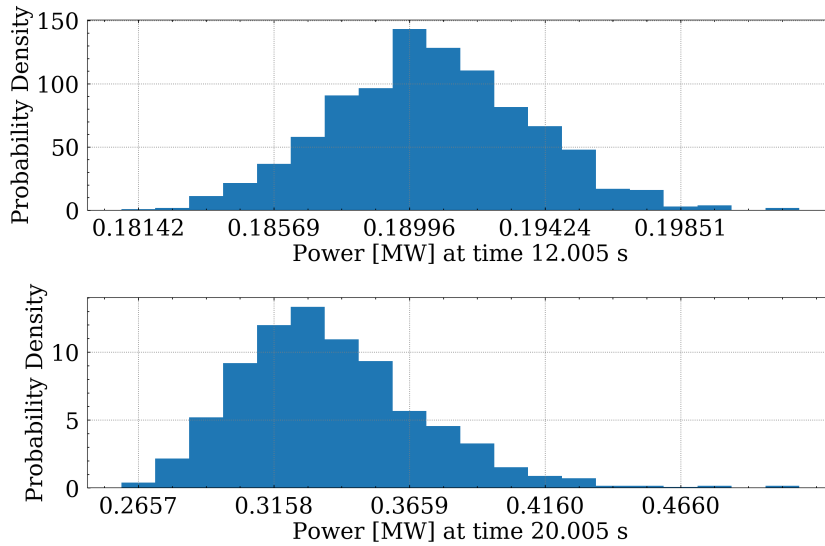


Figure 4.9: Distributions of the power output sample shown in Figure 4.8 at the time points $t_1 = 12.005$ s (top, yellow in Figure 4.8) and $t_2 = 20.005$ s (bottom, green in Figure 4.8) for *Transient 1*.

To confirm any deviation from the assumption of a normal distribution, the Anderson-Darling test statistic (Anderson and Darling, 1952) with a significance level of 5% was

4.5. Uncertainty and sensitivity analysis results

carried out for the power output sample as well as for the reactivity output sample at each time step of the respective time series. The test statistics along with the control rod position are shown in Figure 4.10 as a function of time. The hypothesis test provides statistical evidence that the distribution of the power output values at individual time steps after about 13 s is not a normal distribution. Because of this and the observation that the distribution is skewed, the symmetric 2σ -uncertainty interval may not be an appropriate uncertainty measure and the one-sided or two-sided WTL must be applied instead. The reactivity output sample does not follow a normal distribution at individual time steps after about 24 s. Since this time point comes significantly after the maximum, the application of the 2σ -uncertainty interval in this case is considered acceptable.

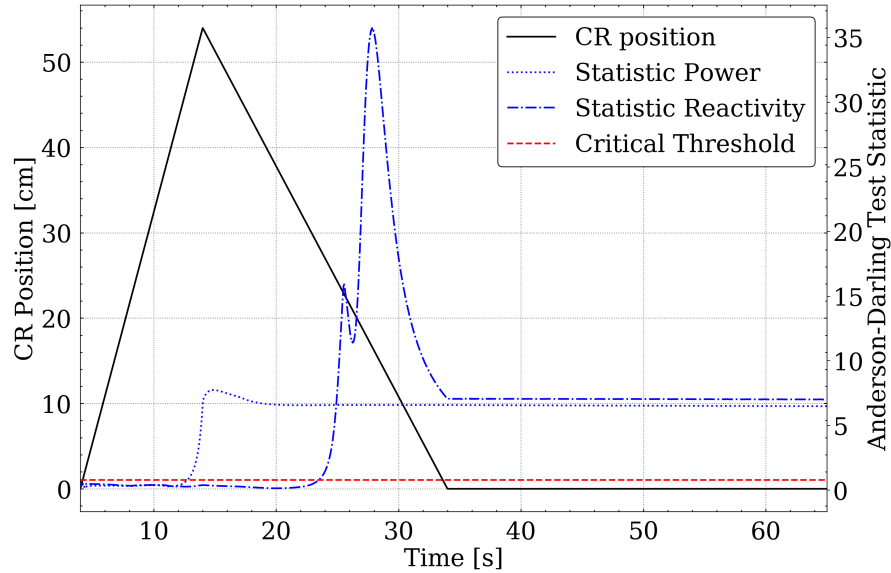


Figure 4.10: Development of the control rod (CR) position and the Anderson-Darling test statistics of both the power output sample and the reactivity output sample, all of *Transient 1*, compared to the critical threshold for power and reactivity, i.e. sign.-level: 5%, normal distribution.

4.5.3 Uncertainty analysis of Transient 2

As shown in Figure 4.11, the reactivity of the nominal calculation has a maximum of 0.967\$ and the mean of the reactivity output sample approaches a maximum of 0.953\$ with a relative uncertainty of 6.38%. The occurrence time of the maximum is in both cases 14.005 s.

In some realisations of the sample calculations, the reactivity exceeds prompt criticality and therefore causes a significant rise in power. This behaviour leads to an

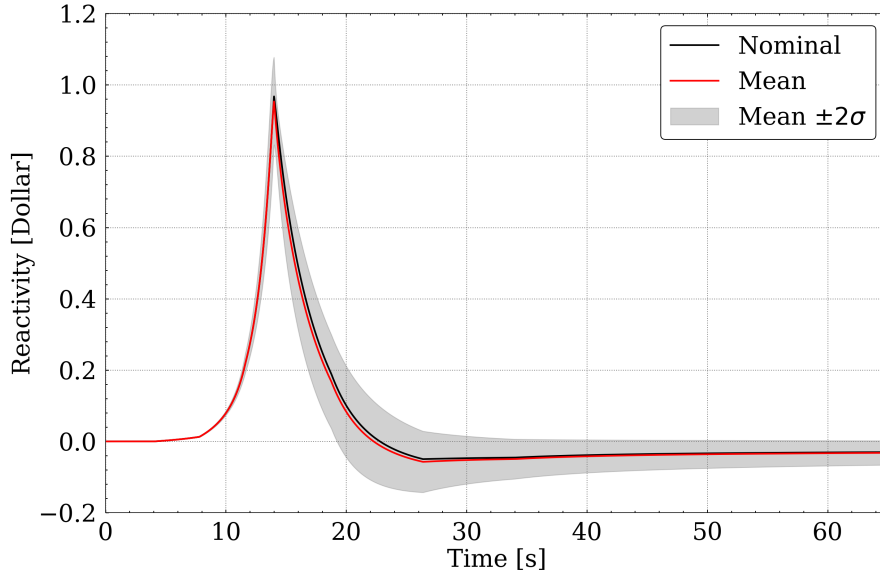


Figure 4.11: Nominal reactivity and sample mean reactivity with 2σ -uncertainty interval for *Transient 2*.

extremely asymmetrical distribution of the power curves at almost all time points of the entire time series. A simple calculation yields a relative standard deviation of 133.72% at the maximum of the sample mean of the power. The strong asymmetry of the distribution along with the large standard deviation rendered the application of uncertainty measures that rely on normally distributed data completely useless in this case. For this reason, instead of the 2σ -uncertainty interval, the one-sided, upper (95 %, 95 %) WTL was evaluated. The two-sided WTL was not considered for this transient because the interest is typically on maximum values in the context of transient safety analysis.

The development over time of the nominal reactor power as well as the mean, the median and the one-sided, upper WTL for the reactor power of the sample calculations are shown in Figure 4.12. The power of the nominal case encounters a maximum of 15.99 MW at 14.26 s. It then decreases to 1.85 MW during the power reversal phase. The sample mean has a maximum of 38.36 MW and the median has a maximum of 16.7 MW. The significant difference between the mean and the median in this case, especially at the time of the maximum, indicates a skewed distribution of the power output sample caused by substantial outliers among the output realisations. The maximum of the sample mean occurs at 14.045 s which is earlier than in the nominal case. The fact that there is a difference in the occurrence times is in contrast to the observation made in *Transient 1*. The light blue area between the lower limit of 0.0 MW and the upper limit given by the one-sided, upper WTL shows the value range that

4.5. Uncertainty and sensitivity analysis results

covers at least 95% of the output realisations at a confidence level of at least 95%. The maximum of the WTL is 189.20 MW at 14.015 s.

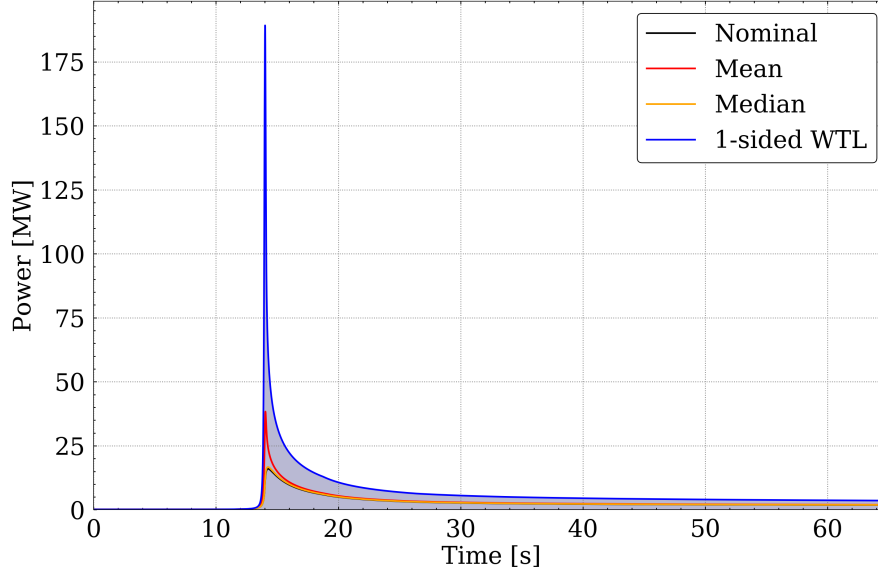


Figure 4.12: Nominal power, and mean, median and one-sided, upper (95%, 95 %) WTL of the power output sample for *Transient 2*.

The central plot in Figure 4.13 again shows the trend of the WTL within the variation of the 1,000 power output realisations (light-grey) of the sample for the time interval 13.6 s – 14.6 s. In addition, Figure 4.13 also shows histograms of the distributions determined of the power maxima as well as of their respective occurrence times. While some realisations reach a maximum power of more than 200 MW, the majority of the output realisations only reach a moderate maximum power. A bimodal distribution is observed for the occurrence times of the power maxima. One mode occurs between the maximum of the nominal case and the maximum of the sample case, and the other mode occurs around 14.6 s.

4.5.4 Sensitivity analyses of Transient 1 and Transient 2

For *Transient 1* and *Transient 2*, the major contributors of the varied nuclide cross sections to the power uncertainty were identified through the calculation of the squared multiple correlation coefficients R^2 (see Section 4.4).

For *Transient 1*, Figure 4.14 shows the development of the R^2 coefficients of the major contributors to the power uncertainty for the time interval 4.515 s – 24.365 s enclosing the control rod movement. In addition, significance bounds and confidence intervals for the R^2 coefficients as calculated with XSUSA are shown.

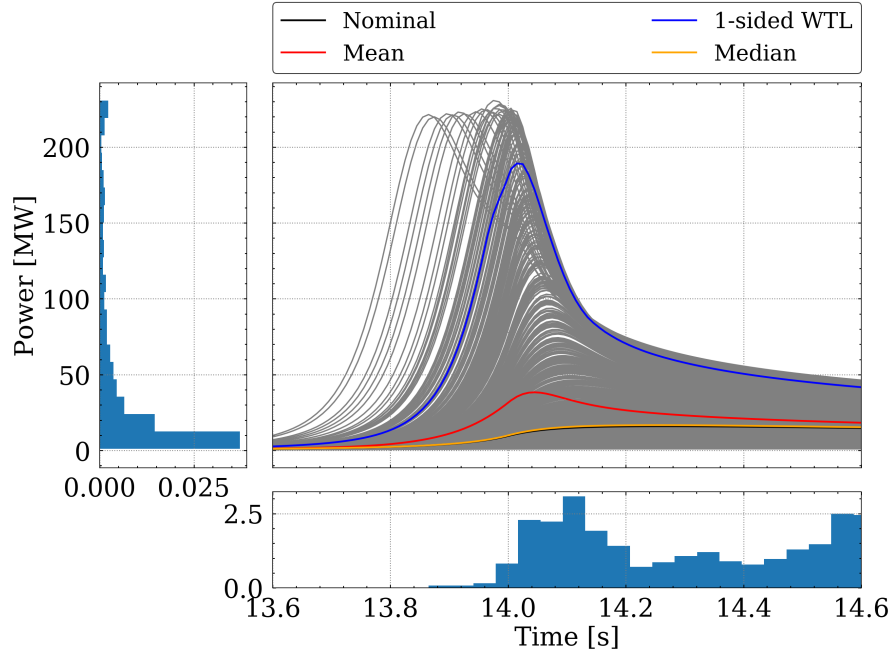


Figure 4.13: *Transient 2*: Power curves (light grey) of the entire sample; mean, median and one-sided, upper (95 %, 95 %) WTL of the power output sample; histograms showing the power maxima and their respective occurrence times; power of the nominal case.

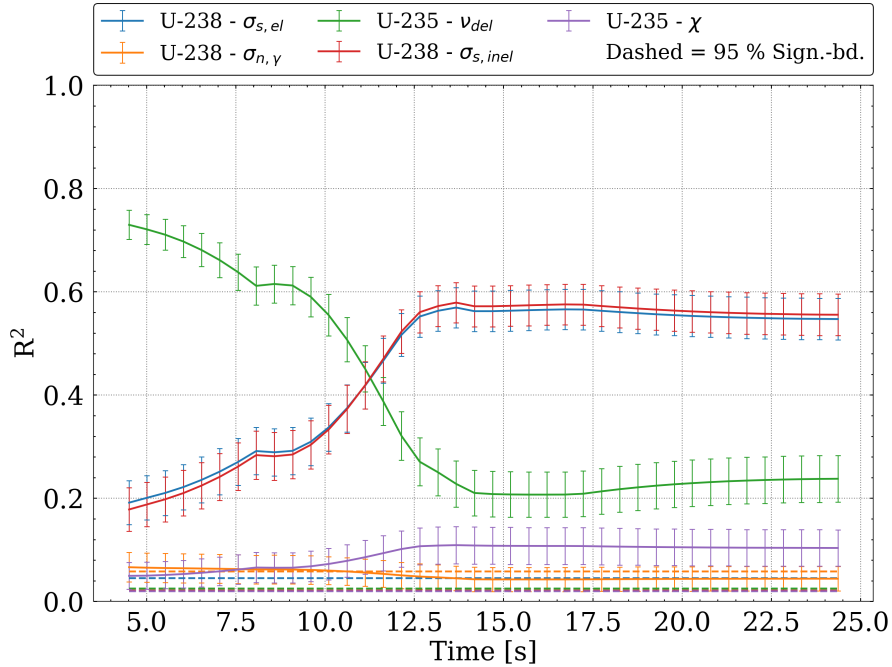


Figure 4.14: R^2 coefficients with confidence intervals and significance bounds of the major contributors to the power uncertainty for *Transient 1*.

4.5. Uncertainty and sensitivity analysis results

In general, the R^2 coefficients undergo significant changes during the control rod withdrawal, while they remain almost constant in the phase of the control rod reinsertion. With beginning of the control rod withdrawal, the uncertainty of the ^{235}U delayed neutron multiplicity ν_{del} is the dominant contributor to the power uncertainty, although its R^2 coefficient exhibits a gradual decrease. At the same time, the R^2 coefficients of the ^{238}U scattering cross sections increase, and, from approximately 11.5 s on, they are the dominant contributors. While the ^{238}U inelastic scattering cross section is the direct contributor to the uncertainty, the significant contribution of the ^{238}U elastic scattering cross section can be explained by strong correlations between the inelastic and elastic scattering cross sections of ^{238}U (Aures et al., 2017c). The contributions from the ^{235}U fission energy spectrum χ and the ^{238}U capture cross section are minor and are therefore considered as unimportant.

For *Transient 2*, the sensitivity analysis identified the same set of varied nuclide cross sections as the major contributors to the power uncertainty as in *Transient 1* (Figure 4.15).

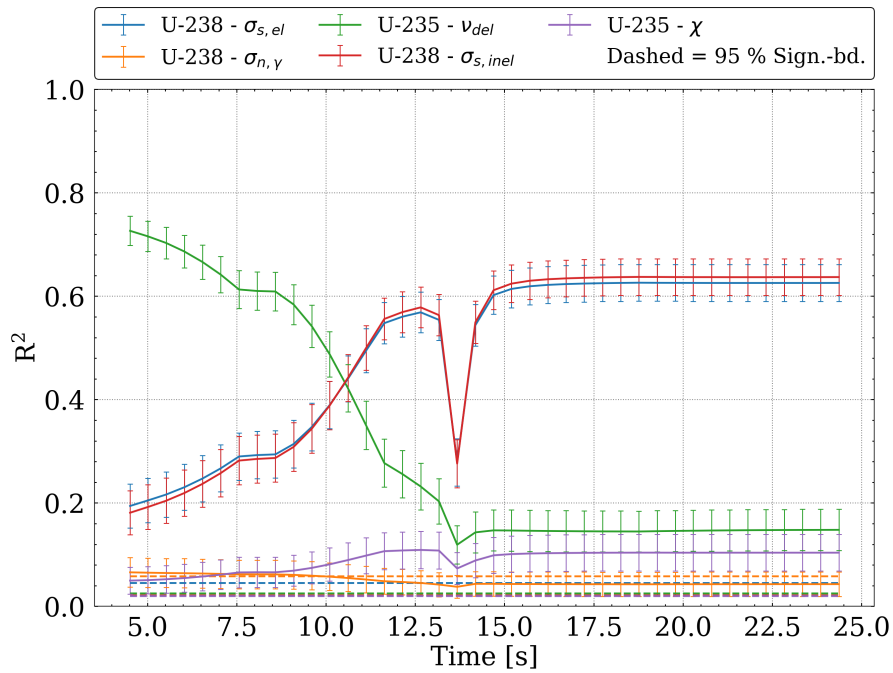


Figure 4.15: R^2 coefficients with confidence intervals and significance bounds of the major contributors to the power uncertainty for *Transient 2*.

The R^2 coefficients for the ^{238}U scattering cross sections, the ^{238}U capture cross section, the ^{235}U delayed neutron multiplicity, and the ^{235}U energy spectrum, show almost the same development over time, but with one exception: in contrast to *Transient 1*, the R^2 coefficients have strong dips in the time interval 13 s – 14 s, particularly

Chapter 4. Impact of nuclear data uncertainties in transient analysis

for the ^{238}U scattering cross sections as the dominant contributors during this phase. The fact that these dips occur in the trends of the R^2 coefficients of the individual nuclide reactions again indicates that the power uncertainty is substantially affected by non-linear effects during this time interval. This interpretation could be validated by unraveling such dips also in the trend of the total R^2 coefficient (cf. Section 4.4).

The large number of input parameters and the limited sample size of 1,000 in this analysis prevented the determination of the total R^2 under the consideration of all uncertain input parameters. To overcome this limitation, the total R^2 coefficients were estimated for both transients on the basis of the reactions of only the most contributing nuclides ^{235}U and ^{238}U . The development over time of the estimated total R^2 coefficients are shown in Figure 4.16. While during the time interval 13 s – 14 s the estimated total R^2 of *Transient 1* decreases only moderately from 0.98 to 0.95, the estimated total R^2 of *Transient 2* encounters a strong dip with a minimum value of 0.71. An explanation of this pattern is given by the presence of strong non-linear effects. It shall be noted that the estimated total R^2 coefficients of both transients are below 1 for the time interval examined as a consequence of the limited number of considered input parameter groups for this estimation.

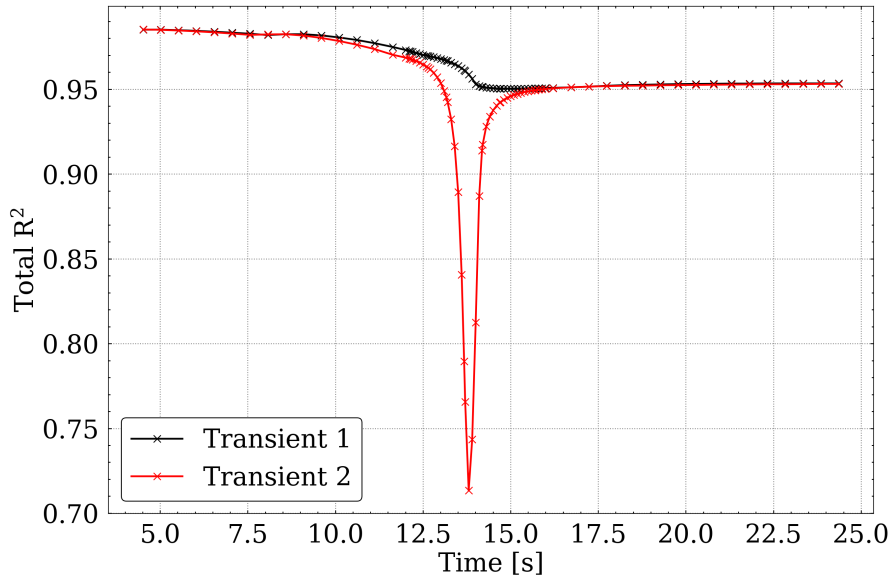


Figure 4.16: Estimated total R^2 coefficients for the power uncertainty of both *Transient 1* and *Transient 2* if only the most contributing nuclides ^{235}U and ^{238}U are considered.

4.6 Summary and discussion

The impact of nuclear data uncertainties on the outcome of reactor transient calculations was investigated. The studied scenarios were two control rod withdrawal transients with nominal reactivity insertions of 0.5\$ and 0.97\$, respectively, for a PWR mini-core model. For this study, the random sampling-based method XSUSA was used to propagate uncertainties of nuclear cross sections, the average numbers of both prompt and delayed neutrons per fission, and the fission spectra through the lattice-physics sequence TRITON/NEWT of the SCALE 6.1 code package for the generation of varied two-group constants libraries. On the basis of these libraries, 1,000 NK/TH calculations with the code system DYN3D-ATHLET were carried out for each transient. The development over time of both the reactivity uncertainty and the reactor power uncertainty was investigated.

In the course of the uncertainty analysis of the complete time series, it was found that the distributional patterns of the analysed quantities of interest change across the problem time and the assumption of normally distributed output values cannot be preserved for the entire problem time. This characteristic is particularly observed for the 0.97\$ transient where outliers in terms of power due to prompt supercriticality caused a highly skewed distribution. Since this behaviour is less pronounced for the reactivity (the assumption of normality is rejected only at the end of the power reversal phase), the uncertainty analysis of the reactivity was performed under the assumption of a normal distribution.

For both transients, a relative uncertainty between 6% – 9% were found for the reactivity at the time when the sample means encounter their respective maximum. Although a moderate increase in reactor power was observed for the 0.5\$ transient, the assumption of normality was already rejected during control rod withdrawal. In case of the 0.97\$ transient it was observed that although the majority of the NK/TH calculations yielded moderate maximum power values, an extremely asymmetrical distribution was caused by some substantial outliers. Because of these findings, the non-parametric WTLs were applied for the statistical analysis of the time series of the reactor power of both transients. Given the fixed sample size of transient calculations, the one-sided, upper (95%, 95%) WTL, and the two-sided (95%, 95%) WTL were determined. On the basis of these WTLs, intervals could be determined that enclose the demanded proportion of power output values at a certain confidence level for each computed time step.

Sensitivity analyses based on the determination of the squared multiple correlation coefficient R^2 were performed to identify the most contributing nuclide reactions

Chapter 4. Impact of nuclear data uncertainties in transient analysis

to the reactor power uncertainty over time. For both transients, the uncertainty is dominated by the same set of nuclide reactions: the ^{235}U delayed neutron multiplicity is the major contributor during the phase of the control rod withdrawal; at the time of the maximum power and beyond, the inelastic and elastic scattering cross sections of ^{238}U were the major contributors. In case of the 0.97\$ transient, the trends of the R^2 coefficients, in particular those of the ^{238}U scattering cross sections, exhibit a strong dip around the time of the maximum power. The explanation for this behaviour is the presence of strong non-linear effects around the time of the maximum power which has a substantial impact on the reactor power uncertainty.

The findings of this study stress the importance of accompanying reactor transient analyses with nuclear data uncertainty propagation. In this way, the resulting uncertainties of not only integral quantities, such as the reactor power, but also of local, safety-relevant output quantities such as the maximum cladding temperature can be determined. The applied WTLs are then a useful uncertainty measure to prove whether a proportion β of output realisations at a statistical confidence level γ are within regulatory limits.

The identification of the nuclide reactions contributing most to the result uncertainties via sensitivity analyses also provides the opportunity to formulate recommendations for further improvements of the underlying cross section data, for example, through improving the evaluations or carrying out additional measurements.

5 Hybrid neutron transport approach for reactor transient analysis

For the simulation of steady-state and dynamic reactor problems of LWRs, the two-step approach consisting of (1) the generation of group constants and (2) the coupled neutron-kinetic and thermal-hydraulic simulation has been state-of-the-art for many years (see Section 1.1). The neutron-kinetic code solves the neutron diffusion equation in few energy groups on a coarse spatial mesh and relies therefore on spatially-homogenised and energy-collapsed group constants. These group constants are usually obtained by multigroup deterministic neutron transport calculations of single assembly configurations in an infinite lattice, i.e. reflective boundary conditions are applied. However, the solution of the neutron transport in this way involves several approximations in terms of energy and space.

The most accurate description of such reactor dynamic problems is obtained using the Monte Carlo method for the simulation of CE neutron transport in combination with an adequate simulation of the thermal-hydraulic phenomena. In recent years, Monte Carlo neutron transport calculations with a detailed space-dependent thermal-hydraulic feedback became an established method for the analysis of steady-state reactor problems of research reactor cores and even LWR and SFR cores (Knebel et al., 2016; Bernnat et al., 2015). However, time-dependent Monte Carlo neutron transport calculations with the consideration of thermal-hydraulic feedback for the analysis of reactor transients is only possible by the use of massive computing clusters (see Section 1.1).

Encouraged by the successful simulations of steady-state reactor problems using the Monte Carlo neutron transport method in combination with thermal-hydraulic feedback, in this chapter, an approach is explored that aims for improving the conventional two-step approach for reactor transient simulations by employing Monte Carlo

full-core calculations.

To this end, the application of the Monte Carlo code Serpent is advantageous because group constants for multiple regions in a full-core model can be obtained by only performing one full-core neutron transport calculation (see Section 2.2). In this way, region-wise group constants are generated under the consideration of the actual neutron flux distribution in the three-dimensional full-core model, including the impact of surrounding assemblies and leakage effects that can cause neutron flux gradients and spectral differences between regions. Moreover, the Serpent full-core calculation allows for the determination of kinetic parameters for the whole reactor core. The successful generation of group constants using a Serpent full-core model and the subsequent application of these group constants in a nodal diffusion calculation has already been demonstrated by Rais (2018) for a research reactor.

This chapter provides a description of the approach and an overview of the technical implementation. The models based on the TMI-1 mini-core for the generation of group constants with Serpent and for the steady-state nodal diffusion calculations with DYN3D and for the coupled NK/TH calculations with DYN3D-ATHLET are described. Group constants determined with both infinite-lattice models and full-core models are compared and their performance is assessed in steady-state DYN3D calculations. Further aspects of the intended approach are assessed, such as the generation of group constants for partially controlled nodes in the nodal diffusion model.

Some methods and results studied in this chapter have been published as a conference paper (Aures et al., 2017d).

5.1 Method description

The approach involves reactor transient simulations with the NK/TH code system DYN3D-ATHLET, in combination with Monte Carlo full-core calculations using Serpent at time steps during the transient. From these Serpent full-core calculations, group constants are obtained that are used to update the group constants libraries which were applied by the NK/TH code system throughout the integration of previous time steps.

The approach is based on the established coupling scheme of the NK/TH code system DYN3D-ATHLET (see Section 2.5.1). First the reactor transient simulation is started with conventionally generated infinite-lattice group constants that are parameterised with respect to the thermal-hydraulic parameters: fuel temperature, moderator density, and boron concentration. The NK/TH code system determines a stationary state

and a critical boron concentration for the reactor core under consideration.

An extension of the coupling scheme is the additional execution of Serpent full-core calculations at times during the transient (Figure 5.1). These Serpent full-core calculations are performed with the current distribution of the thermal-hydraulic parameters and the current position of the control rod.

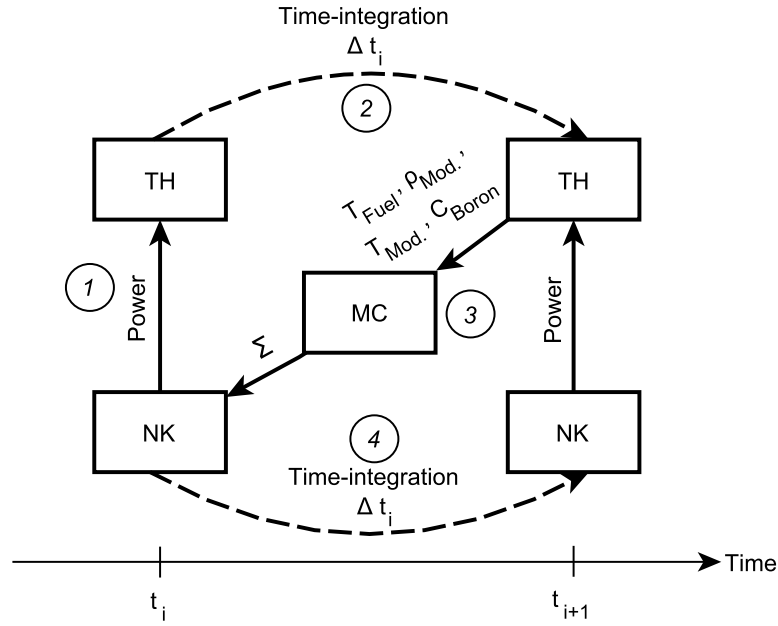


Figure 5.1: Scheme for the hybrid approach with coupled time-dependent neutron-kinetic (NK) and thermal-hydraulic (TH) calculations in combination with Monte Carlo (MC) full-core calculations for the analysis of reactor transients. *Numbers in circles depict the order of the individual calculation steps for the integration of one time step.*

From these Serpent full-core calculations, node-wise group constants (referred to as *full-core group constants*) are obtained, which, in principle, can be used to form new group constant libraries for DYN3D for the integration of the next time step. However, the following challenges have to be considered at this point:

1. the full-core group constants obtained for one node of the full-core model cover only the single thermal-hydraulic condition that was actually implemented for this node in the full-core model, thus it is not possible for the neutron-kinetic code to interpolate group constants for a certain thermal-hydraulic condition from a data grid of thermal-hydraulic parameters;

Chapter 5. Hybrid neutron transport approach for reactor transient analysis

2. reactor transient simulations involve hundreds of time steps, thus the execution of Serpent full-core calculations at each time step is not practicable;
3. the neutron-kinetic code models partially controlled nodes by weighting uncontrolled group constants (control rod withdrawn) and controlled group constants (control rod inserted) in dependence on the actual control rod insertion; however, for a partially controlled node in the Serpent full-core model, neither fully uncontrolled group constants nor fully controlled group constants are obtained.

To circumvent the first challenge, a scheme based on linear extrapolation is developed that allows the generation of group constant libraries parameterised with respect to thermal-hydraulic parameters (Figure 5.2). In this scheme, the infinite-lattice group constants, from which the reactor transient simulation was originally started, serve as a basis. Since these group constants are parameterised with respect to thermal-hydraulic parameters, difference quotients can be determined that describe the change of a group constant with a change of one of the thermal-hydraulic parameters. Then, with the fuel temperature, the moderator density and the boron concentration actually applied in one node of the Serpent full-core model, the corresponding difference quotients are selected and used to linearly extrapolate the full-core group constants for specified absolute ranges of the fuel temperature, moderator density, and boron concentration, respectively. In this way, the neutron-kinetic code can be provided with group constants libraries containing for each node the full-core group constants at the specified thermal-hydraulic state and, in addition, group constants at higher and lower values of the thermal-hydraulic parameters.

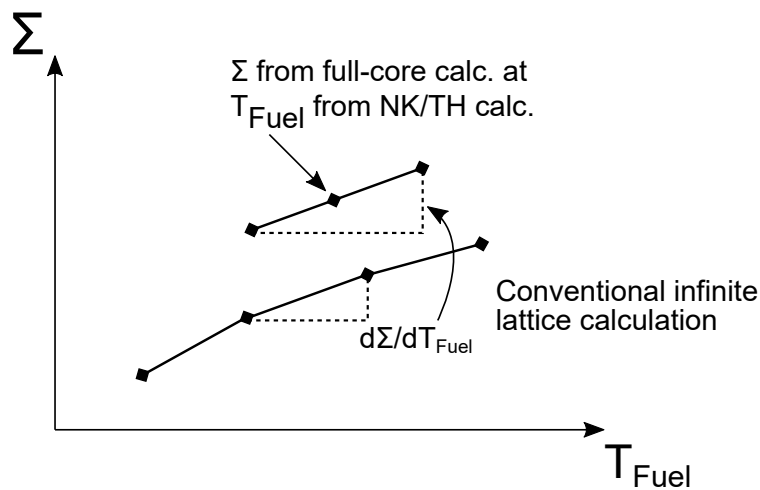


Figure 5.2: Linear extrapolation scheme to parameterise group constants from the Serpent full-core calculation with respect to thermal-hydraulic parameters.

The full-core group constants libraries with the linearly extrapolated values allow the neutron-kinetic code for interpolating group constants for newly resulting thermal-hydraulic conditions after integration of a time step. Thus, for the new thermal-hydraulic conditions, Serpent full-core calculations do not necessarily have to be performed after every time step; instead, they can be performed after larger time intervals. The maximum time interval has to be determined based on the analysed reactor transient and the chosen ranges of the thermal-hydraulic parameters for the extrapolation of the group constants.

To provide the nodal diffusion model with both uncontrolled and controlled group constants for an individual controlled fuel assembly, the scheme illustrated in Figure 5.3 was developed with the assumption that PWR assemblies are almost homogeneous in terms of the geometry and the material compositions in the axial direction. If in the initial state of the reactor transient, the control rod is fully inserted, the Serpent full-core calculation yields controlled group constants for all nodes in which the control rod is inserted. For each fuel assembly in which a control rod is intended to be moved, a set of controlled and a set of uncontrolled group constants need to be provided to the nodal diffusion model. To provide the uncontrolled group constants, an additional Serpent full-core calculation with the first (lowest) node uncontrolled is performed to obtain fully uncontrolled group constants (Figure 5.3a).

When the control rod is moved upwards within the first node, the controlled group constants for this node are obtained from the fully controlled node above (second node). The uncontrolled group constants are still taken from the additional Serpent full-core calculation (Figure 5.3b). This procedure is carried out until the control rod tip reaches the lower edge of the second node.

When the second node becomes partially controlled, the node below (first node) is fully uncontrolled and the node above (third node) is fully controlled. The group constants of the uncontrolled node below are then taken as the uncontrolled group constants for the partially controlled node; similarly, the group constants of the controlled node above are used as the controlled group constants for the partially controlled node (Figure 5.3c).

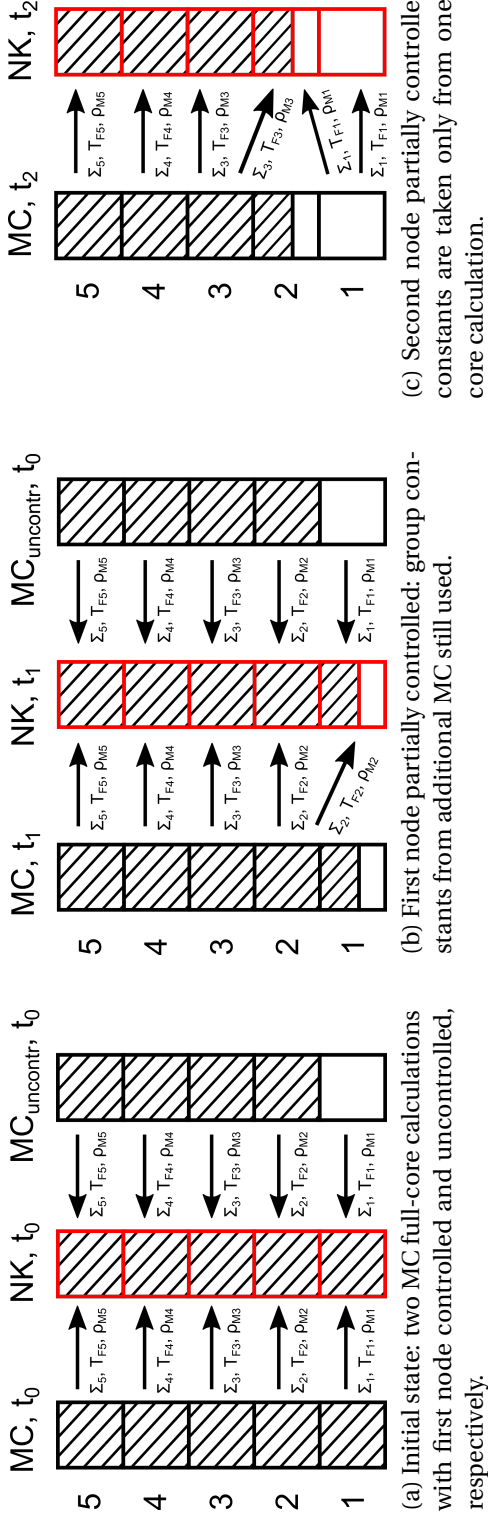


Figure 5.3: Scheme for the assignment of uncontrolled and controlled group constants Σ obtained by an original Monte Carlo (MC) full-core calculation and an additional Monte Carlo (MC_{uncontr}) full-core calculation performed at corresponding thermal-hydraulic parameters (T_F, ρ_M) to model partially controlled nodes in the neutron-kinetic (NK) model.

5.2 Technical implementation

The technical implementation of the hybrid approach as a programme (hereinafter referred to as the *control programme*) was realised using the scripting language Python. Extensive use was made of a development version of the core simulator KMACS to benefit from the various pre- and post-processing methods for both lattice calculations and coupled NK/TH calculations and the sophisticated database for the storage of the group constants and the results of the NK/TH calculations. Moreover, ATHLET 3.1A was used in the form of a shared library, in combination with the Python controller provided with ATHLET. In the following, several aspects of the technical implementation are described in more detail.

Extracting thermal-hydraulic parameters during the DYN3D-ATHLET calculation

When using ATHLET as a shared library, it is possible to associate so-called callback routines with certain events in the ATHLET simulation (Austregesilo et al., 2017). At a certain event, the corresponding callback routine is called before continuation of the ATHLET simulation. For the purpose of the described hybrid approach, the callback routine that is associated with the event of writing result data to ATHLET's output file was activated in the Python controller. (In this study, ATHLET was instructed to write output data after each time step.) In this callback routine, a call to a method in the control programme was implemented to allow for further actions of the control programme before the ATHLET simulation continues. In this call, the current position of the control rod and the ATHLET problem time are passed to the control programme.

Depending on the time step and the specified time interval between two Serpent full-core calculations, the control programme determines whether an update of the group constants based on a Serpent full-core calculation is to be carried out or whether only a simple return to the ATHLET simulation is undertaken.

In case of an update of the group constants, node-wise thermal-hydraulic parameters (fuel temperature, moderator density and temperature, and boron concentration) of the time step integrated last by ATHLET are parsed from the ATHLET output file with an appropriate output file reader included in KMACS and stored in KMACS' database. For this approach, the methods were modified in order to parse and store results obtained in a reactor transient simulation.

Chapter 5. Hybrid neutron transport approach for reactor transient analysis

Monte Carlo full-core calculations with Serpent

For the Serpent full-core calculations, multi-physics interface files of the Cartesian mesh type are generated for the different fuel materials and the moderator material using the thermal-hydraulic parameters stored for every node. From these interface files, Serpent determines the three-dimensional distributions of the temperatures and densities of the individual materials for the neutron transport calculation. The dimensions of the Cartesian mesh are taken from the geometrical core description contained in the KMACS input. The current control rod position is implemented in a template-version of the full-core model input prepared beforehand.

The first full-core calculation is always done before the movement of the control rod takes place. This yields controlled group constants for all nodes in the fuel assembly containing the control rod. Moreover, the additional Monte Carlo full-core calculation with the lowest node uncontrolled is also performed for reasons explained in Section 5.1.

To parse the group constants of the fuel and reflector nodes from the result file of a full-core calculation, a Python module was developed that also stores the parsed data in a data structure that corresponds to the nodes of the nodal diffusion model. For the nodes of a fuel assembly in which a control rod is moved, the assignment of the group constants to the nodes follows the scheme described in Section 5.1.

Extrapolation of the full-core group constants

The linear extrapolation of the full-core group constants on the basis of pre-calculated infinite-lattice group constants is performed with a specially developed Python module. At initialisation of the control programme, the infinite-lattice group constants assigned to each node as well as the thermal-hydraulic parameters by which the group constants are parameterised are obtained from the previously generated KMACS database. For each cross section in the set of group constants of one node, difference quotients are determined from the intervals of the cross section values and the intervals of the thermal-hydraulic parameters. The difference quotients are stored in a data structure. During the reactor transient calculation, for a given node, a cross section type, and a thermal-hydraulic variable and its value, the appropriate difference quotient can be selected for the subsequent linear extrapolation of a cross section obtained in the full-core calculation.

5.3. TMI-1 mini-core models for steady-state and transient analysis

Update of the DYN3D group constants library

When the group constants that were provided to DYN3D have to be updated during the reactor transient simulation, the KMACS method for pre-processing of library files for DYN3D is used to generate new library files containing the extrapolated full-core group constants. The group constants library files used by DYN3D before are replaced. The method in DYN3D that performs a new time step was modified such that the group constants from the newly generated library files are read.

Moreover, in the DYN3D method, a query on a particular GCSM signal of ATHLET was implemented, so that DYN3D only reads the library files and updates the group constants when the group constants library files have actually been updated. The GCSM signal is set by the control programme and forwarded by the Python controller to ATHLET.

5.3 TMI-1 mini-core models for steady-state and transient analysis

The development of the hybrid approach was carried out with the TMI-1 mini-core model. Details of the TMI-1 mini-core were already provided in Section 4.1. Only details are given in the following that are specific to this study or the applied codes.

In the following subsections, the Serpent models for the generation of group constants, the DYN3D nodal diffusion model for the steady-state calculations, and the DYN3D-ATHLET model for the transient calculations are described.

5.3.1 Generation of group constants with Serpent models

Two-group constants for the DYN3D nodal diffusion calculation of the TMI-1 mini-core were determined with different Serpent models: i) a full-core model with regions corresponding to the nodes of the nodal diffusion model, ii) conventional infinite-lattice models and reflector models.

A. Rais found that the original method implemented in Serpent for the calculation of the diffusion coefficient—the so called out-scatter approximation—caused deviations of up to 1500 pcm for the multiplication factor between the nodal diffusion result and the reference Monte Carlo result for small reactor cores with a high neutron leakage (Rais et al., 2017). For such reactor cores, the application of the in-scatter approximation for the calculation of the transport cross section and thus the diffusion coefficient

Chapter 5. Hybrid neutron transport approach for reactor transient analysis

is preferable. However, the direct application of the in-scatter approximation is not practicable due to the Monte Carlo neutron transport method (Leppänen et al., 2016). To offer an improved diffusion coefficient while avoiding the mentioned issues with the direct application of the in-scatter approximation, Serpent allows the calculation of transport cross sections and diffusion coefficients with the so-called transport correction (TRC) method. The TRC method relies on pre-calculated correction factors. If these are properly determined, transport cross sections are obtained that are equivalent to those obtained by the in-scatter approximation. The correction factors are calculated as the ratio of the macroscopic transport cross section to the total cross section determined in a fixed-source calculation of an infinite region filled only with moderator. Further details on this correction method are found in Rais et al. (2017) and Rais (2018).

Full-core model

The Serpent full-core model (Figure 5.4) of the TMI-1 mini-core was built to serve two purposes: i) the generation of individual group constants for each node of the DYN3D nodal diffusion model; ii) the determination of reference results for the quantities of interest such as the multiplication factor and the core power distribution.

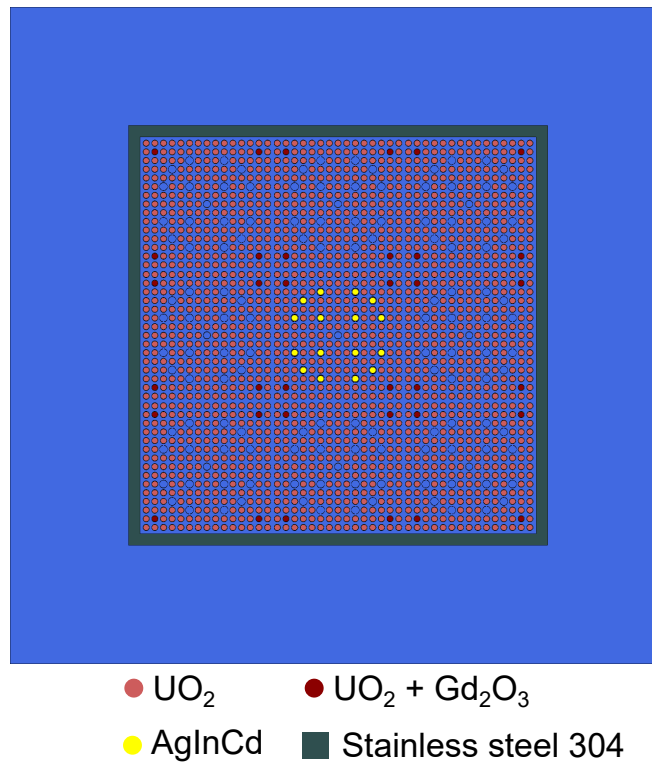


Figure 5.4: Radial view of the Serpent full-core model of the TMI-1 mini-core.

5.3. TMI-1 mini-core models for steady-state and transient analysis

To generate group constants with the Serpent full-core model for every node of the nodal diffusion model, each fuel assembly and each reflector assembly were modelled individually. Furthermore, the assemblies were axially subdivided into 16 units so that an individual set of group constants can be determined for each node. In this way, the full-core model of the TMI-1 mini-core allows for the determination of individual group constants for all nodes.

The core power distribution is obtained using a fission energy detector with a Cartesian mesh that corresponds to the spatial mesh (one mesh cell is one node) of the nodal diffusion model.

A special variant of this model was built for the application within the hybrid approach. The temperatures and densities of the different materials, such as fuel and moderator, are set through several multi-physics interface files (see Section 2.2).

Infinite-lattice models and reflector models

For the determination of the group constants in the conventional manner, Serpent infinite-lattice models and reflector models were generated using the KMACS module that was developed in the course of this thesis (see Section 2.6).

Both the uncontrolled and the controlled infinite-lattice model of the UO_2 fuel assembly have reflective boundary conditions (Figure 5.5). Fuel temperature, moderator density and temperature, and boron concentration are set according to the thermal-hydraulic parameter ranges defined in the KMACS input.

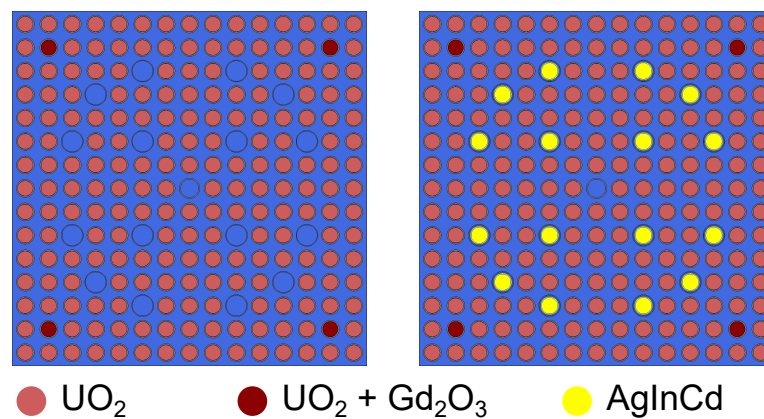


Figure 5.5: Layout of the UO_2 fuel assembly, left: uncontrolled, right: controlled.

The reflector model was built as a symmetric model with two uncontrolled UO_2 fuel assemblies enclosed by radial reflector nodes. The boundary conditions are reflective

in the direction of the y-axis and vacuum in the direction of the x-axis to approximate the spatial neutron flux distribution in a reflector. The group constants are determined in one of the radial reflector nodes.

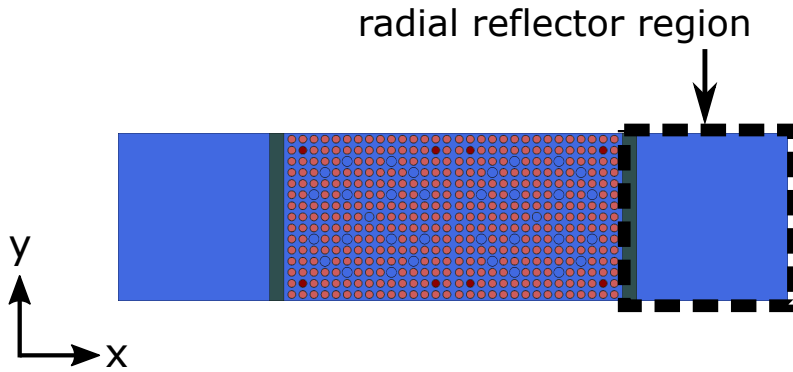


Figure 5.6: Radial reflector model.

5.3.2 DYN3D steady-state model and DYN3D-ATHLET model

In the same way as the Serpent full-core model, the DYN3D nodal diffusion models for both the steady-state and transient calculations were built with an individual modelling of each fuel assembly and each reflector assembly, and with the same axial subdivision, i.e. 16 nodes. This allows the assignment of an individual set of group constants to one node.

For comparison of the steady-state DYN3D nodal diffusion results with the results of the Serpent full-core calculation, fixed thermal-hydraulic parameters were specified for every node in the model instead of applying DYN3D's internal thermal-hydraulic solver.

5.4 Results

This section begins with a comparison of group constants obtained by a Serpent full-core calculation with group constants obtained by Serpent infinite-lattice calculations. Afterwards, results from steady-state nodal diffusion calculations performed with these group constants are presented. The applicability of the developed scheme for modelling partially controlled nodes in the nodal diffusion model with group constants from the full-core calculation is assessed.

5.4.1 Comparison between full-core group constants and infinite-lattice group constants

To study whether it makes a difference if group constants are determined in a two-dimensional infinite-lattice model or in regions of a three-dimensional full-core model, group constants were calculated with the models introduced above and compared. For this study, fixed thermal-hydraulic parameters were implemented in the models, namely: a fuel temperature of 560 K, a moderator density of 0.75206 g/cm^3 , and a boron concentration of 1000 ppm. The full-core calculation was carried out with 400,000 neutrons per cycle, 5,000 active cycles, and 200 inactive cycles. The Serpent infinite-lattice calculations were performed with 10,000 neutrons per cycle, 5,000 active cycles, and 20 inactive cycles.

In case of the full-core model, the group constants were extracted for various regions containing a UO_2 fuel assembly and for various regions with a reflector assembly, as is shown in Figure 5.7. While the regions UO_2_1010 , UO_2_2010 , UO_2_5010 , Refl_10110 , Refl_10210 , Refl_10310 are at the bottom of core, the regions UO_2_1080 , UO_2_2080 , UO_2_5080 , Refl_10117 , Refl_10217 , Refl_10317 are halfway up the core.

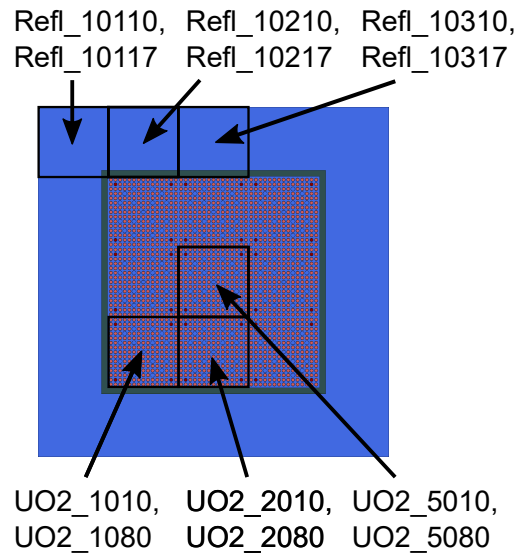


Figure 5.7: Regions in the Serpent full-core model for which the group constants are compared with those obtained by the infinite-lattice models.

The studied group constants encompass the fast and thermal diffusion coefficients D_1 and D_2 , the fast and thermal absorption cross section Σ_{abs_1} and Σ_{abs_2} , the fast and thermal fission neutron production cross section $\bar{\nu}\Sigma_{\text{fis}_1}$ and $\bar{\nu}\Sigma_{\text{fis}_2}$, and the scattering cross section from the fast to the thermal energy group Σ_{12} . The diffusion coefficient based on the originally implemented out-scatter approximation is considered.

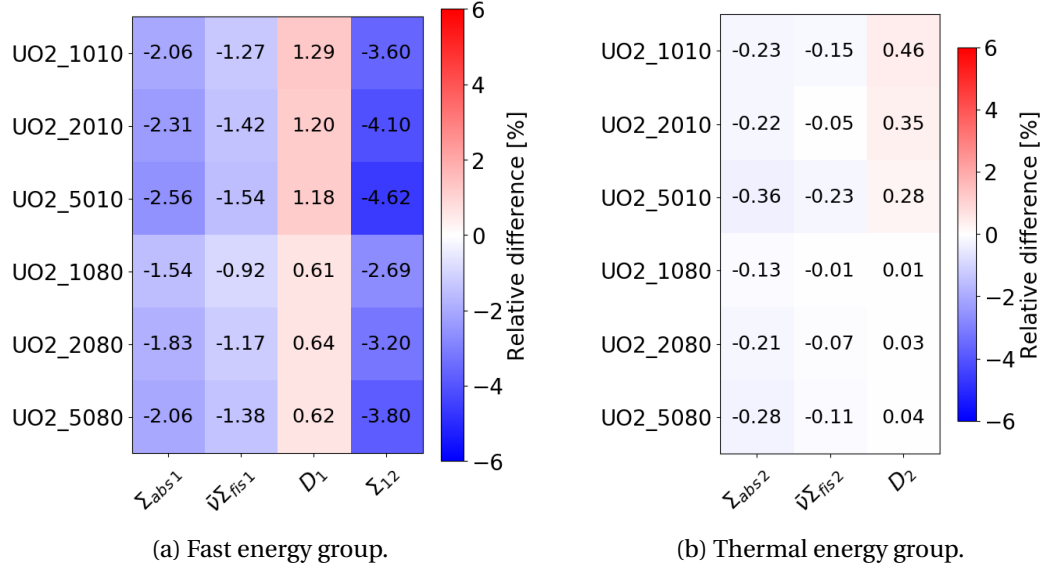


Figure 5.8: Relative difference between the full-core group constants and the infinite-lattice group constants of UO₂ nodes as generated with Serpent.

For regions with a UO₂ fuel assembly, Figure 5.8 compares group constants obtained by the full-core model with those obtained by the infinite-lattice model. In case of the fast energy group, the diffusion coefficients determined in the regions of the full-core model overestimate the one of the infinite-lattice model; a maximum difference of 1.29% is found for the region UO2_1010 which is at the corner position and at the bottom of the core. All other group constants obtained for the regions of the full-core model underestimate the group constants from the infinite-lattice model. A maximum difference of -4.62% is found for the scattering cross section of the region UO2_5010, which is in the centre and at the bottom of the core. Moreover, for this region, always the largest differences between the full-core group constants and the infinite-lattice group constants are observed except for the diffusion coefficient. Since the model is symmetric in the axial direction (control rod is fully withdrawn), it is expected that the same behaviour is observed for the nodes at the top of the core.

The same observations are made for the thermal group constants. However, the differences between the full-core group constants and the infinite-lattice group constants are smaller, namely below 1%. The full-core diffusion coefficients overestimate the infinite-lattice diffusion coefficient; a maximum difference of 0.46% is found for the region UO2_1010. All other full-core group constants underestimate the infinite-lattice group constants; a maximum difference of -0.36% is found for the absorption cross section determined in the region UO2_5010.

Figure 5.9 compares the group constants of the various reflector regions of the full-core model with those of the infinite-lattice reflector model. The fast diffusion coefficients and the scattering cross sections obtained for the regions Refl_10110 and Refl_10117, respectively, are significantly larger—with a maximum difference of 46.31%—than the values from the infinite-lattice calculation. In contrast, for the same regions, the fast absorption cross section is underestimated with a maximum difference of -35.04%, and also the thermal absorption cross section is underestimated with a maximum difference of -13.13%. The reason for the significant differences in the group constants of these two regions is to a large extent due to differences in the model. The steel baffle part in these regions of the full-core model is much smaller than in the infinite-lattice reflector model. The differences observed for the fast and thermal group constants of the other regions are moderate. A maximum difference of 4.39% is found for the fast diffusion coefficient, and a maximum difference of 0.51% is found for the thermal diffusion coefficient.

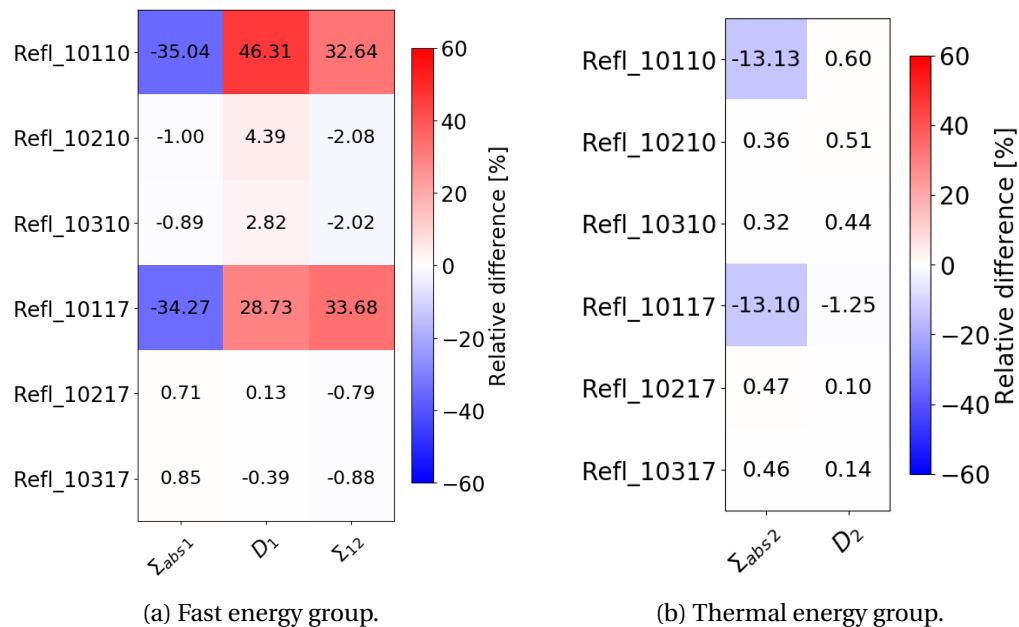


Figure 5.9: Relative difference between the full-core group constants and the infinite-lattice group constants of reflector nodes as generated with Serpent.

The impact of the differences between the full-core group constants and the infinite-lattice group constants on the outcome of steady-state nodal diffusion calculations is investigated in the following subsection.

5.4.2 Performance assessment of group constants from the full-core model and the infinite-lattice models

The performance of the group constants generated with the infinite-lattice models and with the full-core model, respectively, were assessed by applying the various group constants in steady-state DYN3D nodal diffusion calculations of the uncontrolled reactor core. The resulting multiplication factor and the core power distribution were compared with those obtained by the Serpent reference calculation. The same thermal-hydraulic values that were used in Section 5.4.1 for the group constant generation were also specified in the DYN3D nodal diffusion model as fixed, core-wide thermal-hydraulic parameters.

The TRC method was applied in all Serpent calculations to obtain not only the diffusion coefficients based on the out-scatter approximation, but also the diffusion coefficients that are equivalent to those that would result from the in-scatter approximation. In case of the infinite-lattice calculations, assembly discontinuity factors (ADFs) for both the UO_2 fuel assembly and the reflector assembly were determined. Because the determination of ADFs with three-dimensional models is not allowed in Serpent, ADFs from the infinite-lattice calculations were applied as a first approach in the DYN3D calculations with the full-core group constants.

In Table 5.1, multiplication factors determined by DYN3D with either infinite-lattice group constants or full-core group constants are compared with the Serpent reference result. In addition, the impact of the ADFs and the TRC method on the DYN3D multiplication factor is studied. By use of the infinite-lattice group constants, a small impact of the ADFs was found with a maximum impact of about 200 pcm; DYN3D's multiplication factors with or without ADFs show a good agreement with the Serpent reference result. When using the diffusion coefficient based on the TRC method, the multiplication factors increase by about 400 pcm.

The same DYN3D calculations (without and with ADFs, without and with the TRC method) were performed with the full-core group constants. When comparing the multiplication factor obtained by DYN3D based on the full-core group constants with the multiplication factor of the corresponding DYN3D calculation based on the infinite-lattice group constants, it is observed that the use of the full-core group constants results always in a reactivity difference of about -300 pcm. By comparison with the Serpent reference result, the best agreement is found for the DYN3D calculation in which the infinite-lattice ADFs as well as the diffusion coefficient based on the TRC method are applied in addition to the full-core group constants. As the largest impact was expected from the infinite reflector ADFs, an additional DYN3D calcu-

lation was done without the infinite UO2 assembly ADFs but still with the diffusion coefficient from the TRC method. The resulting multiplication factor is also in very good agreement with the Serpent reference result.

Table 5.1: DYN3D calculations with infinite-lattice group constants (inf-lattice GC) or full-core group constants (full-core GC) compared to the Serpent reference result.

Case	UO2 ADFs	Refl. ADFs	TRC	k_{eff}	$\Delta\rho$ [pcm]
Serpent Reference				1.08094(2)	-
DYN3D - inf-lattice GC				1.08252	135
DYN3D - inf-lattice GC	x	x		1.07963	-112
DYN3D - inf-lattice GC			x	1.08745	554
DYN3D - inf-lattice GC	x	x	x	1.08448	302
DYN3D - full-core GC				1.07872	-191
DYN3D - full-core GC	x	x		1.07589	-435
DYN3D - full-core GC			x	1.08407	267
DYN3D - full-core GC	x	x	x	1.08114	17
DYN3D - full-core GC		x	x	1.08057	-32

¹ Values in parentheses are the 1σ statistical uncertainty related to the Monte Carlo result.

Figures 5.10 and 5.11 compare the radial core power distributions obtained by the various DYN3D calculations listed in Table 5.1 with the Serpent reference result. Although symmetric radial core power distributions are obtained by DYN3D, the presented relative differences show variations due to the statistical uncertainty of the Serpent reference result.

The application of infinite-lattice group constants without ADFs and with the original out-scatter diffusion coefficient leads to a core power distribution that is in reasonable agreement with the core power distribution obtained by Serpent. A maximum relative difference of -3.79% is observed in the central fuel assembly (Figure 5.10a). When using ADFs, an excellent agreement between the core power distributions of DYN3D and Serpent with a maximum relative difference of -0.07% is obtained (Figure 5.10b). The application of the diffusion coefficient based on the TRC method does not lead to a significant improvement (Figure 5.10c, d).

DYN3D determines with the full-core group constants a core power distribution that deviates by up to -4.57% from the Serpent reference result (Figure 5.11a). The relative differences are slightly larger but by less than 1% compared to the DYN3D result with infinite-lattice group constants (Figure 5.10a). With the additional application of the infinite UO2 assembly ADFs and the infinite reflector ADFs, DYN3D shows a good agreement with the Serpent reference result with a maximum difference of -0.75%

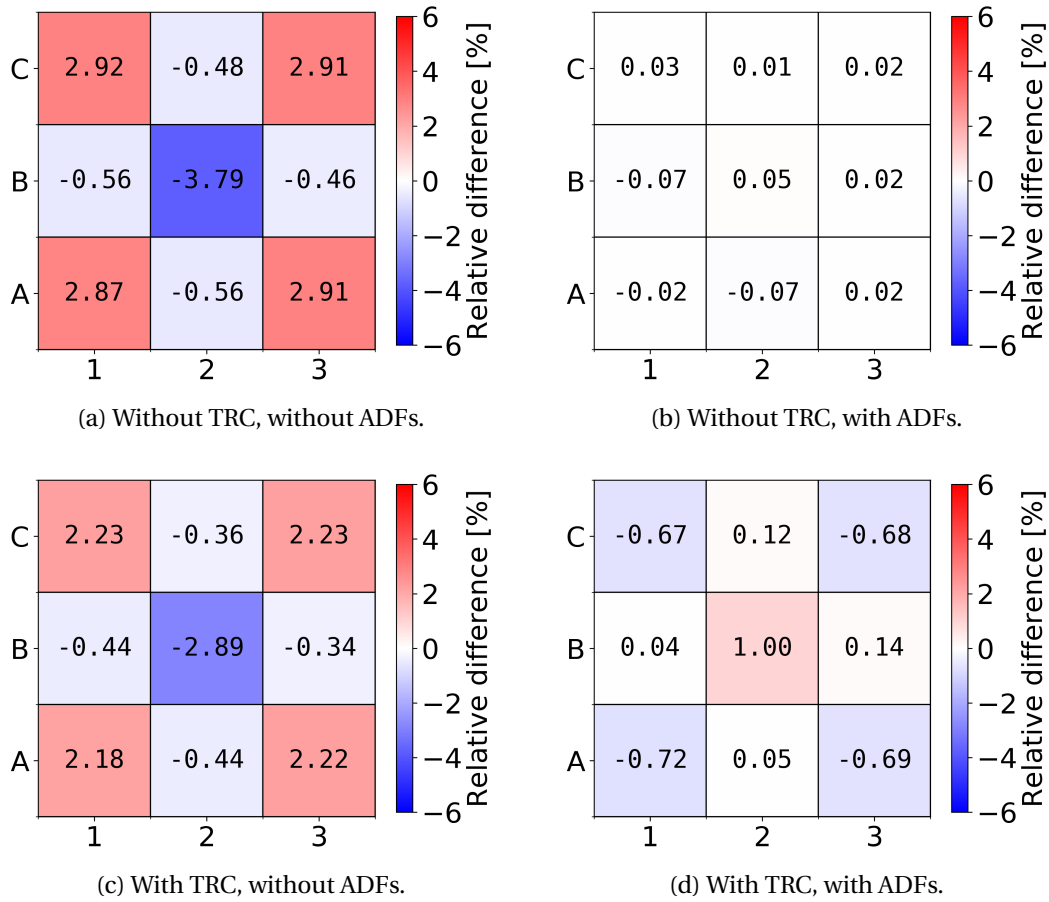


Figure 5.10: Relative difference of the radial core power distribution between DYN3D with infinite-lattice group constants, ADFs, and the diffusion coefficient from the TRC method, and the Serpent reference calculation.

(Figure 5.11b). Without the ADFs but with the diffusion coefficient from the TRC method, a slightly better agreement compared to the case with the original diffusion coefficient is achieved (Figure 5.11c). When using the diffusion coefficient from the TRC method, the infinite UO₂ assembly ADFs, and the infinite reflector ADFs, a very good agreement between DYN3D and Serpent with a maximum difference of 0.26% is obtained (Figure 5.11d). By neglectation of the infinite UO₂ assembly ADFs, the very good agreement remains with a maximum difference of 0.38% (Figure 5.11e).

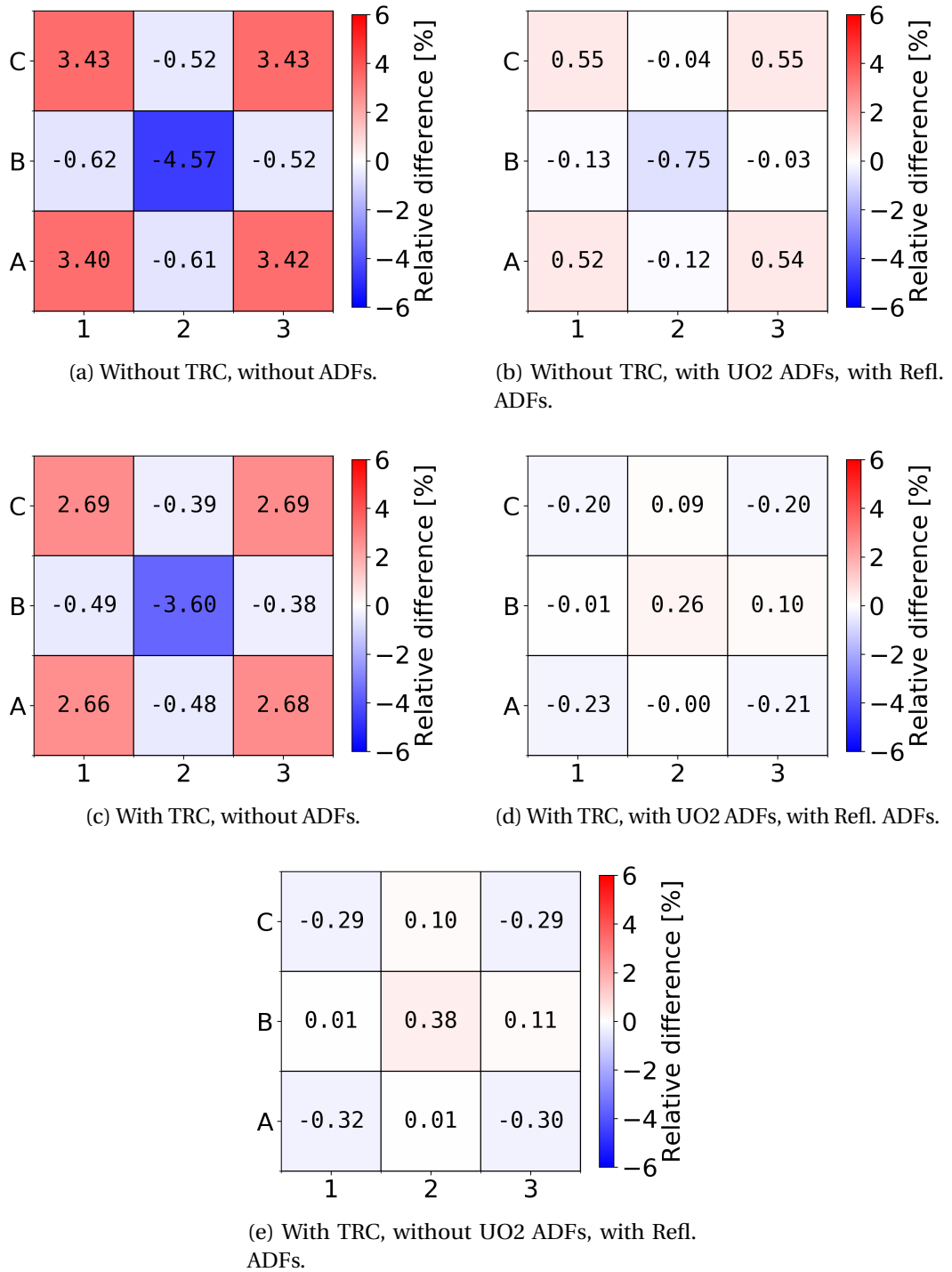


Figure 5.11: Relative difference of the radial core power distribution between DYN3D with full-core group constants, ADFs, and the diffusion coefficient from the TRC method, and the Serpent reference calculation.

5.4.3 Modelling of partially controlled nodes in the nodal diffusion model with group constants from Serpent full-core calculations

The scheme described in Section 5.1 for providing the DYN3D nodal diffusion model with uncontrolled and controlled group constants for the nodes of a fuel assembly in which a control rod is intended to be moved was tested.

First, Serpent full-core calculations with different control rod insertion depths—starting with the fully inserted position and ending at the upper edge of the sixth lowest node—were performed. The same thermal-hydraulic parameters were used as for the calculations in Section 5.4.1. Afterwards, a series of DYN3D calculations were carried out in which the group constants obtained by the Serpent full-core calculations were assigned to the nodes of the DYN3D nodal diffusion model according to the developed scheme. Thus, the control rod was explicitly modelled in the nodal diffusion model. In a second series of DYN3D calculations, group constants from the Serpent full-core calculations were directly applied to the nodal diffusion model. In these calculations, the control rod was implicitly modelled through the group constants of the nodes that were actually controlled in the Serpent full-core calculations. Moreover, in a third series of DYN3D calculations, group constants obtained by Serpent infinite-lattice calculations were applied.

Figure 5.12 shows the resulting multiplication factors in dependence on the control rod insertion as obtained by the three series of DYN3D calculations and the Serpent full-core calculations. The series of Serpent full-core calculations, which serve as a reference, and the series of DYN3D calculations with the direct application of the group constants, referred to as *DYN3D full-core GC directly assigned*, show a gradual increase of the multiplication factor when the control rod insertion is reduced. For the considered control rod insertions, the DYN3D multiplication factors overestimate the Serpent multiplication factors by an average reactivity difference of about 242 pcm.

In case of the series of DYN3D calculations, in which the developed scheme for the assignment of the uncontrolled and controlled group constants to the nodes encompassing a control rod is applied, referred to as *DYN3D full-core GC assigned by scheme*, the multiplication factors first agree with those of the other DYN3D calculation series. However, as soon as the control rod reaches the third lowest node, the multiplication factors obtained for control rod positions that are in the middle of a node are underestimated; the neutron absorption is overestimated. The same behaviour but even more pronounced is observed for the DYN3D calculations based on the infinite-lattice group constants, referred to as *DYN3D infinite-lattice GC*. In this case the effect is

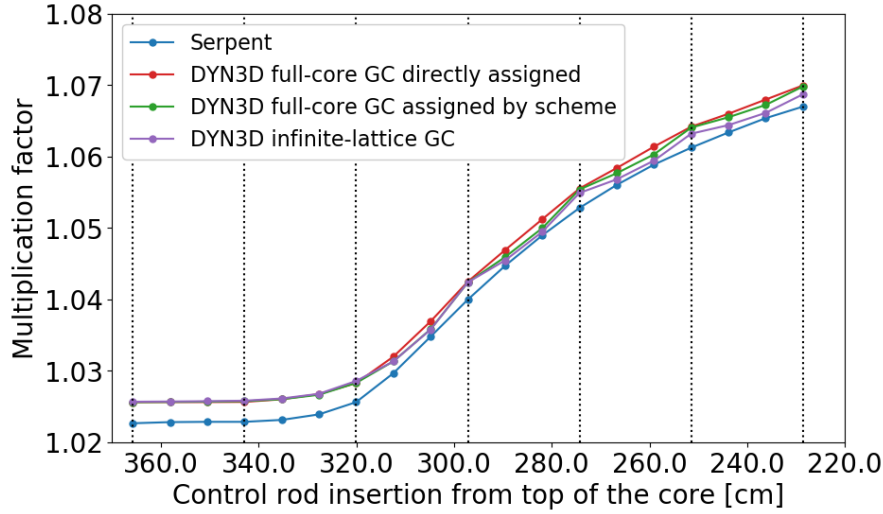


Figure 5.12: Calculated multiplication factor as a function of the control rod insertion. *Serpent*: Serpent full-core calculation; *DYN3D full-core GC directly assigned*: implicit modelling of the control rod through direct application of the group constants from the full-core model; *DYN3D full-core GC assigned by scheme*: explicit modelling of the control rod through the usage of uncontrolled and controlled group constants from the full-core model; *DYN3D infinite-lattice GC*: group constants from infinite-lattice calculations. The dotted lines indicate the node boundaries in the axial direction.

explained by the purely geometrical weighting of the uncontrolled and controlled group constants of partially controlled nodes, as has been observed in previous studies (Pautz, 2002), but the same explanation probably also applies to the series of DYN3D calculations where the developed scheme is applied (*DYN3D full-core GC assigned by scheme*). A reduction of this effect may be achieved by an additional weighting of the group constants with the uncontrolled and controlled neutron fluxes (Grundmann et al., 2005). For this purpose, the appropriate neutron fluxes would have to be determined either in additional DYN3D calculations or from the Serpent full-core calculations.

5.4.4 Linear Extrapolation of full-core group constants

The method for the linear extrapolation of the full-core group constants was tested with a simulation of a delayed supercritical control rod withdrawal transient in the TMI-1 mini-core model. The developed control programme was used to run a DYN3D-ATHLET calculation based on infinite-lattice group constants and to perform the Serpent full-core calculations at certain times. The group constants obtained by the Serpent full-core calculations were linearly extrapolated. However, at this stage, the

Chapter 5. Hybrid neutron transport approach for reactor transient analysis

extrapolated full-core group constants were not provided to the DYN3D-ATHLET calculation.

At a problem time of 4 s, the control rod is withdrawn by 54 cm from the fully inserted position within 5 s. The reactor power as obtained by DYN3D-ATHLET reaches a maximum of 36.4 MW at 10.27 s (Figure 5.13).

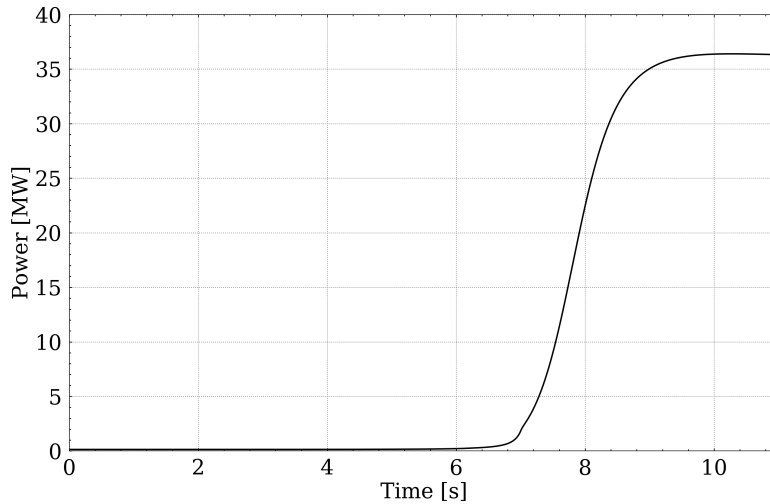
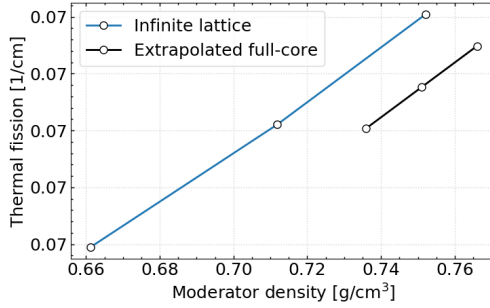


Figure 5.13: Reactor power over time.

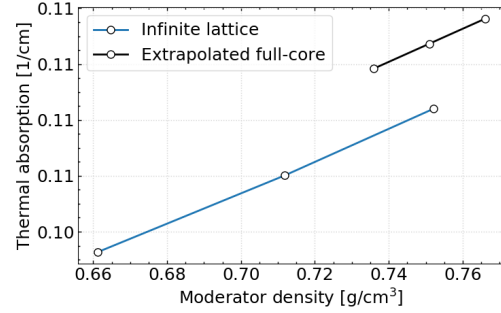
Serpent full-core calculations were performed every second starting at a problem time of 1.5 s. In a first approach, the full-core group constants were linearly extrapolated based on the method described in Section 5.1 with a range of ± 100 K for the fuel temperature, ± 0.015 g/cm³ for the moderator density, and ± 200 ppm for the boron concentration.

As an example, the individual plots in Figure 5.14 show the linearly extrapolated fission and absorption cross sections from the set of group constants of the uncontrolled node UO2_2010 (Figure 5.4). The linear extrapolation is performed on full-core group constants obtained by the Serpent full-core calculation at a problem time of 10.5 s. In addition, the plots show the infinite-lattice cross sections from which the difference quotients for the linear extrapolation were determined. The intention of these plots is to illustrate the result of the linear extrapolation but not to provide a comparison of the actual cross section values because the thermal-hydraulic parameters applied in the Serpent full-core calculation differ from those applied in the infinite-lattice calculations.

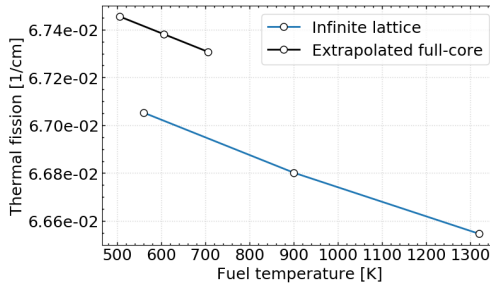
In all cases, the linearly extrapolated cross sections each have the same gradient as the infinite-lattice cross sections in the corresponding thermal-hydraulic parameter interval. It is further observed that the thermal-hydraulic parameter ranges chosen



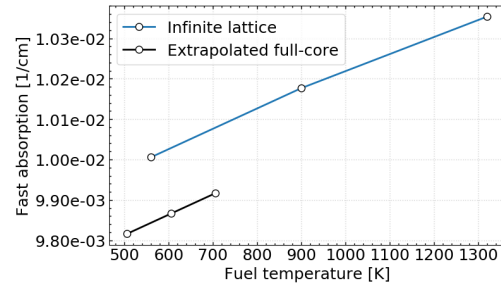
(a) Thermal fission over moderator density.



(b) Thermal absorption over moderator density.



(c) Thermal fission over fuel temperature.



(d) Fast absorption over fuel temperature.

Figure 5.14: Linearly extrapolated fission and absorption cross sections based on Serpent full-core calculations, and fission and absorption cross sections obtained by infinite-lattice calculations.

for the linear extrapolation result in extrapolated cross sections whose associated thermal-hydraulic parameters are outside of the thermal-hydraulic parameter ranges of the infinite-lattice cross sections.

5.5 Summary and discussion

A novel approach was assessed that extends the established two-step approach—infinite-lattice calculations for the generation of group constants and coupled NK/TH calculations—for reactor transient calculations by additional Monte Carlo full-core calculations which are performed at certain times during the transient simulation. The Monte Carlo full-core calculations performed with Serpent allow for the generation of group constants for the individual regions of the three-dimensional full-core model. It was expected that these group constants generated with the actual neutron flux spectra of the full-core model lead to more accurate results in the nodal diffusion calculations compared to the group constants obtained in the conventional infinite-lattice calculations.

Chapter 5. Hybrid neutron transport approach for reactor transient analysis

Various challenges were encountered during the development of this approach:

1. Group constants obtained for a region of a Serpent full-core model cover only a single thermal-hydraulic condition. Therefore, a linear extrapolation scheme was developed to calculate group constants that are parameterised over various thermal-hydraulic conditions.
2. A Serpent full-core calculation at each time step of the transient simulation is not feasible. However, by application of linearly extrapolated group constants libraries, a larger time interval is allowed between two Serpent full-core calculations.
3. Uncontrolled and controlled group constants for partially controlled nodes in the nodal diffusion model cannot be obtained from a single Serpent full-core calculation. Instead, an additional Serpent full-core calculation is performed or group constants from neighbouring uncontrolled or controlled nodes can be applied.

Group constants obtained by a full-core calculation were compared to group constants determined in infinite-lattice calculations. Relative differences of a few percent were observed. The application of the full-core group constants in steady-state DYN3D nodal diffusion calculations resulted in good agreement of the multiplication factor when compared to a Serpent full-core reference calculation. However, a good agreement for the radial core power distribution could only be achieved with additional measures, such as the application of ADFs and the TRC method for the correction of the diffusion coefficients.

The scope of this study included the technical implementation of the presented hybrid approach. However, within the given time frame, the implementation could only be completed for the generation of region-wise group constants with Serpent full-core calculations at times during a reactor transient simulation with DYN3D-ATHLET, the linear extrapolation of the full-core group constants of uncontrolled nodes to obtain group constant libraries parameterised over thermal-hydraulic conditions. Moreover, DYN3D was modified to reload the group constants from the library files before DYN3D integrates the next time step. This functionality has so far only been tested on the same group constants libraries. In terms of the technical implementation, the linear extrapolation of the controlled group constants taken from the neighbouring nodes or the additional Serpent full-core calculation remains open. Finally, the developed hybrid approach will be applied to reactor transient calculations.

6 Summary and recommendations for future research

The methods and results studied in this doctoral research are summarised in the following section. Afterwards, recommendations for future research are provided.

6.1 Thesis summary

The summary of this thesis follows the objectives as specified in Section 1.3.

Assessment of the applicability of Serpent/DYN3D-ATHLET for the analysis of reactor transients in small reactor cores

Seven reactivity accident tests of the SPERT III E-core experimental programme were chosen to assess the applicability of the code sequence Serpent/DYN3D-ATHLET for the simulation of reactor transients in small reactor cores. Delayed supercritical, prompt critical, and prompt supercritical tests at two different reactor conditions—cold-startup and hot-standby—were analysed. The Monte Carlo neutron transport code Serpent was applied for the generation of appropriate group constants libraries using infinite-lattice and reflector models. Based on these group constants, the coupled NK/TH code system DYN3D-ATHLET was used for the time-dependent simulation of the different tests. Excellent agreement was found between the calculated and the experimental reactivity insertions and between the calculated and the experimental maximum powers, respectively. For the majority of the tests, the calculated maximum power occurred at a time that was within two standard deviations of the experimental time. The calculated and the experimental reactivity feedbacks at the time of the maximum power were generally in very good agreement. For most of the

Chapter 6. Summary and recommendations for future research

prompt supercritical tests, the energy releases until the time of the maximum power were in very good agreement. For the delayed supercritical tests, reasonable agreement of slightly less than three standard deviations was obtained. For the prompt critical and prompt supercritical tests from the range of cold-startup tests, the calculated stable reactor periods were found to be in good agreement with the experimental values.

In addition to the transient calculations, static nuclear core characteristics of the SPERT III E-core at cold-startup conditions were analysed with Serpent full-core models and steady-state DYN3D nodal diffusion models. Very good agreement was found for the critical position of the control rod bank, the excess reactivities of both the control rod bank and the transient rod, and the effective point kinetic parameters.

The good agreement between the calculated and the experimental results proves the applicability of DYN3D-ATHLET in combination with group constants from Serpent infinite-lattice calculations for the analysis of reactor transients of small reactor cores.

Propagation of nuclear data uncertainties through reactor transient calculations

To assess the impact of nuclear data uncertainties on the simulation of reactor transient calculations, nuclear data uncertainties were propagated through coupled NK/TH calculations of two control rod withdrawal transients with nominal reactivity insertions of 0.5\$ and 0.97\$, respectively. These transients were studied for the TMI-1 mini-core model at hot zero power conditions. The core consists of 3×3 UO₂ fuel assemblies, and it is surrounded by a water reflector including a steel baffle. The random sampling-based method XSUSA was used to propagate uncertainties of nuclear cross sections, the average numbers of both prompt and delayed neutrons per fission, and the fission spectra through the lattice-physics sequence TRITON/NEWT of the SCALE 6.1 code package. In this way, 1,000 libraries with varied two-group constants parameterised with respect to fuel temperature, moderator density, and boron concentration were generated. These libraries were then applied with DYN3D-ATHLET for the simulations of the control rod withdrawal transients, i.e. in total 1,000 DYN3D-ATHLET calculations were performed for each control rod withdrawal transient.

Assessment of the impact of the nuclear data uncertainties on the outcome of the reactor transient calculations with appropriate uncertainty measures

For both control rod withdrawal transients of the TMI-1 mini-core, uncertainty analyses were performed for both the reactivity and the reactor power as obtained by

DYN3D-ATHLET. It was found that the assumption of a normal distribution may not be valid for the complete time series of these response values. This was particularly observed for the reactor power of the 0.97\$ transient, where some realisations of the sample calculations yielded substantial maximal power values due to prompt supercriticality and thus led to a highly asymmetrical distribution of the reactor power. Although the power increase of the 0.5\$ transient was found to be moderate, the assumption of a normal distribution was also rejected during this control rod withdrawal transient. Because of these findings, the determination of basic uncertainty measures, such as the mean value and the standard deviation, under the assumption of a normal distribution was not appropriate. Thus, the non-parametric Wilks tolerance limits (WTL) were applied for the statistical analysis of the reactor power of both transients at each computed time step. Under consideration of the fixed sample size of 1,000 DYN3D-ATHLET transient calculations, the one-sided, upper (95 %, 95 %) WTL, and the two-sided (95 %, 95 %) WTL allowed the determination of intervals that enclose 95% of the reactor power output realisations with a confidence of at least 95%. In case of the 0.97\$ transient, the one-sided, upper WTL encounters a maximum of 189.20 MW as compared to the nominal transient maximum power of 15.99 MW.

Since the assumption of a normal distribution for the reactivity was rejected only at the end of the power reversal phase, the uncertainty of the reactivity was analysed by calculation of the mean value and the standard deviation under the assumption of a normal distribution. For both transients, relative uncertainties in terms of the standard deviation of 6% – 9% were found for the reactivity at the time when the mean values of the reactor power output realisations reach their respective maximum.

Identification of the most contributing nuclide reactions to the reactor power uncertainty using sensitivity analyses

The identification of the most contributing nuclide reactions to the reactor power uncertainty over time were performed with sensitivity analyses based on the calculation of the squared multiple correlation coefficient R^2 . For both transients, the same set of nuclide reactions was identified: the ^{235}U delayed neutron multiplicity dominated the uncertainty during the phase of the control rod withdrawal; at the time of the maximum power and beyond, the scattering cross sections of ^{238}U were the most contributing nuclide reactions. In case of the 0.97\$ transient, strong dips were observed in the trends of the R^2 coefficients around the time of the maximum power. In particular the R^2 coefficients of the ^{238}U scattering cross sections, which were the dominant contributors in this phase, exhibited these dips. This behaviour indicated the presence of strong non-linear effects in this phase of the transient.

Performance assessment of group constants obtained by a three-dimensional Monte Carlo full-core model

The Monte Carlo code Serpent allows for the generation of group constants for individual regions in a three-dimensional full-core model. In this way, region-wise group constants can be determined under the consideration of the actual neutron flux distribution in the three-dimensional full-core model, i.e. the impact of the neighbouring assemblies and the neutron leakage can be considered in this way. This is in contrast to the conventional approach for group constant generation in which infinite-lattice calculations are performed for individual assemblies of a reactor core, i.e. while neglecting neighbouring effects. The performance of the group constants generated in a full-core model was studied using a three-dimensional Serpent full-core model and a corresponding steady-state DYN3D nodal diffusion model of the TMI-1 mini-core. For each node of the nodal diffusion model, an individual set of group constants was obtained with Serpent using the full-core model for the group constant generation under the assumption of fixed thermal-hydraulic conditions. The calculated multiplication factors and the radial core power distribution were compared between DYN3D and Serpent, while the results obtained with Serpent were considered as reference. When using only the group constants as obtained by the full-core calculation, good agreement was observed between the DYN3D multiplication factor and the Serpent reference result. The radial core power distributions were in reasonable agreement with deviations of up to a few percent. A very good agreement was achieved for the multiplication factor and the radial core power distribution by the additional application of assembly discontinuity factors (ADFs) and transport-corrected diffusion coefficients. ADFs were taken from additional infinite-lattice calculations because the generation of ADFs on the basis of the three-dimensional full-core model was not possible.

Development of a novel approach for the application of group constants from a Monte Carlo full-core model in reactor transient simulations

Based on the conventional two-step approach for the analysis of reactor transients, a novel approach was explored that pursues the generation of region-wise group constants with a three-dimensional Serpent full-core model at selected time steps during the reactor transient simulation. The Serpent full-core calculations were performed under consideration of the actual distributions of the fuel temperature, moderator density and temperature, and boron concentration. The group constants from the full-core model were then used to update the group constants libraries that were used by the NK/TH code system during the integration of previous time steps of this reactor transient simulation.

Various challenges were encountered during the development of this approach: i) each set of full-core group constants is determined only for a single thermal-hydraulic condition, ii) Serpent full-core calculations are not feasible at each time step of the transient simulation, iii) the nodal diffusion model requires uncontrolled and controlled group constants for a fuel assembly in which a control rod is intended to be moved; however, these group constants cannot be obtained from a single Serpent full-core calculation. To overcome these challenges, appropriate schemes were developed. For example, the full-core group constants were linearly extrapolated to obtain group constants libraries parameterised with respect to thermal-hydraulic parameters. Moreover, at the beginning of the transient simulation, an additional Serpent full-core calculation with the control rod not fully inserted can provide the necessary uncontrolled group constants for modelling the control rod withdrawal. Within the given time frame, the technical implementation could only be completed with regard to the execution of Serpent full-core calculations during the reactor transient simulation with DYN3D-ATHLET for the generation of region-wise group constants, the linear extrapolation of the full-core group constants of uncontrolled nodes, and the reloading of the group constant libraries by DYN3D before the next time step is integrated. The linear extrapolation of the controlled group constants remains open, and finally, the proper functioning of the hybrid approach must be proven with simulations of reactor transients.

6.2 Recommendations for future research

The analyses performed in this thesis provide opportunities for future research, as outlined in the following.

Further analysis of the SPERT III reactivity accident tests

During the SPERT III E-core experimental programme, reactivity accident tests were also carried out at the reactor conditions hot-startup and operating power. With a change of the reactor conditions, which also entail different positions of the control rod bank and the transient rod, the reactor core may show a different dynamic behaviour. As was already observed from the analysed reactivity accident tests for the reactor conditions cold-startup and hot-standby, the individual contributions to the total reactivity feedback change with different reactor conditions. While the contribution from the moderator density to the reactivity feedback was negligible in the cold-startup tests, a contribution was observed in the hot-standby tests. Therefore, it is of general interest to prove whether DYN3D-ATHLET with group constants from Serpent can also reproduce the experimental reactivity accident tests performed at

Chapter 6. Summary and recommendations for future research

hot-startup and operating power conditions.

Since DYN3D allows for modelling of control rods that consist of axial segments with different heights and different absorber materials, the existing DYN3D model of the SPERT III core can be enhanced with respect to the additional modelling of the flux suppressors in the control rods. This may lead to a better agreement of the critical position of the control rod bank with the experimental value.

Uncertainty and sensitivity analysis of reactor transient simulations

The uncertainty and sensitivity analyses of the control rod withdrawal transients with respect to nuclear data uncertainties presented in this thesis were performed with the 44-group covariance library of the SCALE 6.1 code package. With the release of SCALE 6.2, a more modern 56-group covariance library mainly based on the ENDF/B-VII.1 nuclear data library became available. One of the relevant differences is the substantial reduction of the uncertainty of the ^{239}Pu neutron multiplicity. It should thus be noted that depending on the nuclides in the considered system and the chosen nuclear data covariance library, different output uncertainties can be expected.

Since the performed uncertainty and sensitivity analyses of the control rod withdrawal transients have proven successful for a small reactor core, the application of the method can be extended to larger reactor cores and more realistic transient events, such as a control rod ejection transient or a boron dilution transient in a PWR core. For example, the PWR MOX/UO₂ Core Transient Benchmark (Kozłowski and Downar, 2007) specifies a control rod ejection transient for a reactor core loaded with UO₂ and MOX fuel. However, it should be noted that the generation of the varied two-group constants libraries takes a great effort, which increases as the number of different fuel assemblies increases.

Furthermore, it is of interest to perform the uncertainty analyses not only for integral quantities such as the reactor power, but also for local safety-relevant output quantities such as the maximum cladding temperature. By application of the one-sided, upper (95 %, 95 %) Wilks tolerance limit, for each time step of the simulation, a maximum cladding temperature can be determined that can be compared with the maximum permissible cladding temperature defined for the particular reactor under consideration.

Input uncertainties arise not only from nuclear data but also from material parameters and geometrical parameters (Ivanov et al., 2016). Therefore, a comprehensive uncertainty analysis should include all the different input uncertainties.

Generation of group constants using Monte Carlo full-core models and their application in nodal diffusion models

The generation of region-wise group constants using three-dimensional Monte Carlo full-core models and the subsequent application of these group constants in nodal diffusion calculations can be further investigated with the aim to achieve a good agreement between the results of a nodal diffusion calculation and the results of a Monte Carlo reference calculation. This study may include in particular the determination of assembly discontinuity factors from the Monte Carlo full-core solution, as it was observed that the application of assembly discontinuity factors led to an improved core power distribution of the nodal diffusion calculation. A possible method is presented, for example, by Hursin et al. (2016). Moreover, it is worth studying whether group constants generated with a higher number of energy groups may lead to a further improved agreement between the nodal diffusion calculation and the Monte Carlo reference calculation.

Hybrid approach to neutron transport for reactor transient analysis

The performance of the hybrid approach must be assessed with simulations of different reactor transients.

In case of the linear extrapolation scheme for the group constants obtained by the Serpent full-core calculation, a further analysis can be performed regarding the proper choice of the thermal-hydraulic parameter ranges used for the extrapolation. Moreover, appropriate criteria must be found for the choice of the time interval between two Serpent full-core calculations.

The purely geometrical weighting of the uncontrolled and controlled group constants used for the modelling of a control rod in the nodal diffusion model can be extended by an additional weighting with neutron fluxes obtained for an uncontrolled and a controlled node. This may lead to a reduction of the overestimation of the neutron absorption observed in the control rod curve. The appropriate neutron fluxes may be obtained by additional nodal diffusion calculations with varied control rod insertions or from Serpent full-core calculations.

As soon as the hybrid approach has proven successful for transients in small reactor cores, it can be applied to transients in larger reactor cores. Moreover, the Serpent full-core calculations allow then for the direct determination of results with a detailed spatial resolution as compared to nodal diffusion calculations, where the pin powers are often obtained in a further step on the basis of the nodal diffusion solution.

A Behaviour of Wilks Tolerance Limits in dependence on the sample size

Since the Wilks tolerance limits (WTLs) are estimated for samples with a finite sample size N , they show a variability from sample to sample. The degree of variability is dependent on the sample size. To demonstrate this dependency, the one-sided, upper (95 %, 95 %) WTL is determined for samples with a sample size of 59, 200, and 500, respectively. The samples were taken from the output sample of the 0.97\$ control rod withdrawal transient (*Transient 2*) with an overall sample size of 1,000 (see Section 4.5.3). It should be noted that the analysis of a time series of response values by the application of WTLs requires that the output realisations of the considered sample are ranked at every time step. For $N = 59$, the one-sided, upper WTL is given by the highest value of the sample, while for $N = 200$ the WTL is given by the 196th highest value, and for $N = 500$ the WTL is given by the 484th highest value. In Figure A.1, the WTLs determined for 16 samples with $N = 59$ are shown along with the WTL determined for the overall sample with $N = 1,000$. A substantial variability between the WTLs of the individual samples is observed. Moreover, the trends of some WTLs exhibit two local maxima. Similarly, the Figures A.2 and A.3 show the WTLs for individual samples with $N = 200$ and $N = 500$, respectively. It is observed that for larger sample sizes the variability between the WTLs is considerably reduced, i.e. an estimated WTL becomes more precise, and the majority of the WTLs have only one maximum. Moreover, the WTLs of the individual samples converge towards the WTL of the overall sample with $N = 1,000$.

The same behaviour of the WTLs was also observed for this output sample but with a randomly selected order of the output realisations.

Appendix A. Behaviour of Wilks Tolerance Limits in dependence on the sample size

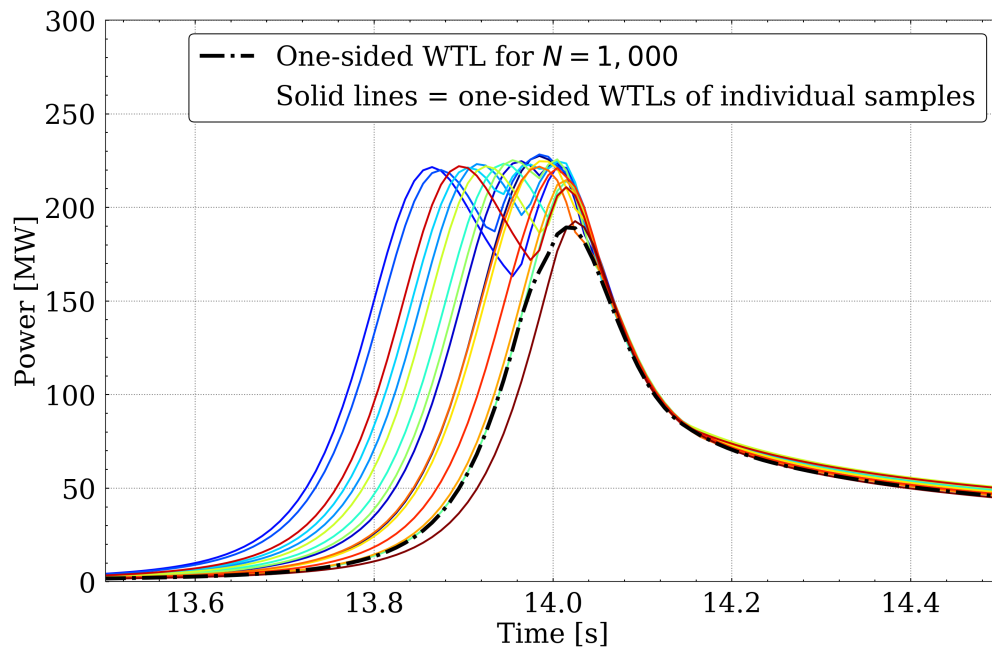


Figure A.1: One-sided, upper (95 %, 95 %) WTLs for samples with a sample size of 59 and for a sample with a sample size of 1,000.

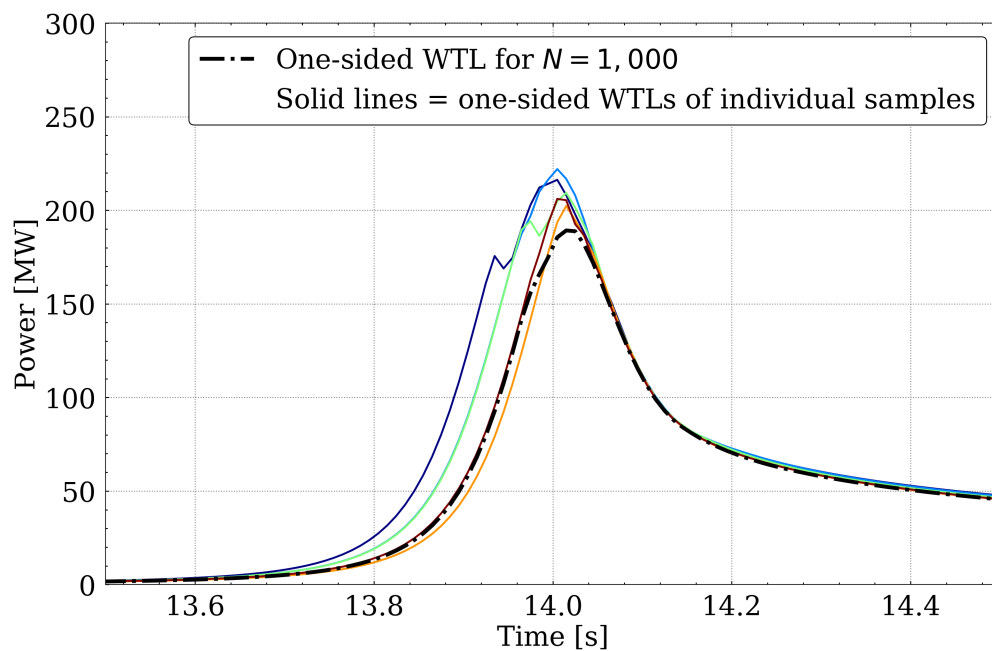


Figure A.2: One-sided, upper (95 %, 95 %) WTLs for samples with a sample size of 200 and for a sample with a sample size of 1,000.

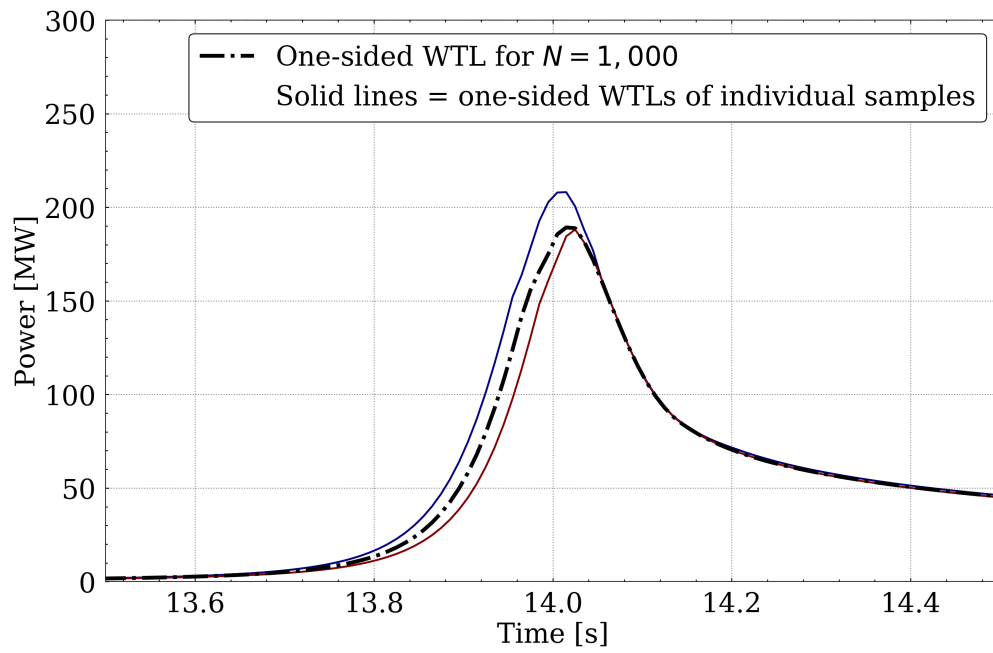


Figure A.3: One-sided, upper (95 %, 95 %) WTLs for samples with a sample size of 500 and for a sample with a sample size of 1,000.

Bibliography

- T. W. Anderson, and D. A. Darling. Asymptotic Theory of Certain "Goodness of Fit" Criteria Based on Stochastic Processes. *The Annals of Mathematical Statistics*, 23: 193–212, 1952.
- S. Aoki et al. Analysis of the SPERT-III E-Core using ANCK Code with the Chord Weighting Method. *Journal of Nuclear Science and Technology*, 46:239–251, 2009.
- T. Arens et al. *Mathematik*. Spektrum Akademischer Verlag Heidelberg, 2012.
- A. Aures et al. Uncertainty Analysis for VVER-1000 Core Simulations with MCNP/ATHLET. In *M&C 2017, Jeju, Korea, April 16–20*, 2017a.
- A. Aures et al. Benchmarking and application of the state-of-the-art uncertainty analysis methods XSUSA and SHARK-X. *Annals of Nuclear Energy*, 101:262–269, 2017b. <https://doi.org/10.1016/j.anucene.2016.11.025>.
- A. Aures et al. Uncertainty in the delayed neutron fraction in fuel assembly depletion calculations. In *ND2016, Bruges, Belgium, September 11 - 16*, 2017c. EPJ Web of Conferences, Vol. 146, ISBN 978-2-7598-9020-0.
- A. Aures et al. Introduction of a Hybrid Deterministic / Stochastic Calculation Model for Transient Analysis. In *M&C 2017, Jeju, Korea, April 16–20*, 2017d.
- A. Aures et al. Uncertainty and sensitivity analysis of PWR mini-core transients in the presence of nuclear data uncertainty using non-parametric tolerance limits. *Annals of Nuclear Energy*, 137:107146, 2020a. <https://doi.org/10.1016/j.anucene.2019.107146>.
- A. Aures et al. Transient Calculations of SPERT III Experiments. In *PHYSOR 2020, Cambridge, United Kingdom, March 30 – April 2*, 2020b.
- H. Austregesilo et al. ATHLET 3.1A – Models and Methods, GRS-P-1 / Vol. 3, Rev. 4. Gesellschaft für Anlagen- und Reaktorsicherheit (GRS) gGmbH, Germany, 2016.

Bibliography

- H. Austregesilo et al. ATHLET 3.1A – Programmer’s Manual, GRS-P-1 / Vol. 2, Rev. 7. Gesellschaft für Anlagen- und Reaktorsicherheit (GRS) gGmbH, Germany, 2017.
- W. Bernnat et al. Monte Carlo Full Core Neutronics Analysis with Detailed Consideration of Thermal-hydraulic Parameters. In *M&C 2015, Nashville, TN, USA, April 19 - 23*, 2015.
- B. R. Betzler. *Calculating Alpha Eigenvalues and Eigenfunctions with a Markov Transition Rate Matrix Monte Carlo Method*. Dissertation, University of Michigan, USA, 2014.
- F. Bostelmann et al. Uncertainty and Sensitivity Analysis in Criticality Calculations with Perturbation Theory and Sampling. In *M&C 2015, Nashville, TN, USA, April 19 - 23*, 2015.
- F. Bostelmann et al. Sensitivity Indices for Nuclear Data Uncertainty Analysis with XSUSA and TSUNAMI. In *BEPU 2018, Lucca, Italy, May 13 - 19*, 2018.
- F. Bostelmann. Systematic Sensitivity and Uncertainty Analysis of Sodium-Cooled Fast Reactor Systems, 2020. Dissertation, n° 7576, EPFL Lausanne, Switzerland.
- F. Bostelmann et al. SCALE/AMPX multigroup libraries for sodium-cooled fast reactor systems. *Annals of Nuclear Energy*, 140:107102, 2020. <https://doi.org/10.1016/j.anucene.2019.107102>.
- D. A. Brown et al. ENDF/B-VIII.0: The 8th Major Release of the Nuclear Reaction Data Library with CIELO-project Cross Sections, New Standards and Thermal Scattering Data. *Nuclear Data Sheets*, 148:1–142, 2018. <https://doi.org/10.1016/j.nds.2018.02.001>.
- L. Cao et al. Neutronics modeling of the SPERT III E-Core critical experiments with MPACT and KENO. *Annals of Nuclear Energy*, 80:207–218, 2015. <https://doi.org/10.1016/j.anucene.2015.02.013>.
- M. B. Chadwick et al. ENDF/B-VII.0: Next Generation Evaluated Nuclear Data Library for Nuclear Science and Technology. *Nuclear Data Sheets*, 107(12):2931–3060, 2006. <https://doi.org/10.1016/j.nds.2006.11.001>.
- M. B. Chadwick et al. ENDF/B-VII.1 Nuclear Data for Science and Technology: Cross Sections, Covariances, Fission Product Yields and Decay Data. *Nuclear Data Sheets*, 112(12):2887–2996, 2011. <https://doi.org/10.1016/j.nds.2011.11.002>.

- CSEWG, 2018. ENDF-6 Formats Manual - Data Formats and Procedures for the Evaluated Nuclear Data Files, CSEWG Document ENDF-102, Report BNL-203218-2018-INRE. Cross Sections Evaluation Working Group, National Nuclear Data Center, Brookhaven National Laboratory, USA, 2018.
- D. E. Cullen. PREPRO 2019, IAEA-NDS-0229. Nuclear Data Services, International Atomic Energy Agency (IAEA), 2019. Rev. 19, 20th August 2019.
- F. D'Auria et al. Technology Relevance of the Uncertainty Analysis In Modelling Project for Nuclear Reactor Safety, 2007. NEA/NSC/DOC(2007)15.
- A. Dokhane et al. Validation of PSI best estimate plus uncertainty methodology against SPERT-III reactivity initiated accident experiments. *Annals of Nuclear Energy*, 118: 178–184, 2018a. <https://doi.org/10.1016/j.anucene.2018.04.022>.
- A. Dokhane et al. Analyses of SPERT-III RIA Experiments with Nuclear Data Uncertainty Quantification using three different Covariance Matrix Libraries. In *PHYTRA4, Marrakech, Morocco, September 17-19, 2018b*.
- J. J. Duderstadt, and L. J. Hamilton. *Nuclear Reactor Analysis*. John Wiley & Sons, 1976. ISBN 0471223638.
- J. Dugone. SPERT III Reactor Facility: E-core Revision, IDO–17036. U.S. Atomic Energy Commission, USA, 1965.
- D. Emendörfer, and K.-H. Höcker. *Theorie der Kernreaktoren - Band 2: Der instationäre Reaktor*. Bibliographisches Institut & F.A. Brockhaus AG, Mannheim, 1993. ISBN 3-411-16051-9.
- D. Ferraro et al. Serpent/SUBCHANFLOW pin-by-pin coupled transient calculations for a PWR minicore. *Annals of Nuclear Energy*, 137:107090, 2020a. <https://doi.org/10.1016/j.anucene.2019.107090>.
- D. Ferraro et al. Serpent/SUBCHANFLOW pin-by-pin coupled transient calculations for the SPERT-III hot full power tests. *Annals of Nuclear Energy*, 142:107387, 2020b. <https://doi.org/10.1016/j.anucene.2020.107387>.
- N. García-Herranz et al. Multiscale neutronics/thermal-hydraulics coupling with COBAYA4 code for pin-by-pin PWR transient analysis. *Nuclear Engineering and Design*, 321:38–47, 2017. <https://doi.org/10.1016/j.nucengdes.2017.03.017>.
- D. Gaston et al. Moose: A parallel computational framework for coupled systems of nonlinear equations. *Nuclear Engineering and Design*, 239(10):1768–1778, 2009. <https://doi.org/10.1016/j.nucengdes.2009.05.021>.

Bibliography

- GIF. A Technology Roadmap for Generation IV Nuclear Energy Systems, 2002. https://www.gen-4.org/gif/jcms/c_40481/technology-roadmap. GIF-002-00.
- H. Glaeser et al. Development of methods and exemplary application for evaluating the prediction capability of computer code calculations, GRS-A-3443. Gesellschaft für Anlagen- und Reaktorsicherheit (GRS) mbH, Germany, 2008.
- A. Grahn et al. Simulation of an MSLB scenario using the 3D neutron kinetic core model DYN3D coupled with the CFD software Trio_U. *Nuclear Engineering and Design*, 315:117–127, 2017. <https://doi.org/10.1016/j.nucengdes.2017.02.002>.
- G. Grandi, and L. Moberg. Qualification of CASMO5 / SIMULATE-3K against the SPERT-III E-core Cold Start-up Experiments. In *PHYSOR 2012, Knoxville, USA, April 15–20, 2012*.
- U. Grundmann et al. DYN3D Version 3.2 - Code for Calculation of Transients in Light Water Reactors (LWR) with Hexagonal or Quadratic Fuel Elements - Description of Models and Methods. Forschungszentrum Rossendorf, Germany, 2005.
- R. E. Heffner, and T. R. Wilson. SPERT III Reactor Facility, IDO–16721. U.S. Atomic Energy Commission, USA, 1961.
- R. Henry et al. Transient CFD/Monte-Carlo Neutron Transport Coupling Scheme for simulation of a control rod extraction in TRIGA reactor. *Nuclear Engineering and Design*, 331:302–312, 2018. <https://doi.org/10.1016/j.nucengdes.2018.03.015>.
- M. Herman et al. EMPIRE: Nuclear Reaction Model Code System for Data Evaluation. *Nuclear Data Sheets*, 108:2655–2715, 2007. <https://doi.org/10.1016/j.nds.2007.11.003>.
- J. Hou et al. Benchmark for Uncertainty Analysis in Modelling (UAM) for Design, Operation and Safety Analysis of LWRs - Volume II: Specification and Support Data for the Core Cases (Phase II), 2014. Version 1.9, NEA/NSC/DOC(2014).
- M. Hursin. *Full Core, Heterogeneous, Time Dependent Neutron Transport Calculations with the 3D Code DeCART*. Dissertation, University of California at Berkeley, USA, 2010.
- M. Hursin et al. Assessment of assembly homogenized two-steps core dynamic calculations using direct whole core transport solutions. *Annals of Nuclear Energy*, 87:356–365, 2016. <https://doi.org/10.1016/j.anucene.2015.09.015>.
- IAEA. *Thermophysical Properties Database of Materials for Light Water Reactors and Heavy Water Reactors*. Number 1496 in TECDOC Series. INTERNATIONAL ATOMIC ENERGY AGENCY, Vienna, Austria, 2006. ISBN 92-0-104706-1.

- IAEA. *Research Reactor Benchmarking Database: Facility Specification and Experimental Data*. Number 480 in Technical Reports Series. INTERNATIONAL ATOMIC ENERGY AGENCY, Vienna, Austria, 2015. ISBN 978-92-0-151714-2.
- K. Ivanov et al. Benchmark for Uncertainty Analysis in Modelling (UAM) for Design, Operation and Safety Analysis of LWRs, Volume I: Specification and Support Data for the Neutronics Cases (Phase I), 2016. Version 2.1, NEA/NSC/DOC(2012)10.
- JANIS (2020). Janis Books. <http://www.oecd-nea.org/janis/book/>.
- M. Kloos, and N. Berner. SUSAN Version 4.1 – Manual of Methods – Software for Uncertainty and Sensitivity Analyses, GRS-P-5 / Vol. 2, Rev. 1. Gesellschaft für Anlagen- und Reaktorsicherheit (GRS) gGmbH, Germany, 2017.
- M. Knebel et al. Validation of the Serpent 2-DYNSUB code sequence using the Special Power Excursion Reactor Test III (SPERT III). *Annals of Nuclear Energy*, 91:79–91, 2016. <https://doi.org/10.1016/j.anucene.2016.01.005>.
- A. J. Koning, and D. Rochman. Modern Nuclear Data Evaluation with the TALYS Code System. *Nuclear Data Sheets*, 113(12):2841–2934, 2012. <https://doi.org/10.1016/j.nds.2012.11.002>.
- A. J. Koning et al. TENDL: Complete Nuclear Data Library for Innovative Nuclear Science and Technology. *Nuclear Data Sheets*, 155:1–55, 2019. <https://doi.org/10.1016/j.nds.2019.01.002>.
- T. Kozłowski, and T. J. Downar. PWR MOX/UO₂ Core Transient Benchmark, 2007. NEA/NSC/DOC(2006)20.
- B. Krzykacz. EQUUS: A Computer Program for the Derivation of Empirical Uncertainty Statements on Results from Large Computer Models, GRS-A-1720. Gesellschaft für Anlagen- und Reaktorsicherheit (GRS) mbH, Germany, 1990.
- S. Langenbuch, and K. Velkov. Capability of the Coupled Code System ATHLET-QUABOX/CUBBOX for Safety Analysis. In *Technical Meeting: Use and Development of Coupled Computer Codes for the Analysis of Accidents at Nuclear Power Plants*, IAEA TECDOC No. 1539, IAEA, Vienna, Austria, November 26–28, 2003.
- S. Langenbuch, and K. Velkov. Overview on the development and application of the coupled code system athlet-quabox/cubbox. In *M&C 2005, Avignon, France, September 12–15*, 2005.
- S. Langenbuch et al. Analysis of the Pressurized Water Reactor Main Steam Line Break Benchmark by the Coupled Code System ATHLET-QUABOX/CUBBOX. *Nuclear Technology*, 142(2):124–136, 2003. <https://doi.org/10.13182/NT03-A3378>.

Bibliography

- J. Leppänen. Development of a Dynamic Simulation Mode in the Serpent 2 Monte Carlo Code. In *M&C 2013, Sun Valley, USA, May 5-9*, pages 117–127, 2013.
- J. Leppänen, and A. Isotalo. Burnup calculation methodology in the Serpent 2 Monte Carlo code. In *PHYSOR 2012, Knoxville, USA, April 15–20*, 2012.
- J. Leppänen. Performance of Woodcock delta-tracking in lattice physics applications using the Serpent Monte Carlo reactor physics burnup calculation code. *Annals of Nuclear Energy*, 37(5):715–722, 2010. <https://doi.org/10.1016/j.anucene.2010.01.011>.
- J. Leppänen et al. Calculation of effective point kinetics parameters in the Serpent 2 Monte Carlo code. *Annals of Nuclear Energy*, 65:272–279, 2014. <https://doi.org/10.1016/j.anucene.2013.10.032>.
- J. Leppänen et al. The Serpent Monte Carlo code: Status, development and applications in 2013. *Annals of Nuclear Energy*, 82:142–150, 2015. <https://doi.org/10.1016/j.anucene.2014.08.024>.
- J. Leppänen et al. Overview of methodology for spatial homogenization in the Serpent 2 Monte Carlo code. *Annals of Nuclear Energy*, 96:126–136, 2016. <https://doi.org/10.1016/j.anucene.2016.06.007>.
- G. Lerchl et al. ATHLET 3.1A – Validation, GRS-P-1 / Vol. 3, Rev. 4. Gesellschaft für Anlagen- und Reaktorsicherheit (GRS) gGmbH, Germany, 2016a.
- G. Lerchl et al. ATHLET 3.1A User’s Manual, GRS-P-1 / Vol. 1, Rev. 7. Gesellschaft für Anlagen- und Reaktorsicherheit (GRS) gGmbH, Germany, 2016b.
- E. Lewis. *Fundamentals of Nuclear Reactor Physics*. Academic Press, 2008. ISBN 978-0-12-370631-7.
- C. Liu. Development and optimization of fast solution algorithms for the fuel depletion equations, Master’s thesis, EPFL Lausanne, Switzerland, 2014.
- R. E. MacFarlane. An Introduction to the ENDF Formats. In *Workshop on Nuclear Data and Nuclear Reactors: Physics, Design and Safety, Trieste, Italy, March 13 – April 14*, 2000.
- R. E. MacFarlane, and A. C. Kahler. Methods for Processing ENDF/B-VII with NJOY. *Nuclear Data Sheets*, 111(12):2739–2890, 2010. <https://doi.org/10.1016/j.nds.2010.11.001>.

- C. M. Mattoon et al. Generalized Nuclear Data: A New Structure (with Supporting Infrastructure) for Handling Nuclear Data. *Nuclear Data Sheets*, 113(12):3145–3171, 2012. <https://doi.org/10.1016/j.nds.2012.11.008>.
- R. K. McCardell et al. Reactivity accident test results and analyses for the SPERT III E-core - A small oxide-fueled, pressurized-water reactor, IDO–17281. U.S. Atomic Energy Commission, USA, 1969.
- NEA. International Handbook of Evaluated Criticality Safety Benchmark Experiments. OECD/NEA, 2015. NEA/NSC/DOC(95)03.
- C. E. Obenchain. PARET - A Program for the Analysis of Reactor Transients, IDO–17282. Idaho National Laboratory, USA, 1969.
- A. P. Olson. Neutronics Calculations for SPERT-III, E-Core, ANL/GTRI/TM-13/10. Argonne National Laboratory, USA, 2012.
- N. Otuka et al. Towards a More Complete and Accurate Experimental Nuclear Reaction Data Library (EXFOR): International Collaboration Between Nuclear Reaction Data Centres (NRDC). *Nuclear Data Sheets*, 120:272–276, 2014. <https://doi.org/10.1016/j.nds.2014.07.065>.
- I. Pasichnyk et al. Influence of nuclear data uncertainties on a rod ejection transient. In *AMNT 2013, Berlin, Germany, May 14-16, 2013*.
- A. Pautz, and A. Birkhofer. DORT-TD: A Transient Neutron Transport Code with Fully Implicit Time Integration. *Nuclear Science and Engineering*, 145:299–319, 2003. <https://doi.org/10.13182/NSE03-A2385>.
- A. Pautz. *Rechenmodellentwicklung für die Analyse von Reaktivitätstransienten mit Neutronentransporttheorie und gekoppelter Thermofluidodynamik für Hochfluss-Forschungsreaktoren*. Dissertation, Technische Universität München, München, Germany, 2002.
- Y. Périn. *Development of a Multi-Physics, Multi-Scale simulation tool for LWR safety analysis*. Dissertation, Technische Universität München, München, Germany, 2016.
- Y. Périn et al. Multi-scale coupled code systems: from coarse-mesh to high-fidelity lwr core calculations. *KERNTECHNIK*, 76, 2011.
- A. J. M. Plompen et al. The joint evaluated fission and fusion nuclear data library, jeff-3.3. *Eur. Phys. J. A*, 56:181, 2020. <https://doi.org/10.1140/epja/s10050-020-00141-9>.
- N. Porter. Wilks’ formula applied to computational tools: A practical discussion and verification. *Annals of Nuclear Energy*, 133:129–137, 2019.

Bibliography

- M. Pusa. Rational Approximations to the Matrix Exponential in Burnup Calculations. *Nuclear Science and Engineering*, 169(2):155–167, 2011. <https://doi.org/10.13182/NSE10-81>.
- A. Rais et al. Neutronics modeling of the CROCUS reactor with SERPENT and PARCS codes. In *M&C 2017, Jeju, Korea, April 16–20, 2017*.
- A. Rais. Performance assessment of a 3-D steady-state and spatial kinetics model for the CROCUS reactor, 2018. Dissertation, n° 8248, EPFL Lausanne, Switzerland.
- B. T. Rearden, and M. A. Jessee. SCALE Code System, ORNL/TM-2005/39, Version 6.2.3, 2018. Oak Ridge National Laboratory, Oak Ridge, Tennessee, Available from Radiation Safety Information Computational Center as CCC-834.
- U. Rohde et al. The reactor dynamics code DYN3D – models, validation and applications. *Progress in Nuclear Energy*, 89:170–190, 2016. <https://doi.org/10.1016/j.pnucene.2016.02.013>.
- A. Santamarina et al. The JEFF-3.1.1 Nuclear Data Library, JEFF Report 22, Validation Results from JEF-2.2 to JEFF-3.1.1, 2009. NEA No. 6807.
- SCALE, 2011. Scale: A Comprehensive Modeling and Simulation Suite for Nuclear Safety Analysis and Design, Version 6.1, June 2011. ORNL/TM-2005/39, Available from Radiation Safety Information Computational Center at Oak Ridge National Laboratory as CCC-785.
- A. Seubert et al. The time-dependent 3D discrete ordinates code TORT-TD with thermal-hydraulic feedback by ATHLET models. In *PHYSOR 2008, Interlaken, Switzerland, September 14–19, 2008*.
- K. Shibata et al. JENDL-4.0: A New Library for Nuclear Science and Engineering. *Journal of Nuclear Science and Technology*, 48(1):1–30, 2011. <https://doi.org/10.1080/18811248.2011.9711675>.
- B. L. Sjenitzer. *The Dynamic Monte Carlo Method for Transient Analysis of Nuclear Reactors*. Dissertation, TU Delft, Delft, The Netherlands, 2013.
- W. M. Stacey. *Nuclear Reactor Physics*. WILEY-VCH Verlag GmbH & Co., 2007. ISBN 978-3-527-40679-1.
- R. J. J. Stamm’ler, and M. J. Abbate. *Methods of Steady-State Reactor Physics in Nuclear Design*. Acad. Press, 1983. ISBN 0126633207.
- Studsvik Scandpower. HELIOS Methods, 2012. Version 1.12.

- T. Taxelius et al. Quarterly Technical Report SPERT Project, IDO-17245. U.S. Atomic Energy Commission, USA, 1967.
- T. Viitanen. Implementing a Doppler-preprocessor of cross section libraries in reactor physics code Serpent, 2009. M.Sc. Thesis.
- T. Viitanen, and J. Leppänen. Target Motion Sampling Temperature Treatment Technique with Elevated Basis Cross-Section Temperatures. *Nuclear Science and Engineering*, 177(1):77–89, 2014. <https://doi.org/10.13182/NSE13-37>.
- A. Wald. An Extension of Wilks' Method for Setting Tolerance Limits. *Ann. Math. Statist.*, 14(1):45–55, 03 1943. <https://doi.org/10.1214/aoms/1177731491>.
- J. Wang et al. Review on neutronic/thermal-hydraulic coupling simulation methods for nuclear reactor analysis. *Annals of Nuclear Energy*, 137:107165, 2020. <https://doi.org/10.1016/j.anucene.2019.107165>.
- C. J. Werner, et al. MCNP6.2 Release Notes, 2018. Los Alamos National Laboratory, report LA-UR-18-20808.
- D. Wiarda et al. AMPX-6: A Modular Code System for Processing ENDF/B, ORNL/TM-2016/43, 2016. Oak Ridge National Laboratory, Oak Ridge, Tennessee.
- S. S. Wilks. Statistical Prediction with Special Reference to the Problem of Tolerance Limits. *Ann. Math. Statist.*, 13(4):400–409, 12 1942. <https://doi.org/10.1214/aoms/1177731537>.
- M. L. Williams. Resonance Self-Shielding Methodologies in SCALE 6. *Nuclear Technology*, 174:149–168, 2011. <https://doi.org/10.13182/NT09-104>.
- A. Zhu et al. Transient Methods for Pin-resolved Whole Core Transport Using the 2D-1D Methodology in MPACT. In *MC 2015, Nashville, USA, April 19–23*, 2015.
- M. Zilly, and J. Bousquet. Multi-Cycle Depletion with the GRS Core Simulator KMACS: BEAVRS Cycles 1 and 2. In *M&C 2019, Portland, Oregon, USA, August 25–29*, 2019.
- M. Zilly, and Y. Périn. KMACS Validation Report, GRS-P-8 / Vol. 2, Rev. 0. Gesellschaft für Anlagen- und Reaktorsicherheit (GRS) gGmbH, Germany, 2018.
- M. Zilly et al. PWR Cycle Analysis with the GRS Core Simulator KMACS. In *AMNT 2018, Berlin, Germany, May 29–30*, 2018.
- A. Zoia, and E. Brun. Reactor physics analysis of the SPERT III E-core with Tripoli-4. *Annals of Nuclear Energy*, 90:71–82, 2016. <https://doi.org/10.1016/j.anucene.2015.11.032>.

Bibliography

W. Zwermann et al. Influence of Nuclear Covariance Data on Reactor Core Calculations. In *2nd International Workshop On Nuclear Data Evaluation for Reactor applications*, CEA Cadarache Château, France, September 29 - October 2, 2009.

Thesis-related publications

A. Aures et al., Introduction of a Hybrid Deterministic / Stochastic Calculation Model for Transient Analysis. In *M&C 2017, Jeju, Korea, April 16–20, 2017*.

A. Aures et al. Reactor Simulations with Nuclear Data Uncertainties. In *BEPU 2018, Lucca, Italy, May 13–19, 2018*.

A. Aures et al. Uncertainty and sensitivity analysis of PWR mini-core transients in the presence of nuclear data uncertainty using non-parametric tolerance limits. *Annals of Nuclear Energy*, 137:107146, 2020a. <https://doi.org/10.1016/j.anucene.2019.107146>

A. Aures et al. Transient Calculations of SPERT III Experiments. In *PHYSOR 2020, Cambridge, United Kingdom, March 30–April 2, 2020b*.

Alexander Aures

München, Germany

alexander.aures@mailbox.org

Experience:

since 02/2013

Gesellschaft für Anlagen- und Reaktorsicherheit (GRS) gGmbH,
Garching, Germany

Scientific employee in the Nuclear Fuel Department

- Neutron transport and burnup calculations,
- Development and application of the core simulator KMACS,
- Uncertainty and sensitivity analyses with respect to nuclear data uncertainties,
- Processing of nuclear data.

04/2011 – 11/2011

Culham Centre for Fusion Energy, Abingdon, United Kingdom
Intern

- Neutron transport and activation calculations to determine tritium breeding in future fusion devices.

10/2009 – 04/2011

Institute for Reactor Safety and Reactor Technology,
RWTH Aachen University, Aachen, Germany

Student research assistant

- Student research project: *Application of the NJOY module ERRORR for determination of standard deviations of cross-sections and fission neutron yields*,
- Neutron transport calculations for light water reactor applications,
- Simulation of severe accidents propagation in containments of light water reactors.

04/2008 – 10/2009

Institute for Technical Thermodynamics,
RWTH Aachen University, Aachen, Germany

Student research assistant

- Student research project: *Calculation of thermal conductivity of gases and liquids based on the kinetic theory of gases and friction theory*,
- Development and application of a database with Perl.

Education:

2014 – 2020

École polytechnique fédérale de Lausanne, Lausanne, Switzerland
Ph.D. in Nuclear Engineering: *A Hybrid Approach to Neutron Transport with Thermal-hydraulic Feedback for Reactor Transient Analysis*

2009 – 2012

RWTH Aachen University, Aachen, Germany
Major studies to achieve Dipl.-Ing. in Mechanical Engineering
Thesis: *Determination of the nuclide inventory of a light water reactor core of type Konvoi in equilibrium state by application of the reactor physics code Serpent*

2005 – 2009

RWTH Aachen University, Aachen, Germany
Intermediate exam in Mechanical Engineering

Skills:

Programming:

Python, Fortran, C, Perl

Software:

Serpent, MCNP, DYN3D, XSUSA, SCALE, NJOY

Languages:

German (native)
English (advanced)